Investigation of Interlayer Burr Formation in the Drilling of Stacked Aluminum Sheets

A Thesis
Presented to
The Academic Faculty

by

Cody Hellstern

In Partial Fulfillment
of the Requirements for the Degree
Master of Science in Mechanical Engineering

George W. Woodruff School of Mechanical Engineering
Georgia Institute of Technology

May 2009

Investigation of Interlayer Burr Formation in the Drilling of Stacked Aluminum Sheets

Approved by:

Dr. Shreyes N. Melkote
(ME, Georgia Tech), Committee Chair

Dr. Steven Danyluk
(ME, Georgia Tech)

Dr. Rhett Mayor
(ME, Georgia Tech)

Date Approved: May 13, 2009

Dedicated to my parents and grandparents
for always encouraging and assisting me
throughout my nineteen years of education.

ACKNOWLEDGEMENTS

I would like to thank the following people for their support in the completion of this thesis:

- My research advisor, Dr. Shreyes Melkote, for his constant support in guiding me in my work and helping me to complete this thesis.
- John Morehouse for regularly providing assistance and helpful insight.
- Steven Sheffield for teaching me how to use the PMRC equipment and always being available for help.
- Thomas Newton for his thorough introduction of this project as well as all of the other PMRC students.
- Dr. Steven Danyluk and Dr. Rhett Mayor for reviewing and providing advice on this thesis.
- The Lockheed Martin Manufacturing Research and Integration department for their financial support and supplies of materials for testing.
- Finally, I would like to thank all of my family and friends who have supported me along the way.

TABLE OF CONTENTS

DEDICATION iii

ACKNOWLEDGEMENTS iv

LIST OF TABLES x

LIST OF FIGURES xi

LIST OF SYMBOLS xv

SUMMARY xvii

INTRODUCTION 1

1.1 Background and Motivation 1

1.2 Problem Statement 4

1.3 Research Goals 4

1.4 Thesis Outline 5

LITERATURE REVIEW 6

2.1 Motivation 6

2.2 Introduction to Drilling 6

2.2.1 Factors Affecting Drilling 6

2.2.2 Standard Drill Geometries 7

2.2.3 Drill Materials 7

2.2.4 Other Drill Geometries 7

2.2.5 Drilling Forces 9

2.2.6 Drill Wear 10

2.3 Introduction to Burrs 11
2.3.1 Types of Burrs 11
2.3.2 Burr Formation Mechanism 13
2.3.3 Burr Measurements 14
2.3.4 Burr Problems 15
2.4 Burr Investigations 16
2.4.1 Experimental Investigations – Drilling Parameters 16
2.4.2 Experimental Investigations – Drilling Geometries 17
2.4.3 Experimental Investigations – Wear and Workpiece Material 17
2.4.4 Empirical Burr Modeling 17
2.4.5 Finite Element Modeling of Burrs 18
2.4.6 Analytical Burr Modeling 19
2.5 Interlayer Burrs 22
2.5.1 Interlayer Burr Formation 22
2.5.2 Interlayer Burr Prevention 23
2.5.3 Multilayered Modeling Problems 25
2.5.4 Interlayer FEM Investigations 26
2.6 Summary 26
INTERLAYER DRILLING BURR EXPERIMENTS 28
3.1 Goal and Approach 28
3.2 Parameter Selection 28
3.3 Experimental Procedure 32
3.4 Measurements 35

3.4.1 Drilling Forces 35
3.4.2 Burr Heights 36
3.4.3 Burr Widths 38
3.4.4 Drill Wear 40
3.5 Results 42
3.5.1 Burr Heights 42
3.5.2 Burr Widths and Change in Separation 45
3.5.3 Drill Wear 46
3.5.4 Drilling Thrust and Torque 48
3.5.5 Summary 49
3.6 Discussion 51
3.7 Summary 52
CLAMPING METHODS INVESTIGATION 54
4.1 Goal and Approach 54
4.2 Ideal Clamping Attributes 54
4.2.1 Clamping Functionality 55
4.2.2 Clamping Practicality 56
4.2.3 Current Clamp Comparisons 57
4.3 New Clamping Ideas 58
4.3.1 Long I-Beam Concept 59
4.3.2 Long Hand Clamp Concept 59
4.3.3 Magnetic Clamp Concept 60
4.3.4 Single-sided Clamping Concept 60

4.3.5 Evaluation of Concepts 61
4.4 Analysis of Single-sided Clamping Idea 63
4.5 Prototypes 68
4.6 Prototype Testing 70
4.7 Summary 72
ANALYTICAL MODEL FOR INTERLAYER BURR FORMATION 73
5.1 Goal and Approach 73
5.2 Analysis of Previous Models 74
5.3 Finding Appropriate Model 75
5.4 Sofronas Model Derivation 78
5.4.1 Finding Burr Initiation Height 78
5.4.2 Finding Final Burr Geometry 85
5.5 New Model Assumptions 87
5.6 New Model Calculations 91
5.7 Possible Model Completion Methods 93
5.8 Calibration with Experimental Results 94
5.9 Summary 96
CONCLUSIONS 98
6.1 Overview 98
6.2 Experimental Findings 98
6.2.1 Interlayer Drilling Burr Experiments 98
6.2.2 Clamping Methods Investigation 99
6.2.3 Interlayer Burr Formation Analytical Model 100

6.3 Future Work 100

APPENDIX A: MATLAB CODE FOR DETERMINING BREAKTHROUGH THRUST AND TORQUE 102

APPENDIX B: EXIT BURR HEIGHT RESULTS 104

APPENDIX C: ENTRY BURR HEIGHT RESULTS 107

APPENDIX D: BURR WIDTH RESULTS 110

APPENDIX E: AVERAGED DRILL FLANK WEAR RESULTS 112

APPENDIX F: DRILL OUTER CORNER WEAR RESULTS 117

APPENDIX G: MATLAB CODE FOR DETERMINING RESULTS OF INTERLAYER MODEL 122

REFERENCES 125

LIST OF TABLES

Table 3.1: Summary of drills studied (all #10 size or 4.91 mm dia.) 29

Table 3.2: Drilling conditions utilized in Phase II. 31

Table 3.3: Averaged measurements for each drill over all holes 50

LIST OF FIGURES

Figure 1.1: Entry and exit burr formation 2

Figure 1.2: Interlayer burr formation [2] 3

Figure 2.1: Standard drill geometry parameters [2] 8

Figure 2.2: Step drill parameters [5] 9

Figure 2.3: Drill wear measurements [9] 11

Figure 2.4: Types of drilling burrs [5] 12

Figure 2.5: Aluminum drilling exit burr [2] 13

Figure 2.6: Burr height and width 15

Figure 2.7: Finite element model of drilling burr formation [31] 19

Figure 2.8: Sofronas model of drilling exit burr formation [34] 21

Figure 2.9: Kim model of drilling exit burr formation [36] 22

Figure 2.10: Interlayer burr types [37] 23

Figure 2.11: Hand clamp 24

Figure 2.12: Cleco clamps 25

Figure 3.1: Drills 1, 2 and 3 from left to right. 29

Figure 3.2: Step drill parameters used [5] 31

Figure 3.3: Fadal VMC 15 vertical machining center 33

Figure 3.4: Experimental setup with dynamometer, fixture, frame material and skin material 34

Figure 3.5: De-Sta-Co model 424 squeeze action clamp 34

Figure 3.6: Example drilling forces over time for one hole 36

Figure 3.7: Optical comparator method of measuring burr heights [2] 37

Figure 3.8: Optical comparator 38

Figure 3.9: Mitutoyo toolmaker's microscope 39

Figure 3.10: Typical burr width measurements 40

Figure 3.11: Typical drill flank wear measurements 42

Figure 3.12: Skin exit burr height as a function of hole number 44

Figure 3.13: Frame entry burr height as a function of hole number 44

Figure 3.14: Skin exit burr widths as a function of hole number 46

Figure 3.15: Averaged flank wear for each drill as a function of hole number 47

Figure 3.16: Averaged outer corner wear for each drill as a function of hole number 47

Figure 3.17: Breakthrough thrust force for each drill as a function of hole number 48

Figure 3.18: Breakthrough torque for each drill as a function of hole number 49

Figure 3.19: Formation of burr with regular drill 51

Figure 3.20: Formation of burr with step drill 52

Figure 4.1: Gap formation in unclamped sheets 56

Figure 4.2: Hand clamp and cleco clamp in use [2] 58

Figure 4.3: Long I-beam concept 59

Figure 4.4: Long hand clamp concept 60

Figure 4.5: Magnetic clamp concept 60

Figure 4.6: Single-sided clamping concept 61

Figure 4.7: Resulting deformation of pushing (in) 64

Figure 4.8: Resulting von Mises stress of pushing (psi) 65

Figure 4.9: (a) Drill starting position; (b) Worst case drill position 67

Figure 4.10: Spring prototype 69

Figure 4.11: Compressible rubber prototype 70

Figure 4.12: Clamping concept skin exit burr height results 72

Figure 5.1: Sofronas model variables [34] 75

Figure 5.2: High speed video captures of exit burr formation in single aluminum layer 77

Figure 5.3: Sofronas initiation height parameters [34] 84

Figure 5.4: High speed captures of interlayer formation 88

Figure 5.5: Sofronas model initiation point and new model initiation point 90

Figure 5.6: Predicted and observed values of burr heights vs. feed rates with c = 0.02594 (averaged from observed values of all three) 96

Figure B.1: Individual burr exit heights for drill 1 104

Figure B.2: Individual burr exit heights for drill 2 104

Figure B.3: Individual burr exit heights for drill 3 105

Figure B.4: Averaged burr exit heights for drill 1 (with std bars) 105

Figure B.5: Averaged burr exit heights for drill 2 (with std bars) 106

Figure B.6: Averaged burr exit heights for drill 3 (with std bars) 106

Figure C.1: Individual burr entry heights for drill 1 107

Figure C.2: Individual burr entry heights for drill 2 107

Figure C.3: Individual burr entry heights for drill 3 108

Figure C.4: Averaged burr entry heights for drill 1 (with std bars) 108

Figure C.5: Averaged burr entry heights for drill 2 (with std bars) 109

Figure C.6: Averaged burr entry heights for drill 3 (with std bars) 109

Figure D.1: Burr exit widths for drill 1 110

Figure D.2: Burr exit widths for drill 2 110

Figure D.3: Burr exit widths for drill 3 111

Figure E.1: Average flank wear for drill 1 (for each side) 112

Figure E.2: Average flank wear for drill 1 (for each run averaged) 112

Figure E.3: Average flank wear for drill 1 (with std bars) 113

Figure E.4: Average flank wear for drill 2 (for each side) 113

Figure E.5: Average flank wear for drill 2 (for each run averaged) 114

Figure E.6: Average flank wear for drill 2 (with std bars) 114

Figure E.7: Average flank wear for drill 3 (for each side) 115

Figure E.8: Average flank wear for drill 3 (for each run averaged) 115

Figure E.9: Average flank wear for drill 3 (with std bars) 116

Figure F.1: Outer corner wear for drill 1 (for each side) 117

Figure F.2: Outer corner wear for drill 1 (for each run averaged) 117

Figure F.3: Outer corner wear for drill 1 (with std bars) 118

Figure F.4: Outer corner wear for drill 2 (for each side) 118

Figure F.5: Outer corner wear for drill 2 (for each run averaged) 119

Figure F.6: Outer corner wear for drill 2 (with std bars) 119

Figure F.7: Outer corner wear for drill 3 (for each side) 120

Figure F.8: Outer corner wear for drill 3 (for each run averaged) 120

Figure F.9: Outer corner wear for drill 3 (with std bars) 121

LIST OF SYMBOLS

Chapter IV

k	compressible material stiffness constant
pl	height of drill point
d_0	initial distance between end of drill and end of clamping fixture
t	thickness of one layer of material

Chapter V

t_0	burr initiation height of Kim model
y_1	burr initiation height of Sofronas model
$\vec{F}$	total drilling force vector
τ_ω	material shear strength
$\left\|\vec{A}\right\|$	magnitude of area needed to be sheared
$\overrightarrow{V_{drill}}$	drill velocity vector
$\left\|\Delta\overrightarrow{v_{slab}}\right\|$	relative velocity of the sheared slab material
$\vec{V}_1$ and $\vec{V}_2$	vectors used to determine total sheared area
$\vec{V}_1$* and $\vec{V}_2$ *	vectors used to determine total sheared area
x_1* and z_1	parameters defining total sheared area
β	drill point angle
d	height of cut for each drill cutting lip
δ, γ, and ε	dimensionless parameters used to find initiation height
f	drill feed per revolution
F_{xy} and F_z	components of drilling cutting force
λ	drill friction angle

υ	drill normal rake angle
H	drill helix angle
q	ratio of drill's web thickness to diameter
R_0	drill radius
R_i	inner radius of burr initiation material
r	incremental radius
h	incremental burr height
t	incremental burr thickness
ε_θ	circumferential strain
ε_r	radial strain
ε_t	thickness strain
H	final burr height
T	final burr thickness

SUMMARY

During the drilling process, sharp edges of material called burrs are produced and protrude from the original surface. When a through-hole is drilled, burrs form on both the entry and exit surfaces around the hole, requiring expensive deburring operations to be performed in order to meet part specifications. A common hole producing operation in aircraft assembly is drilling holes through multiple sheet metal layers in order to fasten them together. However, at the interface between two layers, burrs form on both the exit of the first layer (termed “skin”) and entry of the second layer (termed “frame”). Consequently, the layers frequently need to be taken apart, deburred, and put back together again before being fastened, resulting in additional costs and increased assembly time.

The goal of this thesis was to understand the role of key factors such as drill geometry, drill wear and clamping conditions on burr formation at the interface of two thin sheets of 2024-T3 aluminum so that interlayer burr formation could be minimized. This problem was approached from three different angles. First, an experimental study was performed to find the drill geometry parameters for minimization of interlayer burrs and to ascertain the relationship between the average burr size and drill wear. Next, a new kind of clamping system for holding sheet metal layers together during drilling was designed, prototyped, and tested for its effectiveness. Finally, a preliminary analytical model of interlayer burr formation was created in order to better understand the burr

formation process in stacked layers of sheet metal and to better understand the effect that each drilling parameter has on the resulting burr size.

Results showed that interlayer burr heights tend to be somewhat reduced with lower point angle drills and significantly reduced with the use of step drills. It was also found that drill wear does not have a significant effect on burr sizes when drilling through 2024-T3 aluminum stacks. The prototyped clamping system, which works by pushing the layers together from one side, was found to reduce burr size and can be easily used in addition to existing clamping methods. The analytical model for interlayer burr formation was calibrated and compared with experimental results and was found to correctly predict the trend in burr height with increase in feed rate. Finally, the thesis provides recommendations for further research including improvements to the analytical model for interlayer burr formation.

CHAPTER I

INTRODUCTION

1.1 Background and Motivation

Drilling is a machining process used to create or enlarge holes into or through a workpiece material. The process is performed with the use of a drill, which works by rotating at a fast speed while simultaneously being fed into the workpiece, removing incremental amounts of workpiece material. The drill itself, which performs the cutting action, has multiple cutting edges and flutes running along its length that allow the chips of workpiece material to be carried away.

During the drilling process, burrs form on both the entry and exit surfaces as a result of plastic deformation of the workpiece material. Burrs are simply small amounts of attached material that protrude from the original entry and exit surfaces around the drilled hole. An illustration of the drilling process as well as both entry and exit burr formation is shown in Figure 1.1. They are generally unwanted, and commonly need to be removed depending on the specific desired part geometry. If they are not removed, they can cause misalignment with adjacent parts. Because of strain-hardening effects, burrs are typically harder than the original material [1], meaning that contact between two adjacent parts with the burr in between can cause cracks to form and can reduce the overall fatigue life of the assembly. The burrs can also get detached from the surface and

get trapped between mating surfaces leading to three-body abrasion and eventual failure of the assembly, among numerous other potential problems.

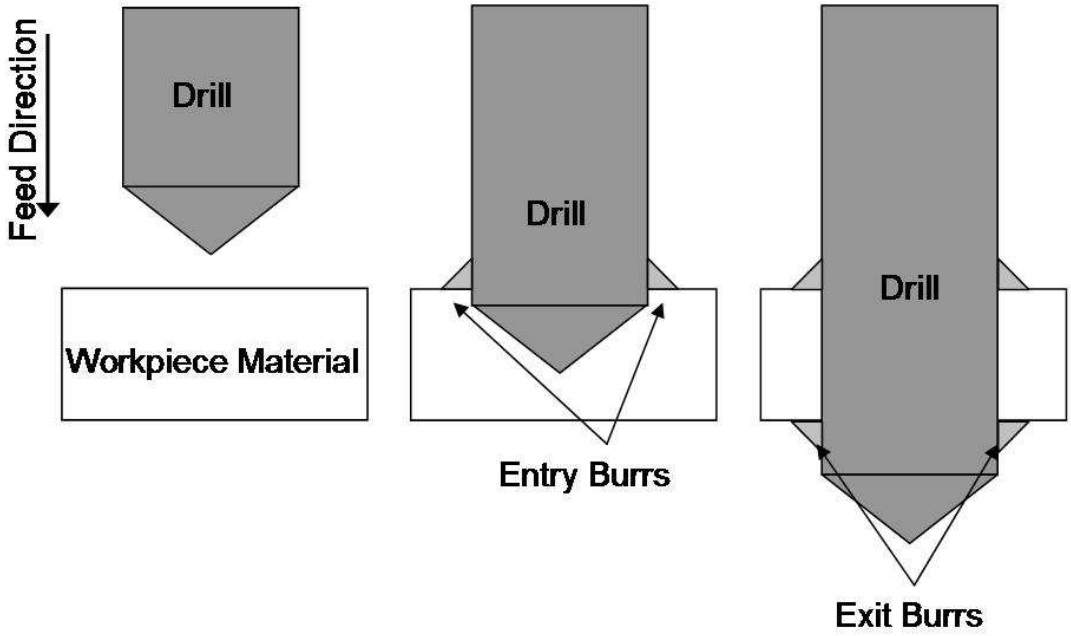

Figure 1.1: Entry and exit burr formation

One common application of drilling is in the creation of through-holes in stacks of sheet metal layers, frequently performed in the aerospace industry so that the layers can be fastened together with rivets. However, because burrs form at the entry and exit of workpiece materials, burrs will exist at the exit of the top layer and the entry of the bottom layer, leaving hardened, protruding material at the interface of the sheet metal layers called interlayer burrs. An illustration of stacked sheet metal drilling and interlayer drilling burr formation is shown in Figure 1.2. Because of the aforementioned problems associated with burrs, the drilled layers then need to be destacked so that the

burr material can be removed through a deburring operation before the layers are stacked together once more and fastened.

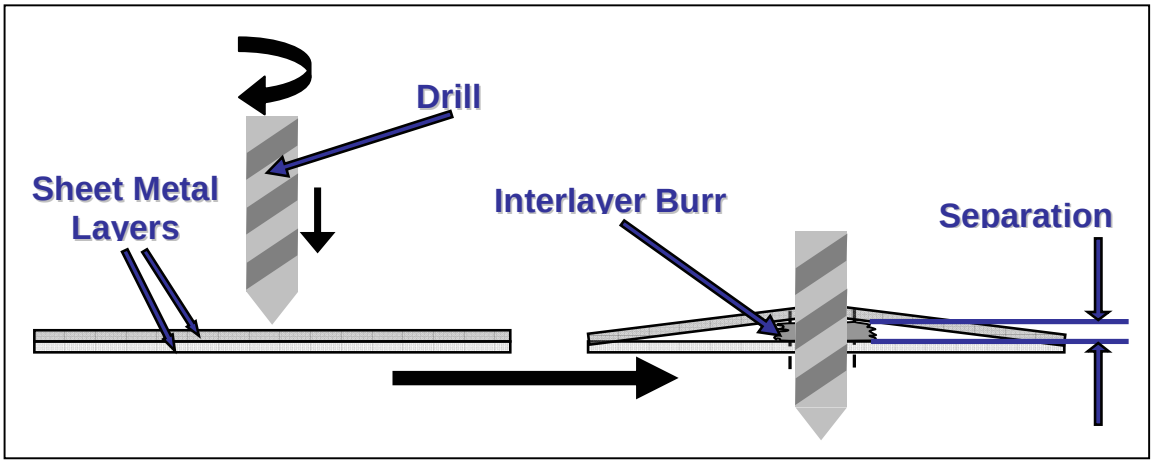

Figure 1.2: Interlayer burr formation [2]

Products such as large aircraft can require up to millions of through holes to be made, most of which require deburring operations in order to meet safety requirements. Thus, the formation of interlayer burrs and the resulting destacking and deburring operations that need to be performed can be very costly and time-consuming.

Although much work has been done to reduce burr formation in general, little has been studied regarding interlayer burr formation in between sheet metal layers. Specifically, more needs to be known regarding the relationship between burr formation and drill wear, the ideal clamping conditions to reduce interlayer burr sizes, and the interlayer burr formation process in general.

1.2 Problem Statement

As stated in the previous section, interlayer burr formation is costly in the aircraft industry due to the necessary destacking of the layers and subsequent deburring operations. Although it may not be possible to eliminate burr formation completely, any reduction in interlayer burr sizes could reduce deburring costs and possibly eliminate the need for some deburring operations depending on the safety specifications of the assembly being produced. With this ultimate goal in mind, this thesis addresses the following questions:

- What specific drill geometry will minimize interlayer burr sizes not just initially, but throughout its useful life?
- Do interlayer burr sizes increase significantly with drill wear, and is there a point at which burr sizes increase dramatically?
- What are the ideal sheet metal clamping conditions for minimizing burrs and how can they be implemented?
- How could interlayer burr formation be modeled mathematically so as to gain a greater understanding of the effects of different drilling parameters?

1.3 Research Goals

The research work detailed in this thesis will attempt to answer the questions posed in the previous section, with the ultimate goal of significantly reducing interlayer burr sizes in drilling of holes in stacked sheet metal layers. To do this, the following goals were established:

- To conduct experiments to determine the relationship between drill wear and interlayer burr sizes, and to find a burr-minimizing drill geometry.
- To conceptualize, design, prototype, and test multiple sheet metal clamping concepts for interlayer burr minimization.
- To create a mathematical model of interlayer burr formation as a function of various drilling parameters and conditions in order to identify ideal drilling conditions.

1.4 Thesis Outline

Chapter II details more information about drilling and burr formation as well as gives an overview of previous research pertinent to the research goals listed above. The experimental work studying interlayer burr formation with respect to different drill geometries and wear conditions is described in Chapter III. Chapter IV describes work done to create and implement an ideal clamping method for sheet metal layers in drilling. Chapter V presents a mathematical model of interlayer burr formation, and Chapter VI summarizes the key conclusions of this thesis and provides recommendations for future work on this topic.

CHAPTER II

LITERATURE REVIEW

2.1 Motivation

The following literature review was conducted in order to obtain the necessary background knowledge for the topics studied in this thesis. Additionally, it was desired to find which topics had been studied extensively and which topics were relatively untouched and needed further examination. Based on the research goals listed in the previous chapter, the topics studied in the literature review include drilling in general, burr formation in general, experimental and analytical models related to burrs, and interlayer burr formation.

2.2 Introduction to Drilling

2.2.1 Factors Affecting Drilling

Although the drilling process might seem simple due to the fact that it only requires the tool to be fed in one direction and only results in circular holes, the amount of complexity in analyzing the process can be large. Galloway [3] categorized five criteria for measuring drill performance including speed, drill life, efficiency of metal removal, hole accuracy, and hole surface finish, and listed over 60 factors that can affect those criteria divided into the properties of the drill, workpiece, machine, and drilling conditions.

2.2.2 Standard Drill Geometries

Figure 2.1 shows many of the different drill geometry parameters that are typically varied in commercially available twist drills [4]. The two factors varied for the experimental investigations later in Chapter III are the point angle and presence or absence of a step as they were found to be two of the most influential factors on resulting burr sizes.

2.2.3 Drill Materials

Standard drills are typically made of either steels such as high carbon steel or high speed steel or carbides such as tungsten carbide. Coatings are also frequently applied to the outside surface of drills in order to increase their resistance to wear and improve the quality of the holes produced. Typical coating materials are black oxide, which is a layer of Fe_3O_4 formed on the surface of a tool through a reaction with the iron content of the tool, and titanium nitride. For the experimental investigations in this thesis, high speed steel drills with black oxide coating were used.

2.2.4 Other Drill Geometries

Apart from the standard twist drill geometry parameters discussed above, there are other drill geometry options that can be created. Figure 2.1 compares some of the drill geometry options discussed previously such as helix angle, point angle, and coating as well as the options for having a split point or a step drill [2]. As seen in the figure, a split point drill has a rake face with two different inclination angles. Another type of drill geometry is the multifacet drill, which has been shown to create improved surface finishes compared to standard twist drills [42].

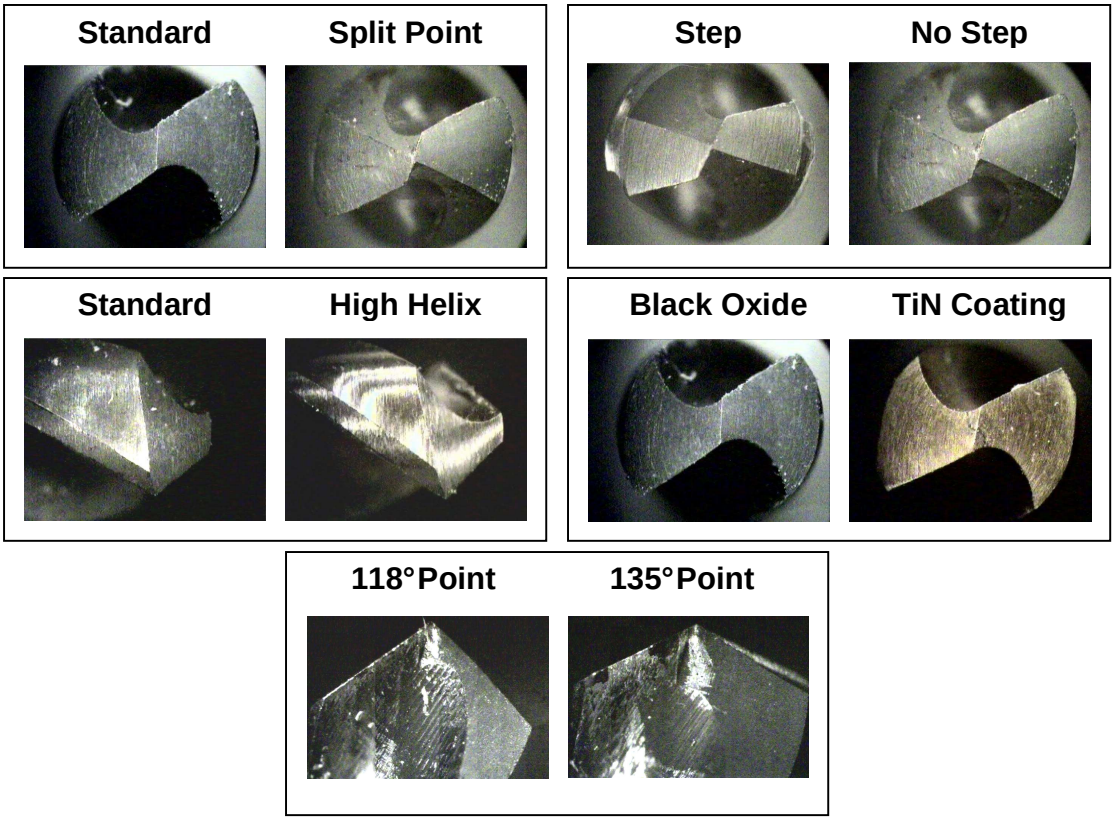

Figure 2.1: Standard drill geometry parameters [2]

A step drill, as shown in Figure 2.2, is a regular drill with a small portion of the diameter reduced at the tip of the drill. Therefore, when a step drill is used, a smaller diameter hole is created before the final diameter is cut out. Thus, a step drill can be thought of as a tool that drills its own pilot hole. Because of this, after a burr is formed as a result of the first diameter, the second diameter removes some of the first burr and forms another smaller burr [5]. Experimental investigations have shown that step drills tend to form smaller burrs than conventional drill geometries [5, 6]. The parameters of a step drill that can be varied include the ratio of D_2 to D_1, L, and θ_2. One study varied the

ratio of D_2 to D_1 and found that it should not be less than 0.6 in order to maintain good cutting conditions [7].

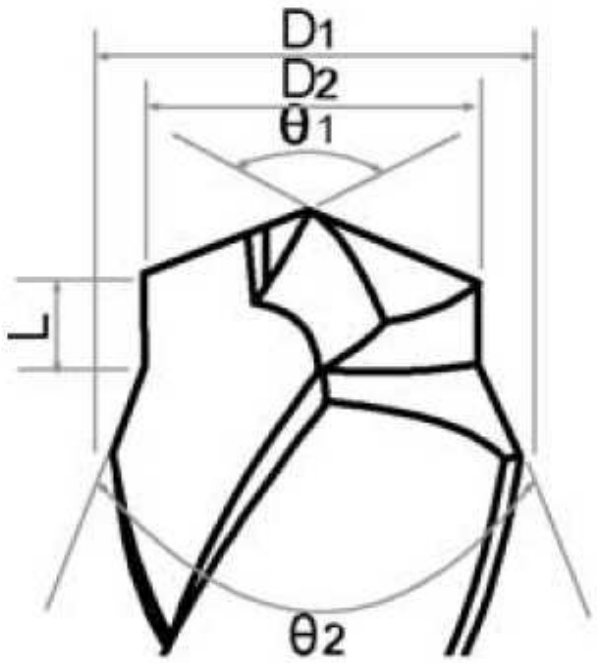

Figure 2.2: Step drill parameters [5]

2.2.5 Drilling Forces

The two forces typically measured in drilling experiments are the drilling thrust force and torque, which can be measured using a dynamometer. Some attempts have been made to model the drilling forces as a function of the various parameters. An analytical model was created to find the forces resulting just from the chisel edge of the drill [8]. Another model by Williams [35] modeled both the thrust force and torque for both the chisel edge and the main cutting edges. One experimental investigation found that a lower point

angle results in a lower thrust but a higher torque [3], and another found empirical equations for the thrust and torque of step drills [7].

2.2.6 Drill Wear

Drills, like all cutting tools, wear down as a result of their use. Wear can be in the form of material removed from the drill itself or from workpiece material adhering to the tool. Tool wear can negatively affect a part's accuracy and surface finish and can lead to higher cutting forces and temperatures. The rate of drill wear is affected by the drilling parameters, the workpiece material properties, and the drill geometry, material, and coating type. An experimental study found that a drill's point angle has the largest effect on drill life among the geometry parameters in the cutting of steel with a feed of 0.01 in/rev [3]. One investigation identified six types of wear affecting drills [9]. Figure 2.3 shows the two types of drill wear measured in the experiments in Chapter 3. The flank wear, shown on the right, can be measured as an average value of the wear running the length of the cutting lip. The outer corner wear, shown on the left, is simply a single measure of the amount of flank wear at the very end of the cutting lip.

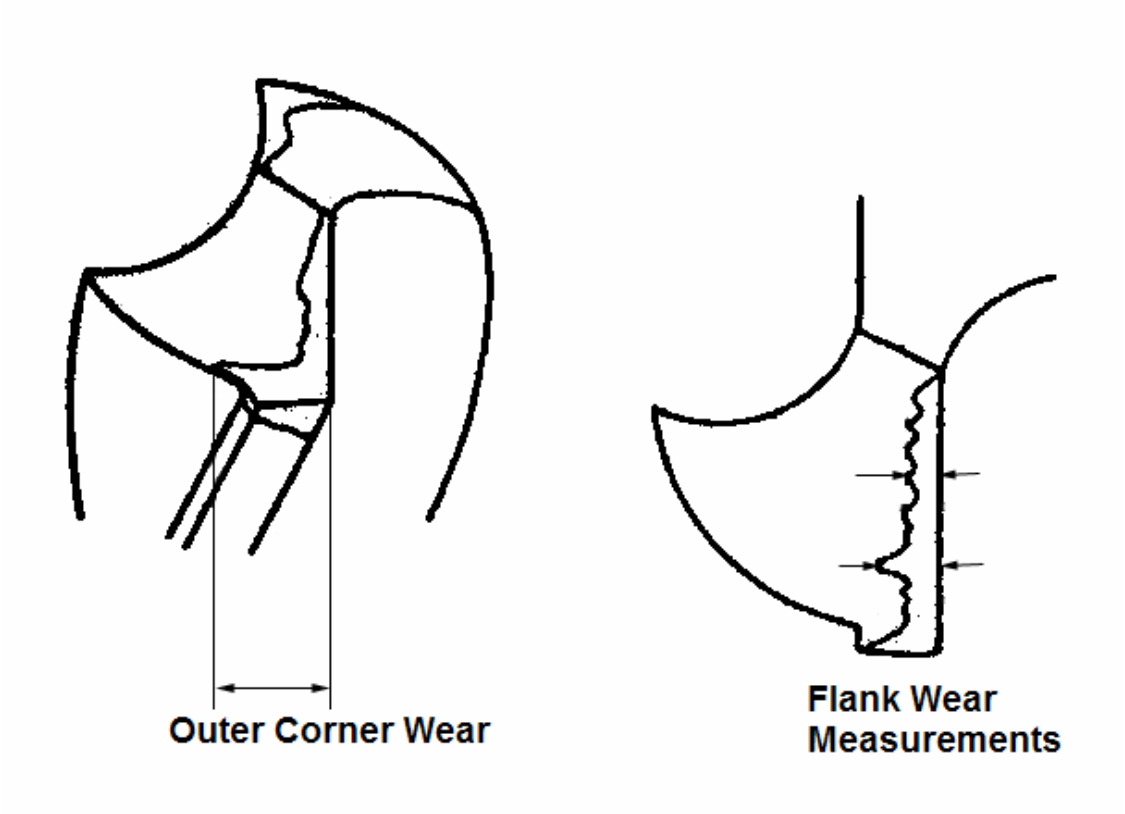

Figure 2.3: Drill wear measurements [9]

2.3 Introduction to Burrs

2.3.1 Types of Burrs

Depending on the specific machining operation being performed and all of the variable parameters discussed previously, different types of burrs can form. The following four different burr formation types have been identified in the literature as: a Poisson burr caused by material bulging under compression, rollover and tear burrs formed by a chip being pushed or torn away respectively instead of sheared, and a cut-off burr caused by raw material separating before a separation cut is finished [10]. Three different kinds of drilling burrs, all of which are rollover burrs, have been identified. They include the

following: a uniform burr, which is small and even around the hole; a crown burr, which is tall and jagged, and a rolled-back burr, which is long burr material that has rolled under itself [11]. In Figure 2.4, “Type A” is a small uniform drilling burr, “Type B” is a large uniform burr, and “Type C” is a crown burr. Figure 2.5 shows a typical drilling burr in aluminum, similar to the ones observed in the current study and shown in Chapter 3. As can be seen, the burr most closely resembles a uniform burr, despite the fact that the burr thickness is somewhat variable around the diameter of the hole. This variability reflects the fact that burr formation is very random, and will generally form in a slightly different way for every hole.

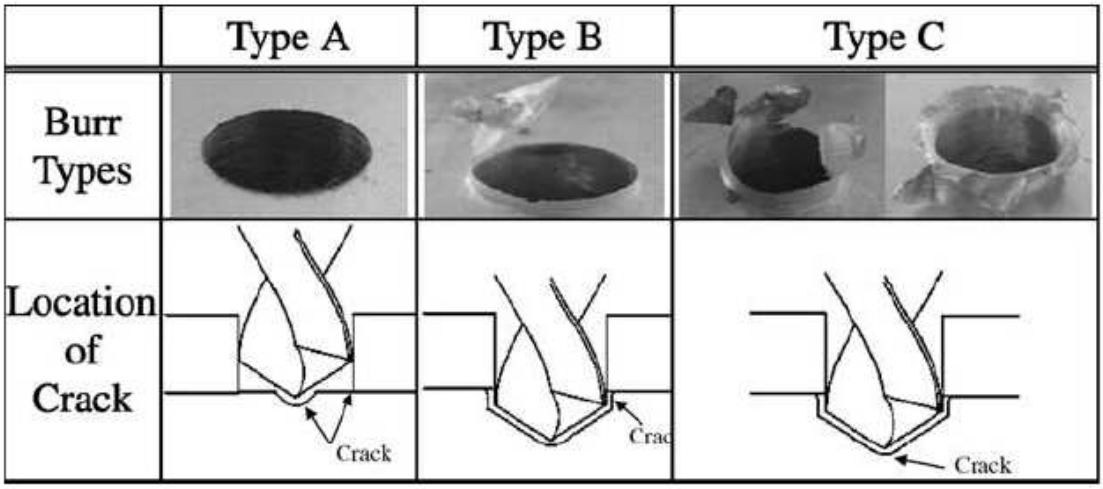

Figure 2.4: Types of drilling burrs [5]

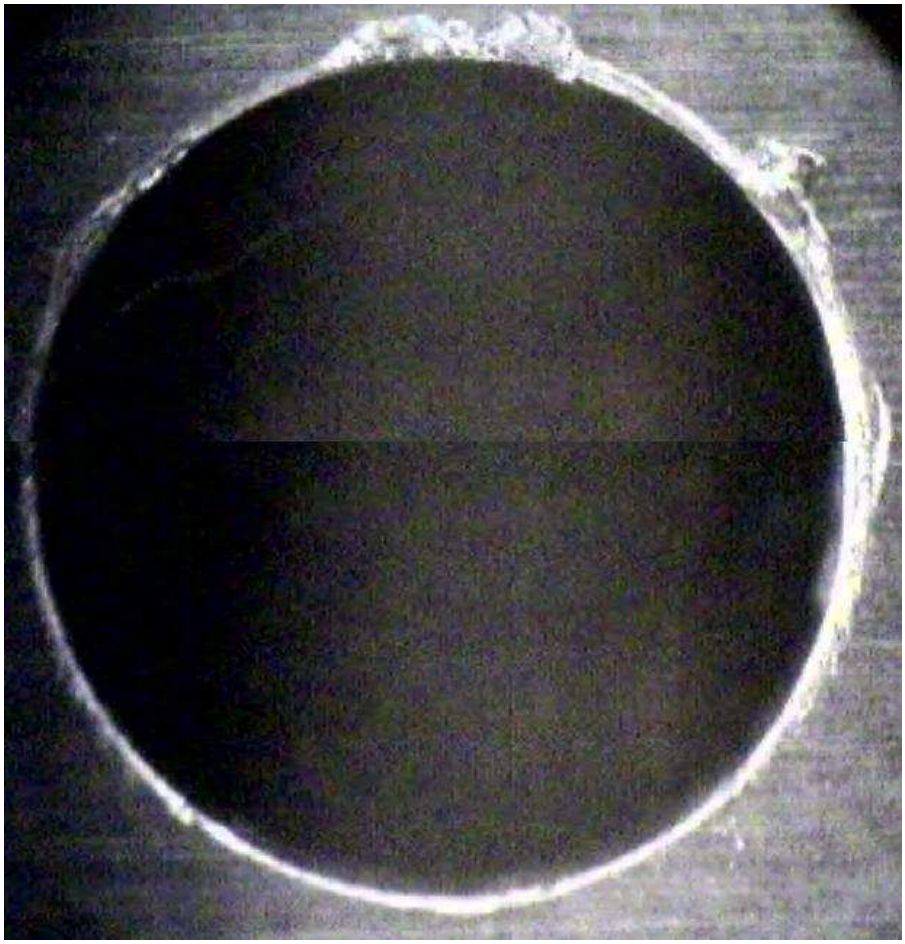

Figure 2.5: Aluminum drilling exit burr [2]

2.3.2 Burr Formation Mechanism

Machining burrs typically form as a result of material being plastically deformed rather than cut towards the entrance or exit of a machined feature. One investigation defined three different stages in burr formation for orthogonal cutting as initiation, at which point plastic deformation begins; development, during which material deformation increases while the amount of material being cut decreases; and formation [12], when only plastic deformation occurs and the burr is formed into its final shape. Another more detailed explanation listed eight different stages, with differences being made between ductile and

brittle materials [13]. Such modeling of burr formation can be used to gain a greater understanding of how they can be reduced. For example, a study by Aurich [1] stated that cooling the workpiece, such as with the use of coolant fluids, helps to reduce burr heights by lowering the material's rate of plastic deformation.

2.3.3 Burr Measurements

There are many different burr characteristics that can be measured, and many different methods for measuring them. Burr geometry characteristics include the burr height and thickness and whether or not the burr is rolled over on itself. An illustration of a burr's height and width is shown in Figure 2.6. Although the burr height is the most commonly measured characteristic, it has been stated that a burr's thickness contributes more to deburring costs than a burr's height [14]. Claus listed several different ways in which burrs can be measured, including contact methods, such as the use of micrometers or profilometers, and optical methods, such as measuring the length of a burr's shadow from a light with a known angle or finding the difference in microscope table displacements [15]. Franke, et. al. classified all of the burr measurement methods and performed an evaluation to directly compare six of the different techniques [41]. Multiple studies have suggested that optical burr measurement methods are superior to contact methods due to the small sizes of burrs making contact methods inaccurate [16, 17]. Recently, more advanced optical techniques have been employed which are capable of obtaining an accurate 3D image of the entire burr such as interferometry or conoscopic holography [40]. Regardless of the type of measurement used, multiple studies have reported that

burrs are so variable that they require a large number of measurements to be statistically accurate [14, 16].

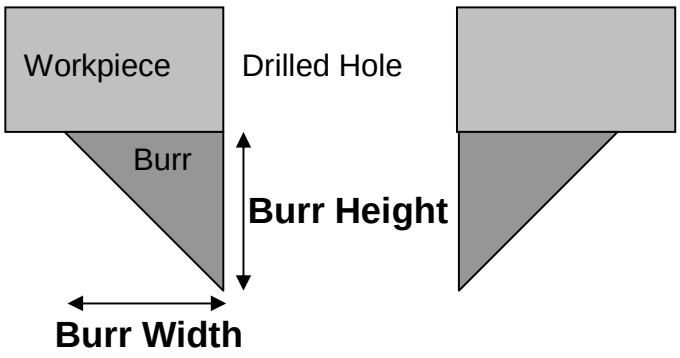

Figure 2.6: Burr height and width

2.3.4 Burr Problems

As mentioned in Chapter 1, some of the main problems associated with burrs are that they cause misalignment between adjacent parts and can reduce the fatigue properties of assembled systems. Other problems include the introduction of stress risers in critical areas [11], operator danger of getting cut by sharp burrs, and poor part aesthetics [15]. Additional problems are caused when burrs break off and move between assembled parts. For example, because burrs are typically harder than their parent material due to strain hardening effects [1], the relative motion of the burr trapped between mating surfaces can cause cracks to form. Broken-off burrs can also cause interference with other product operations, such as shorting out electronic equipment [15].

For industrial situations, however, the main negative effect felt by burrs is the cost of deburring operations. Although deburring costs vary depending on the specific application and deburring method used, one study found equations to calculate the

removal costs [18]. It has also been reported that deburring costs associated with removing interlayer burrs from aircraft structures can account for up to 30% of total manufacturing costs [19]. The danger from not removing interlayer burrs from aircraft is that serious structural safety problems can occur [20].

2.4 Burr Investigations

Because of the aforementioned problems with burrs, much prior work has gone into reducing the size of drilling burrs. This work has taken the form of experimental investigations to find which drilling geometries, parameters, and material properties minimize burr sizes, as well as finite element modeling and analytical modeling. However, a vast majority of these investigations focus on drilling burrs formed in a single layer of material.

2.4.1 Experimental Investigations – Drilling Parameters

Many investigations have studied the effects of drilling spindle speeds and feed rates on the resulting burr sizes. The feed per revolution is the most commonly experimentally varied parameter. Many studies have all shown that lower feed rates tend to reduce burr heights and/or thicknesses [21, 22, 13, 23, 2], possibly because of lower resulting thrust forces which reduce the amount of bending of burr material. Fewer experiments have been performed and fewer conclusive results have been made regarding changes in spindle speed, but one study found that higher spindle speeds tend to reduce burr thicknesses [24].

2.4.2 Experimental Investigations – Drilling Geometries

The two most commonly varied drilling geometry parameters in burr studies are the helix angle and point angle. Multiple studies have shown that higher helix angles tend to reduce burr heights [21, 22, 2]. It has also been commonly observed that lower (steeper) point angles tend to minimize burrs [21, 2].

2.4.3 Experimental Investigations – Wear and Workpiece Material

Very few investigations have been made regarding the relationship between drill wear and burr sizes. One study found that drill wear does significantly increase the sizes of burrs for miniature holes [25]. Another limited series of tests also found that burrs increased with drill wear but the study only considered up to fifty holes [26].

Regarding the workpiece material properties, it is commonly known that higher material ductility values result in larger burrs due to the smaller forces required for plastic deformation. Another study also found that higher workpiece hardness values result in lower burr thicknesses [24].

2.4.4 Empirical Burr Modeling

Most models used to predict burr sizes are empirical models. In empirical models, results from experiments are used to create a mathematical equation which outputs burr sizes as a function of the different parameters varied. Multiple empirical models have been obtained to predict the sizes of drilling burrs, varying parameters such as the helix angle,

point angle, feed rate, and workpiece hardness [21, 27, 18, 28]. However, these models are created with a finite number of experiments using discrete parameter values and specific materials. Thus, they are not always capable of accurately predicting burr sizes for any given set of drilling parameters and any given material.

2.4.5 Finite Element Modeling of Burrs

Many finite element models have been developed to predict drilling burr formation. One model employed a 2D analysis based on temperature and stress distributions and verified the model using experimental data [29]. Other models have employed a 3D analysis of burr formation [30, 31]. An example of a finite element model of drilling burr formation is shown in Figure 2.7. Vijayarghavan [19] discussed how interlayer burr formation could be modeled and gave details regarding the necessary use of thermal and mechanical contact elements, failure, and crack propagation. Although no complete finite element model has been created for interlayer sheet metal burr formation like this thesis focuses on, finite element models have been used to study the effect of having a thick backup material against the machining exit surface [30, 31, 32]. It has been found that the use of a backup material, or more specifically a backup material level with the predefined machined surface, is the best way to minimize burr formation, due to the fact that it does not allow any room for a burr to form and provides a force that opposes the plastic deformation of burr material.

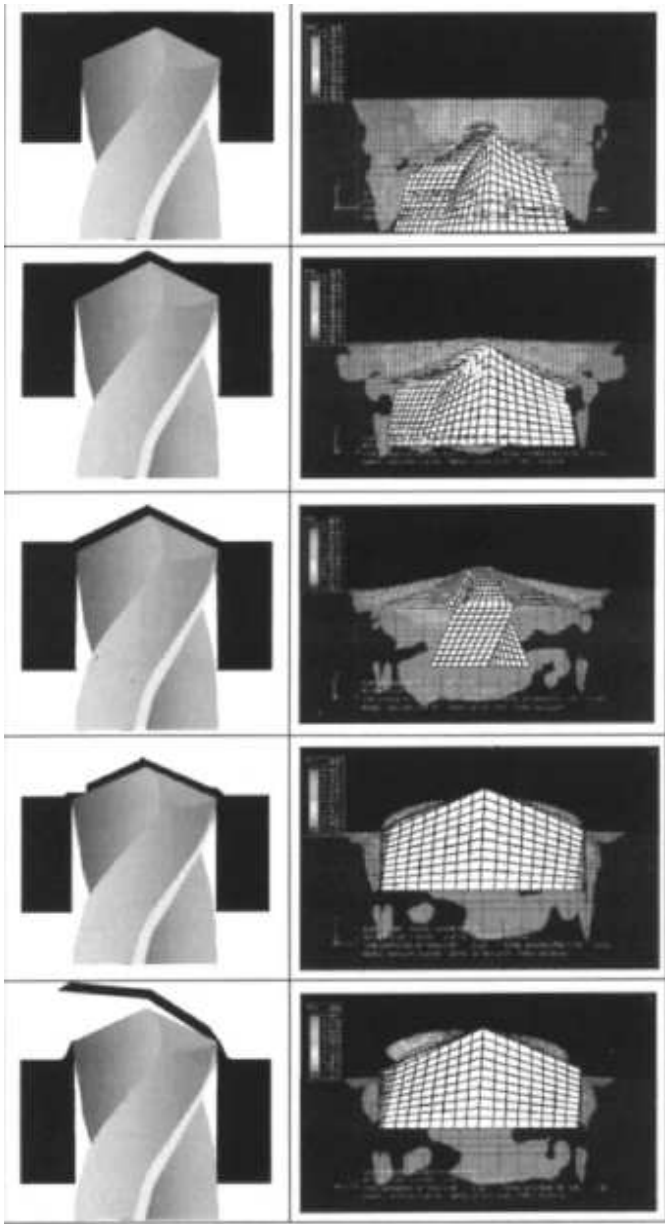

Figure 2.7: Finite element model of drilling burr formation [31]

2.4.6 Analytical Burr Modeling

Analytical burr models attempt to use mathematical equations to find quantitative values of burr geometry parameters. Many of these models have been created for orthogonal

cutting, and then experimentally verified by testing parameters such as the rake angle and chip thickness [33] or the spindle speed [12].

Some models have also been created specifically for drilling burrs, but exclusively in single layered materials. Sofronas [34] created a model for finding exit burr heights and thicknesses as a function of the drilling geometries and parameters. The model works through an energy rate balance equation which finds the point at which the downward cutting force of the drill is equivalent to the force required to plastically deform the remaining material underneath the drill into a burr. The model then assumes that this remaining material under the drill no longer gets cut and completely plastically deforms into the final burr shape. In Figure 2.8, the remaining material under the drill at the burr initiation point is indicated in dotted lines, while the final resulting burr shape is in solid lines. The derivation of this model uses another model by Williams [35], which gives the drilling cutting forces as a function of drill geometry. The analytical model for interlayer burrs created in Chapter 5 of this thesis builds off this model by Sofronas.

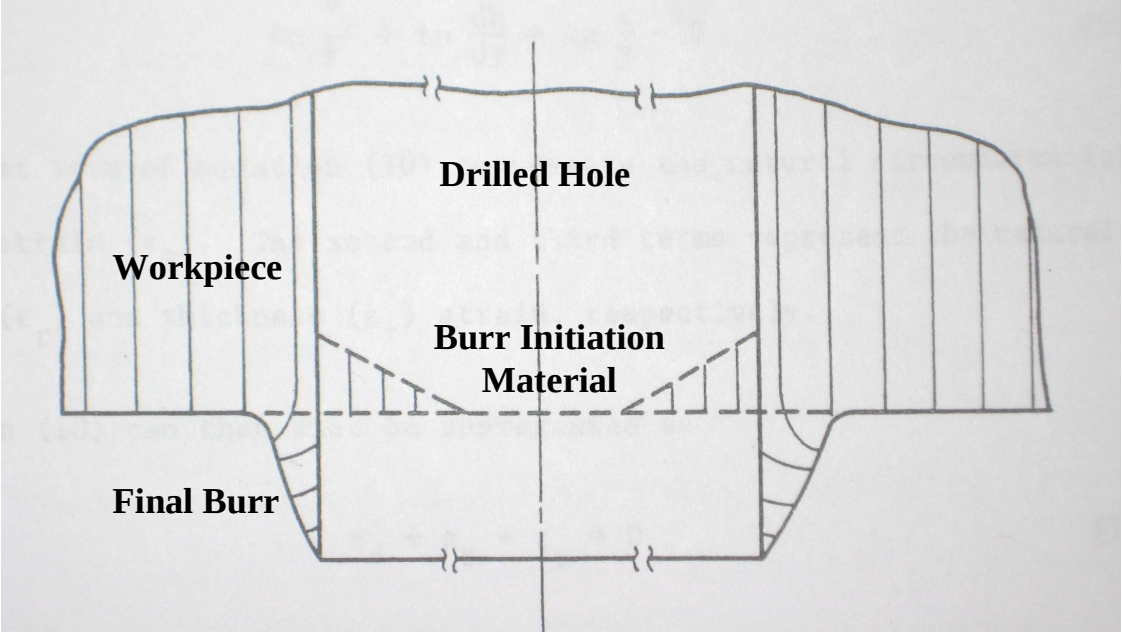

Figure 2.8: Sofronas model of drilling exit burr formation [34]

Another analytical drilling burr model was developed by Kim [36]. This model is similar to the Sofronas model in that it uses an energy balance equation to predict the burr initiation point. However, it implies that burr initiation takes place before the drill tip has exited the workpiece rather than after and that the final burr shape is formed by a crown burr being stretched rather than material being plastically deformed around a hinge. Consequently, this model is only applicable in the case of ductile workpiece materials that are capable of forming crown burrs. Figure 2.9 shows the assumed stages of this burr formation model.

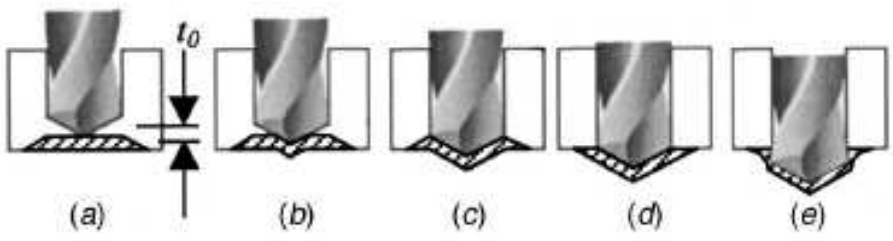

Figure 2.9: Kim model of drilling exit burr formation [36]

2.5 Interlayer Burrs

In industrial situations, such as in aerospace and automotive production, stacks of sheet metal layers are typically drilled through so that they can be fastened together with rivets. As explained previously, because of the interlayer burrs that form between the layers and the problems associated with them, the stacks frequently need to be disassembled and deburred before being reassembled and riveted, resulting in a loss of time and money. Among all machining operations performed on stackups, drilling is by far the most prevalent [19]. An illustration of the interlayer burr formation process is shown in Figure 1.2.

One of the advantages of using stackups is that they are capable of providing better strength-to-weight ratios than single layers [19, 37]. Stackups can also be made of different materials, such that each layer provides a different functionality [19].

2.5.1 Interlayer Burr Formation

One investigation identified six different kinds of interlayer burrs that can form depending on whether or not there is a thick layer of sealant between the layers and

whether the burr forms straight downwards, rolls away from the hole, or rolls into the hole [37]. An illustration of these burrs is shown in Figure 2.10. If layers have different bending properties, then gaps could more easily form while the layers are being bent by the drill, allowing more room for burrs to form [39].

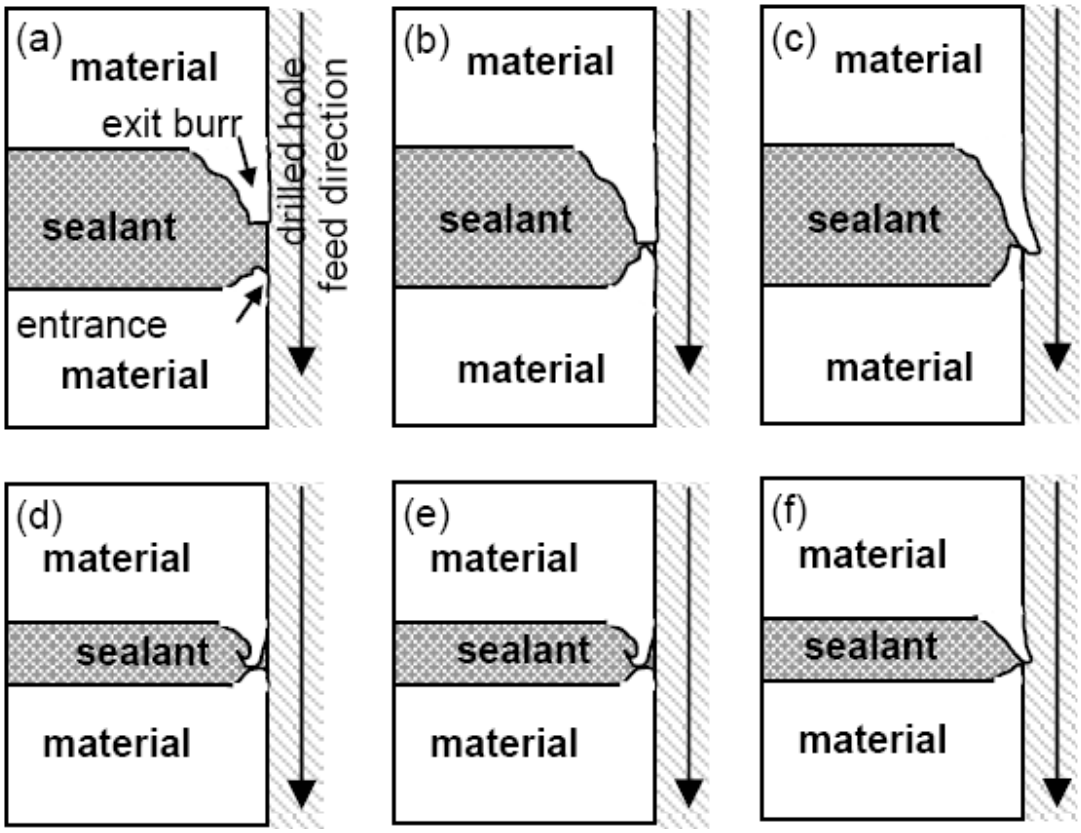

Figure 2.10: Interlayer burr types [37]

2.5.2 Interlayer Burr Prevention

The primary way in which interlayer burrs can be prevented is through the use of clamping systems to hold the sheet metal layers together during drilling. This is due to

the fact that when the layers are held together tightly around the area of the hole being drilled, there is no room for burr formation to occur.

In the aerospace industry, two commonly used sheet metal clamping methods are the hand clamp and the cleco clamp. The hand clamp is a simple squeeze action clamp that locks the layers together from both sides and is illustrated in Figure 2.11. The cleco clamp is a spring-loaded hole clamp that gets pushed into an existing hole and expands to lock the two layers together. Cleco clamps are shown in Figure 2.12. Both types of clamps are discussed further in section 4.2.3.

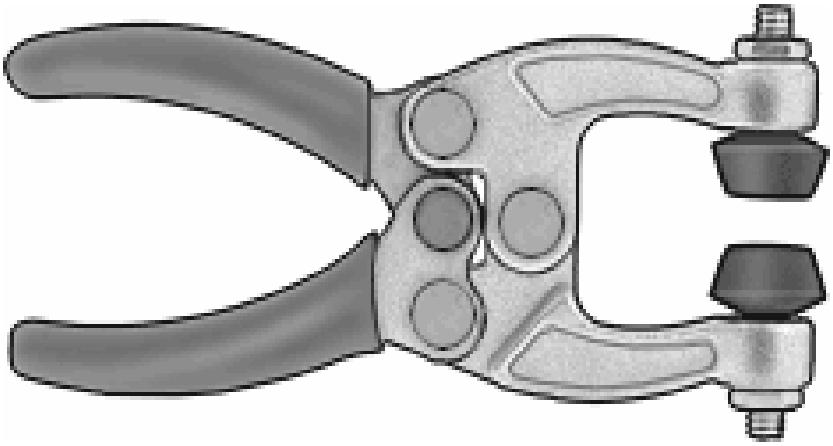

Figure 2.11: Hand clamp

Figure 2.12: Cleco clamps

2.5.3 Multilayered Modeling Problems

A problem with studying drilling of multiple layers is that it is a fundamentally different problem than drilling through a single layer of material, such that single layer results cannot be easily applied [19]. One study identified new factors that need to be taken into account such as clamping position and strength, burr accumulation, and stacking order if different materials are used [38]. Some properties that would need to be taken into account for finite element modeling include having a break from steady state conditions while the drill is between layers, having geometric constraints on burr formation, and having temperature property differences between the different layers [19]. It has also

been stated that tool wear accelerates interlayer burr formation and needs to be modeled [38].

2.5.4 Interlayer FEM Investigations

It has been stated that the amount of gap formation between layers is the single most important factor affecting burr formation as a gap is needed for a burr to be able to geometrically form [30]. A finite element model of interlayer burr formation was created by Choi [39], which modeled the gap formation between the layers. It was found that the material directly below the drill tip would experience a large plastic deformation immediately prior to the drill exiting the layer. The clamping location relative to the hole was found to only have a major effect of the elastic bending of the material. Consequently, higher thrust force values were found to have the largest correlation with levels of plastic deformation, gap formation, and burr sizes. It was also found that both layers would vibrate during the process and that these vibrations would contact the burrs and affect their final size and shape [20].

2.6 Summary

Many studies have been conducted related to drilling and burr formation in general, and research has been performed on the shapes and sizes and burrs formed specifically by drilling. Experimental investigations have shown that drilling burr sizes tend to be reduced with lower feed rates, higher helix angles, lower point angles, and lower workpiece material ductility values. Models to predict drilling burr formation have also been created based on empirical data, finite element simulations, and analytical

equations. Regarding interlayer burr formation, only a few general studies and finite element simulations have been performed.

Apart from the topics listed above that have been studied, there are some areas of drilling, burr formation, and interlayer burr formation that are relatively unexplored. Very little work has been done to ascertain the correlation between drill wear and burr formation, which is needed for industry in order to understand how frequently drills need to be changed to avoid increasingly large burrs. Almost no experimental investigations on interlayer burr formation have been performed, and no analytical model of interlayer drilling burr formation has been reported. Therefore, this thesis addresses the aforementioned deficiencies in the literature through experimental studies and analytical modeling.

CHAPTER III

INTERLAYER DRILLING BURR EXPERIMENTS

3.1 Goal and Approach

This chapter will detail the work undertaken to find a suitable drill geometry capable of minimizing interlayer burr heights not just initially, but throughout its useful life during which the drill wears. First, experimental parameters had to be selected based on previous findings. Next, an experimental setup and a systematic experimental procedure were developed and executed. Many forms of measurements, including the drilling forces, drill wear, and burr sizes, were made during the tests and later analyzed. Through the experiments, the effects of various drill geometry parameters on interlayer burr sizes were identified, including the effect of drill wear.

3.2 Parameter Selection

According to the results from previous experimental investigations discussed in Chapter II, two of the most influential factors on burr formation for both single and stacked layers are the presence or absence of a step and the point angle of the drill tip [5, 2]. Step drills were chosen for study as opposed to other non-conventional geometries such as chamfer drills and round drills due to the results of a study indicating the superiority of step drills [6]. Because of the importance of these two factors, it was desired that the specific drill geometries to be studied be able to isolate the effects of

these two factors. Therefore, it was decided that a total of three different drill geometries would be studied. This would allow the effect of one of the factors to be isolated between the first and second drill geometry and the other factor to be isolated between the second and third. No more than three different drill geometries were used due to the extensive time required to run tests throughout the drill lifetimes and due to the fact that two replications were made for each geometry. The three drills chosen for study in these experiments are as listed in Table 3.1. Figure 3.1 shows a picture of the three drill geometries.

Table 3.1: Summary of drills studied (all #10 size or 4.91 mm dia.)

	Helix Angle	**Point Angle**	**Coating**	**Point Type**
Drill 1	30°	118°	Uncoated Tip	Split/Step
Drill 2	30°	118°	Black Oxide	Split/No Step
Drill 3	30°	135°	Black Oxide	Split/No Step

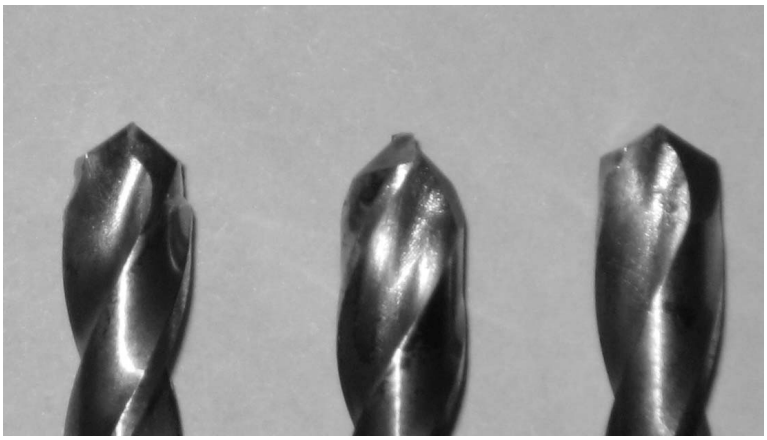

Figure 3.1: Drills 1, 2 and 3 from left to right.

The study by Newton, et. al. [2] on the effects of various drilling parameters on interlayer burr formation was given particular importance due to the fact that it was performed in the same laboratory and under very similar conditions as in this thesis. Drill 1 was selected since it has most of the optimal drill parameters identified in Newton, et. al.'s study, including the step, 118° point angle, a split point, and a black oxide coating. Note that Drill 1 had an uncoated portion on the tip since the coating was removed when the step was ground. Drill 2 was selected so that it would be similar to Drill 1 but without the step, in order to isolate the effect of the step as much as possible. Drill 3 was chosen to be identical to Drill 2 except for the point angle, which was 135°, thereby isolating the effect of the point angle. All of the drills were #10 in size (4.91 mm or 0.1935" diameter) and made of high speed steel. The specific geometry of the step is shown in Figure 3.2. Therefore, to summarize the drill selection process, Drill 1 was chosen to have as many optimal parameters as possible identified in the previous study; Drill 2 was chosen to isolate the effect of having a step, and Drill 3 was chosen to isolate the effect of point angle.

The drilling process parameters and conditions used in the experiments are indicated in Table 3.2. The relatively low feed rate of 0.004 in/rev (0.1016 mm/rev) was chosen because of the clear indication from previous studies [21, 2] that lower feed rates produce smaller burrs. Hand clamps were chosen as opposed to other forms of clamping due to their ease of use and their frequency of use in industry. A more detailed description of typical clamping methods for stacked sheets is given in Section 4.2.3. The

workpiece material consisted of two sheets of 1/16” (1.59 mm) thick Aluminum 2024-T3, fixed together at a clamping distance of 25 mm on either side of the hole.

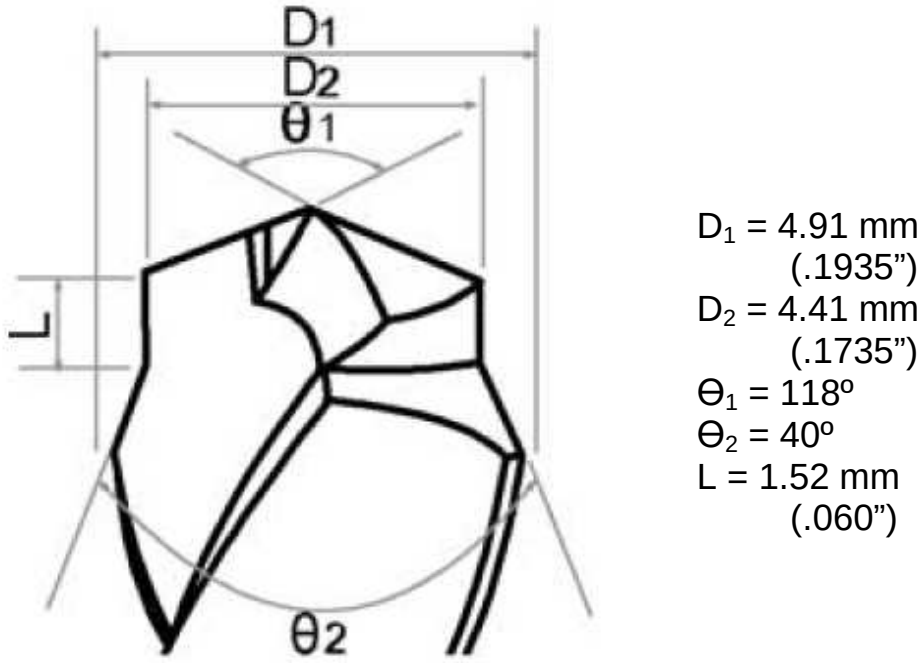

Figure 3.2: Step drill parameters used [5]

Table 3.2: Drilling conditions utilized in Phase II.

Feed Rate	0.004 in/rev (0.1016 mm/rev)
Speed	4500 rpm
Clamp Type	Hand clamps
Clamp Distance	25 mm on either side of hole
Workpiece	Aluminum 2024-T3

3.3 Experimental Procedure

During the experiments, holes were drilled in a Fadal VMC 15 vertical machining center seen in Figure 3.3. A Kistler 9272 drilling force dynamometer, capable of measuring both drilling thrust and torque, was clamped into the machine, and an aluminum fixture was bolted to the dynamometer. The purpose of the fixture was to provide a link between the dynamometer and the samples being drilled. An angular piece of 2024-T3 aluminum frame material with a thickness of 1/16" (1.59 mm) was then screwed to the side of the fixture, and a piece of flat 2024-T3 aluminum skin material, also 1/16" (1.59 mm) thick, was clamped on top of the frame material using two hand clamps as shown in Figure 3.4. The clamps used were De-Sta-Co model 424 squeeze action clamps, which are rated at 890 N and seen in Figure 3.5.

Figure 3.3: Fadal VMC 15 vertical machining center

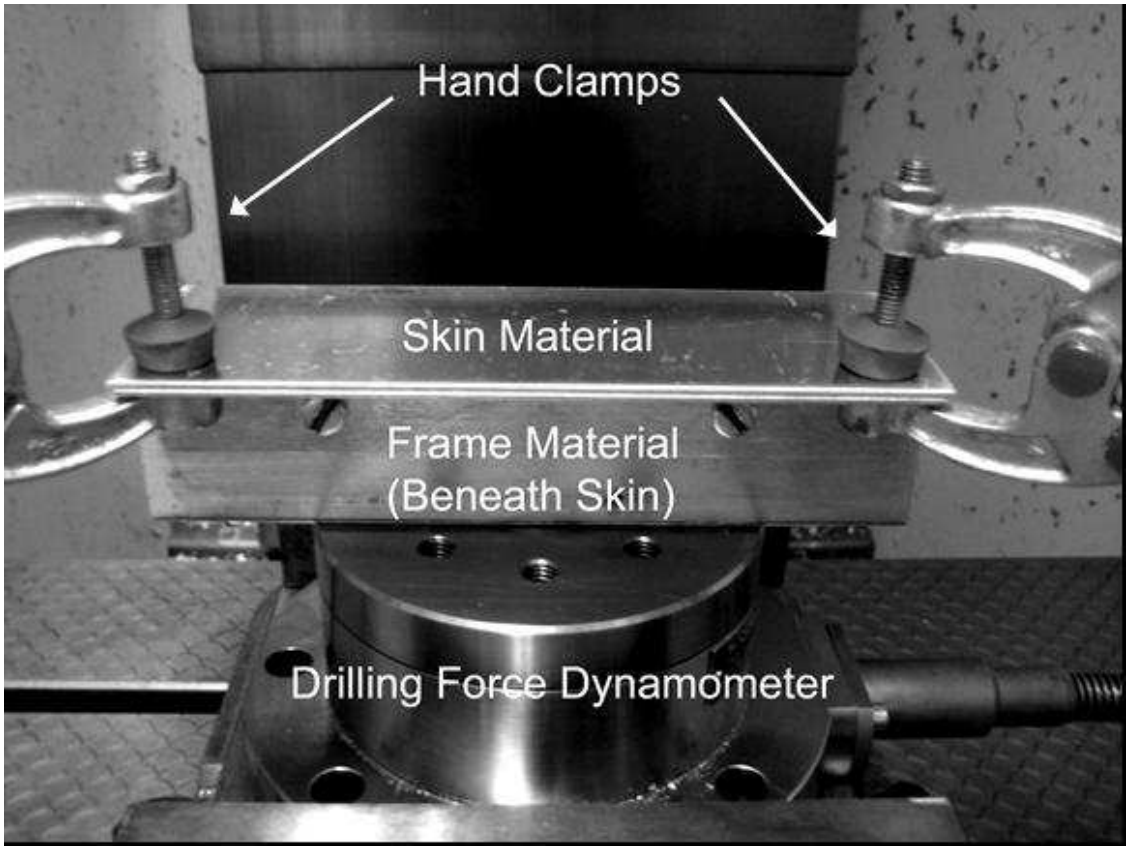

Figure 3.4: Experimental setup with dynamometer, fixture, frame material and skin material

Figure 3.5: De-Sta-Co model 424 squeeze action clamp

Each of the three drills mentioned in the previous section were used to drill 1500 holes. This number was established from preliminary testing that indicated an increase in

the flank wear rate around 1500 holes. All holes were drilled without coolant in a setup similar to the one shown in Figure 3.4. Two replications of the experiment were performed for each drill geometry.

3.4 Measurements

3.4.1 Drilling Forces

The thrust force and torque were recorded as a function of time for all holes drilled. This was accomplished by running the output from the Kistler 9272 drilling force dynamometer to a Kistler 5010 amplifier. The amplified output was then run to a computer's data acquisition card and read using National Instruments LabVIEW at a sampling frequency of 1000 Hz.

For each hole drilled, the instantaneous thrust force and torque at the moment the chisel edge of the drill broke through the first sheet (i.e. the "breakthrough thrust" and "breakthrough torque") were then determined from the data and used to create plots of thrust force and torque as a function of hole number (ranging from 1 to 1500). Appendix A presents the MATLAB code used for finding the breakthrough forces and plotting them. Essentially, the breakthrough forces were determined by finding the point in time at which the thrust forces began to increase (the point at which the tip of the drill touches the top layer) and calculating at what point the tip would break through based on the drilling feed rate. The breakthrough force was then taken as a moving average of 26 milliseconds around this point. The moving average was taken as opposed to a single measurement in order to account for the fact that variations in material thickness might change the exact breakthrough time by a few milliseconds. Figure 3.6 below shows an

example graph of the drilling thrust force and torque vs. time during the drilling of one hole. The instantaneous position at which the breakthrough forces are recorded is marked with a red line, while the points in time at which the chisel edge breaks through the bottom of the second layer and at which drilling is complete are marked with green and blue lines respectively.

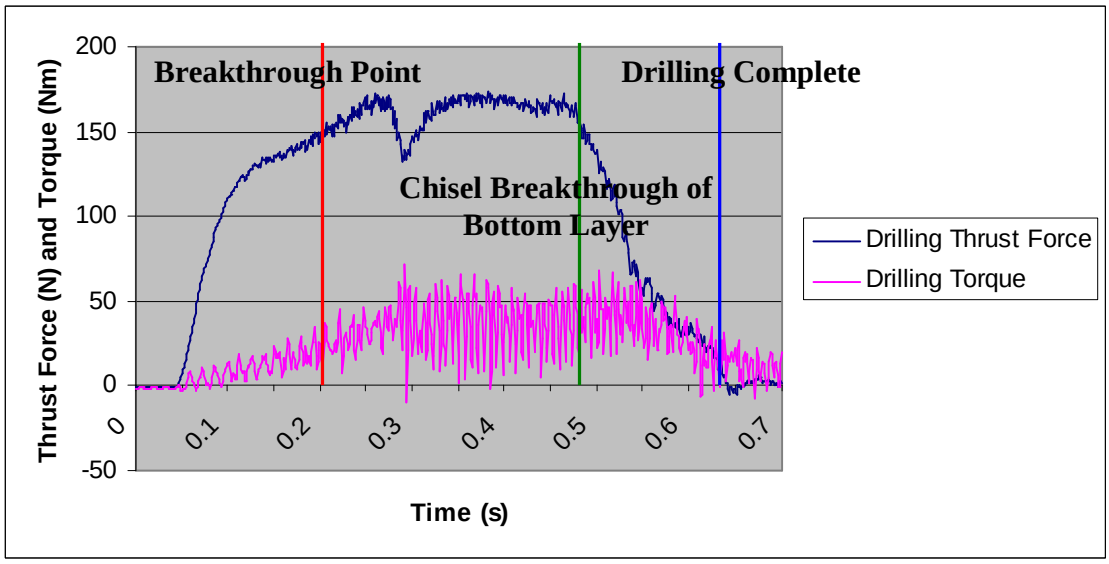

Figure 3.6: Example drilling forces over time for one hole

3.4.2 Burr Heights

The sizes of interlayer burrs formed at the drill exit from the skin material (skin exit burr) and drill entry in the frame material (frame entry burr) were measured once every 50 holes, for a total of 31 burr measurements in each 1500 hole experimental run. The interlayer burr size was measured utilizing three different methods.

The first and primary method involved measuring the burr heights using an optical comparator and a gage block. Figure 3.7 illustrates this method. First, the optical

comparator center line was set to the top of the 0.05” (1.27 mm) thick gauge block, and the current vertical position of the table was recorded. Next, the table was moved up until the center line coincided with the top of the burr being measured, and the corresponding vertical displacement was recorded, allowing a calculation of the burr height to be made. This procedure was used to measure both the skin exit burr and frame entry burr heights. In order to reduce variability, measurements of the maximum burr height were repeated four times. This was accomplished by rotating the workpiece by 30-50 degrees and recording the maximum burr height in each of the four views. The highest three burr measurements were then averaged to obtain a single measure of the burr height. The optical comparator used was a Starret Sigma HB400, and is shown in Figure 3.8.

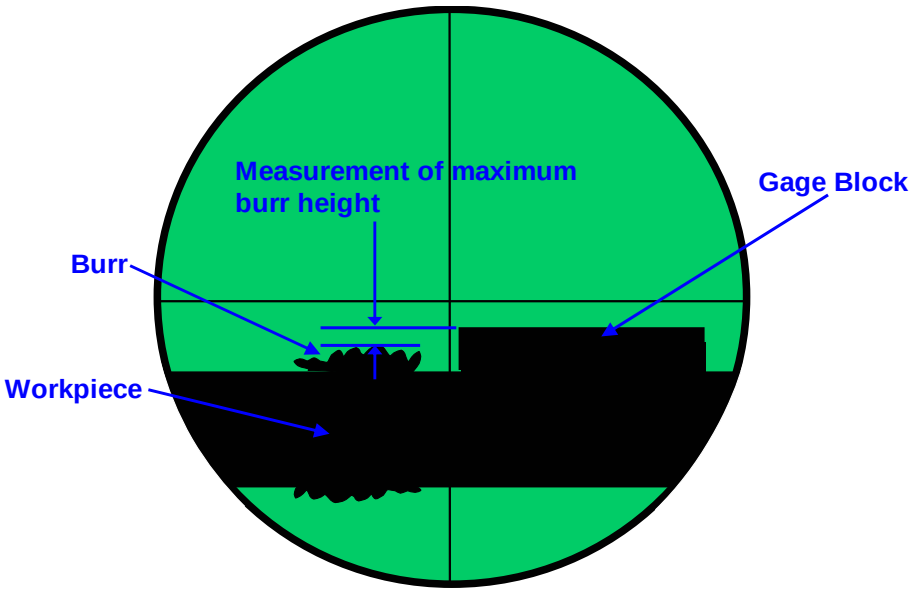

Figure 3.7: Optical comparator method of measuring burr heights [2]

Figure 3.8: Optical comparator

The second method of measuring the interlayer burr sizes involved finding the change in separation between the skin and the frame as a result of the drilling process. This was done by measuring the thickness between the top of the first layer and the bottom of the second layer with a micrometer both before and after drilling. The difference between the two was taken as a measure of the interlayer burr height.

3.4.3 Burr Widths

In addition to the burr heights, the burr widths (or thicknesses) were also measured. The procedure used to quantify the burr widths consisted of measuring the widths of the skin

exit burrs using a Mitutoyo toolmaker's microscope, pictured in Figure 3.9. An example image showing burr width measurements is shown in Figure 3.10. Images were taken at a magnification of 100x, and the width lines were made using Motic Images Plus measuring software. For each hole, a total of fifteen measurements were made around the diameter and averaged. Like each of the burr height measuring methods mentioned above, burr width measurements were made once every 50 holes in each experimental run.

Figure 3.9: Mitutoyo toolmaker's microscope

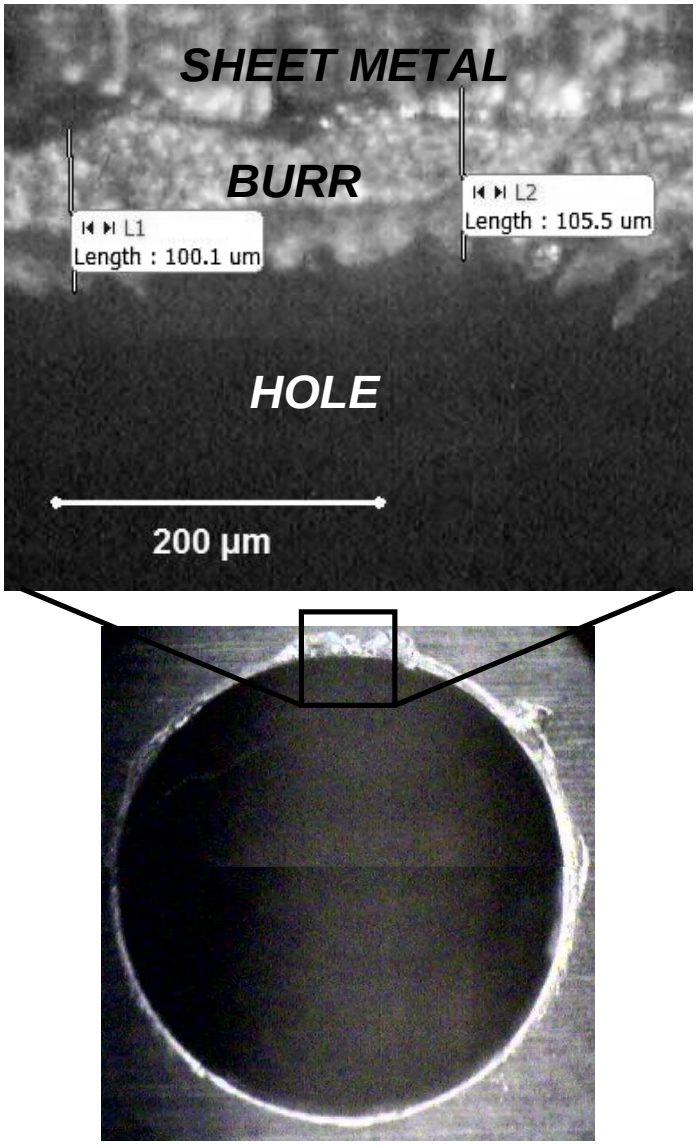

Figure 3.10: Typical burr width measurements

3.4.4 Drill Wear

Measurements of the drill flank wear and outer corner wear were taken once every 100 holes using the toolmaker's microscope. Very few standardized methods exist for measuring drill wear; however, the method used in this study is similar to that used in a

previous study [9]. Figure 2.3 illustrates the way in which the outer corner wear and flank wear were measured. Figure 3.11 shows an example image of the flank and outer corner wear measurements made at the very edge of one of the drill cutting lips. The flank wear was calculated by averaging a total of 18 measurements made along the two cutting lips. The outer corner wear was calculated by averaging the outermost wear measurement on each of the two cutting lips on the drill. In Figure 3.11, which was taken at the end of one of the cutting lips, all 3 measurements indicated are part of the 18 used to calculate the average flank wear. In addition, the outermost measurement on the cutting lip was also averaged with the outermost wear measurement on the opposite cutting lip (not shown in Figure 3.11) to obtain the average outer corner wear.

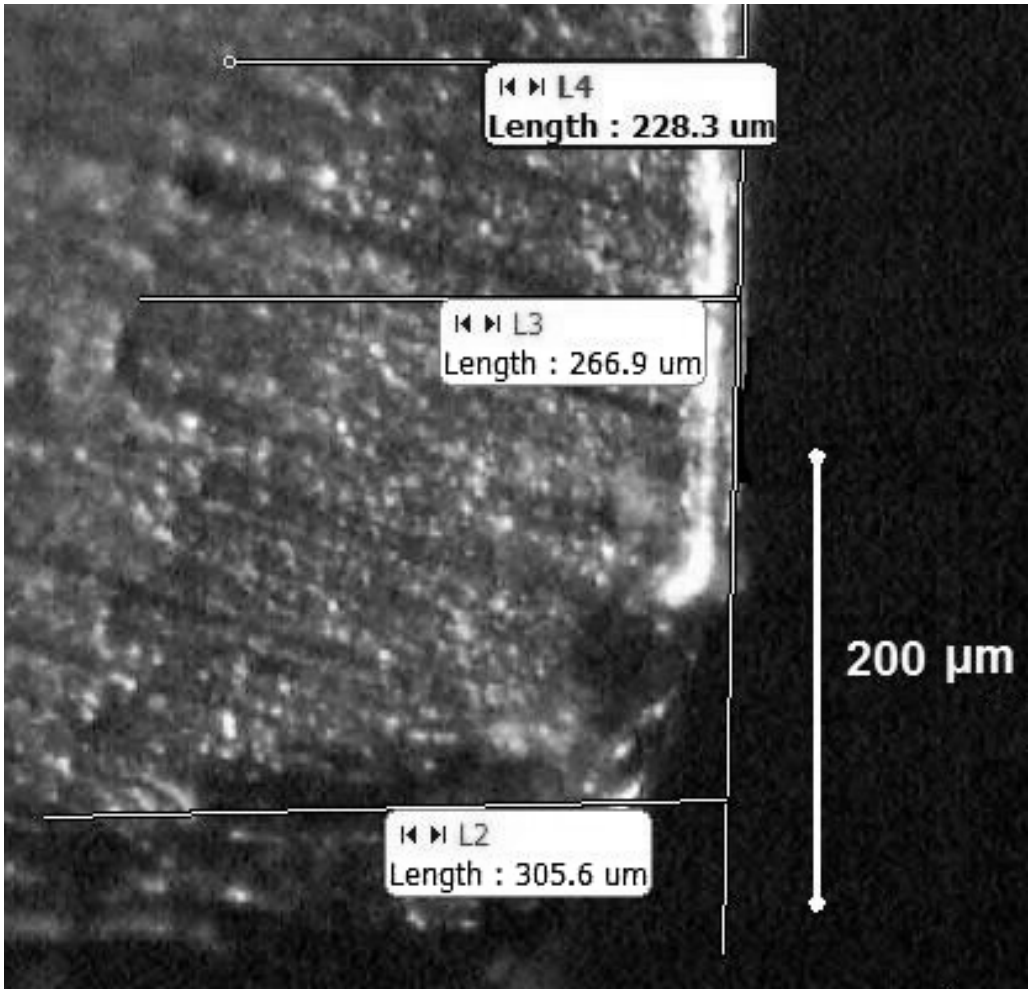

Figure 3.11: Typical drill flank wear measurements

3.5 Results

3.5.1 Burr Heights

The graph in Figure 3.12 shows the average skin exit burr height as a function of the number of holes drilled for each drill that was studied. Full results for both runs of each drill geometry as well as their standard deviations are included in Appendix B. As can be seen, Drill 1 (step drill) produced the smallest mean exit burr height throughout its entire

lifetime, while Drills 2 and 3 produced larger burrs. It is also interesting to note that the increase in skin exit burr height with hole number (or drill wear) is negligibly small for Drill 1 and very mild for Drills 2 and 3. Another apparent advantage of using the step drill is that it produces less variable burr heights than the other two drills, whose heights seem more random in nature. This is an important finding with respect to the ultimate goal of eliminating industrial destacking and deburring processes. If, for example, the average burr height produced by Drill 1 was found to be acceptable without deburring, the lack of variability would reduce the probability of unexpectedly large and potentially hazardous burrs being formed.

The average frame entry burr heights, plotted as a function of the number of holes drilled, is shown in Figure 3.13. Full frame entry height results are located in Appendix C. From the graph it is not apparent which drill performed the best due to the large variability in the measurements. However, on average, Drill 1 still produced the smallest burrs. Table 3.3 at the end of this section contains a summary of the various averaged measurements made for each drill.

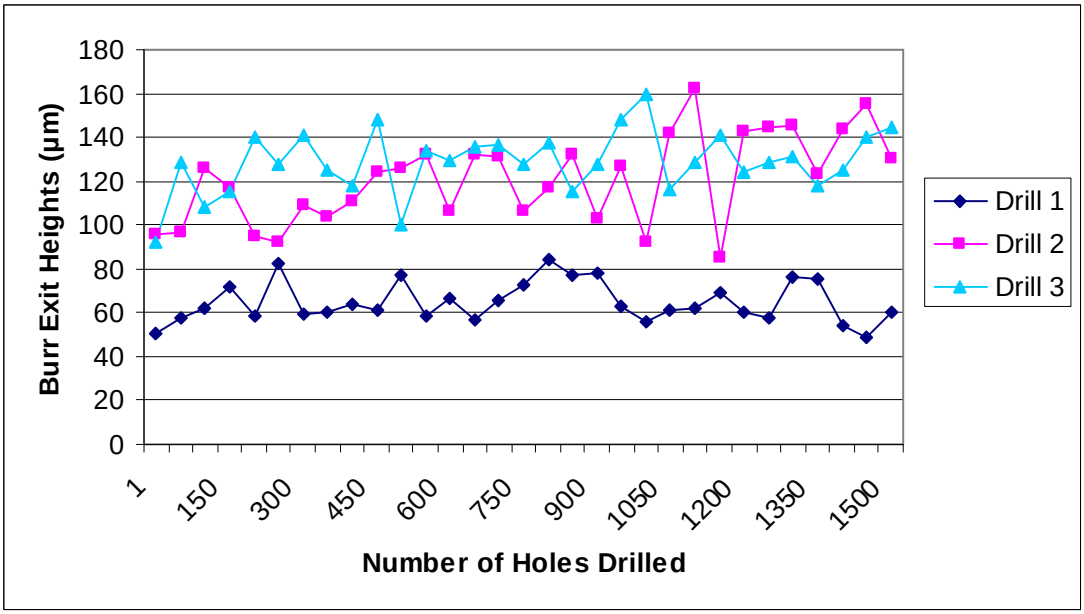

Figure 3.12: Skin exit burr height as a function of hole number

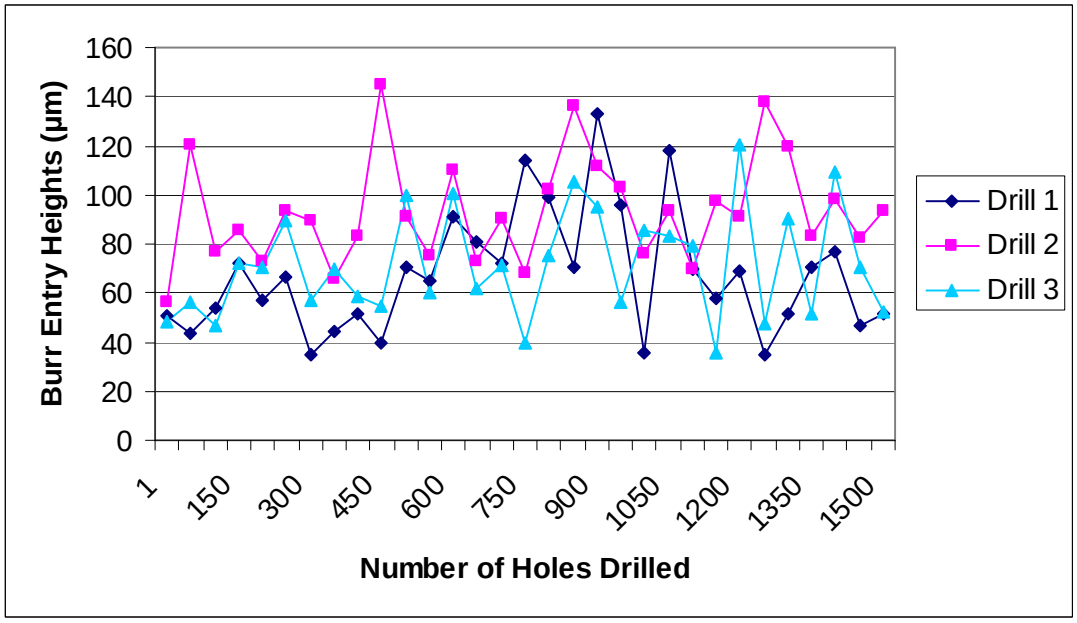

Figure 3.13: Frame entry burr height as a function of hole number

3.5.2 Burr Widths and Change in Separation

The widths of the skin exit burrs as a function of the number of holes drilled can be seen in Figure 3.14. Full burr width results are included in Appendix D. The graph clearly shows that Drill 1 (step drill) produced thinner burrs than either of the other two drills, while Drill 3 (135° point angle, split/no step) produced slightly thinner burrs than Drill 2 (118° point angle, split/no step). The effect of drill wear (with hole number) on the skin exit burr widths is imperceptible for Drill 1, while its effect on the burr widths produced by Drills 2 and 3 is somewhat more evident.

The measurements of change in separation between the two metal sheets as a result of drilling displayed a large amount of variability, making the graphs of separation as a function of hole number difficult to interpret. However, the average change in separation for each drill over all holes drilled is listed in Table 3.3.

An interesting finding from both the burr height and burr width results was that the amount of drill wear had no significant effect on the resulting burr sizes. Rather, burr sizes stayed nearly constant over the 1500 holes drilled for each geometry. One possible explanation for this is that the softness of the aluminum allows material to be cut easily regardless of the drill wear.

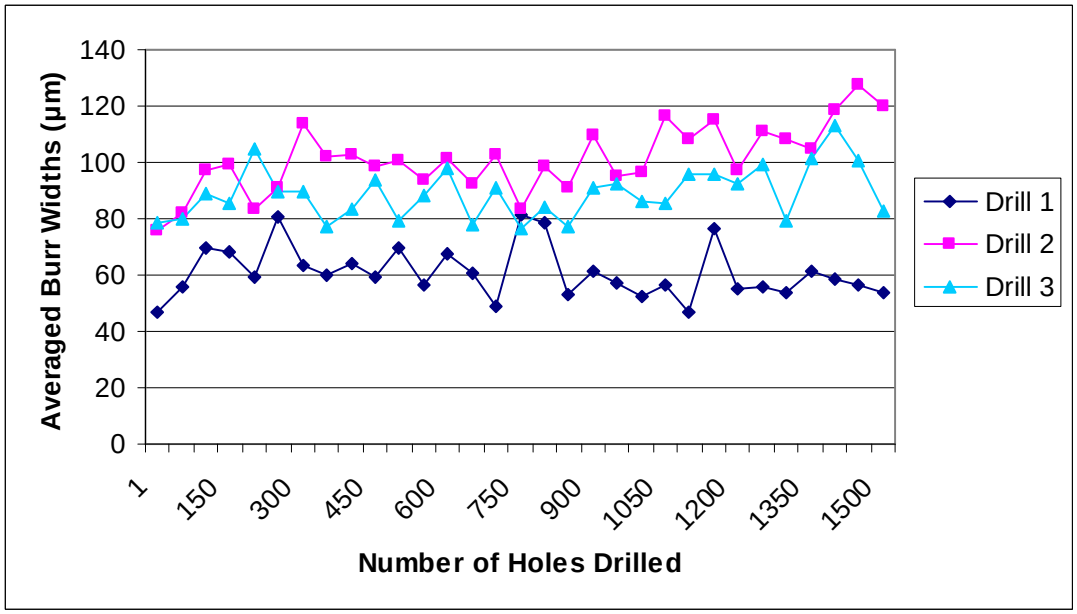

Figure 3.14: Skin exit burr widths as a function of hole number

3.5.3 Drill Wear

The averaged flank wear for each drill as a function of the number of holes drilled is shown in Figure 3.15. The averaged outer corner wear is shown in Figure 3.16. Full average flank wear and outer corner wear results are included in Appendices E and F, respectively. From the graphs it is evident that the wear for Drill 1 (step drill) was smaller than the wear for Drills 2 and 3 over 1500 holes. It is possible that this finding is partially due to the fact that Drill 1 has a step ground into it, making the area over which measurements were made slightly smaller. However, it is apparent from the graph that it takes longer for Drill 1 to reach any given amount of wear than it takes Drills 2 or 3.

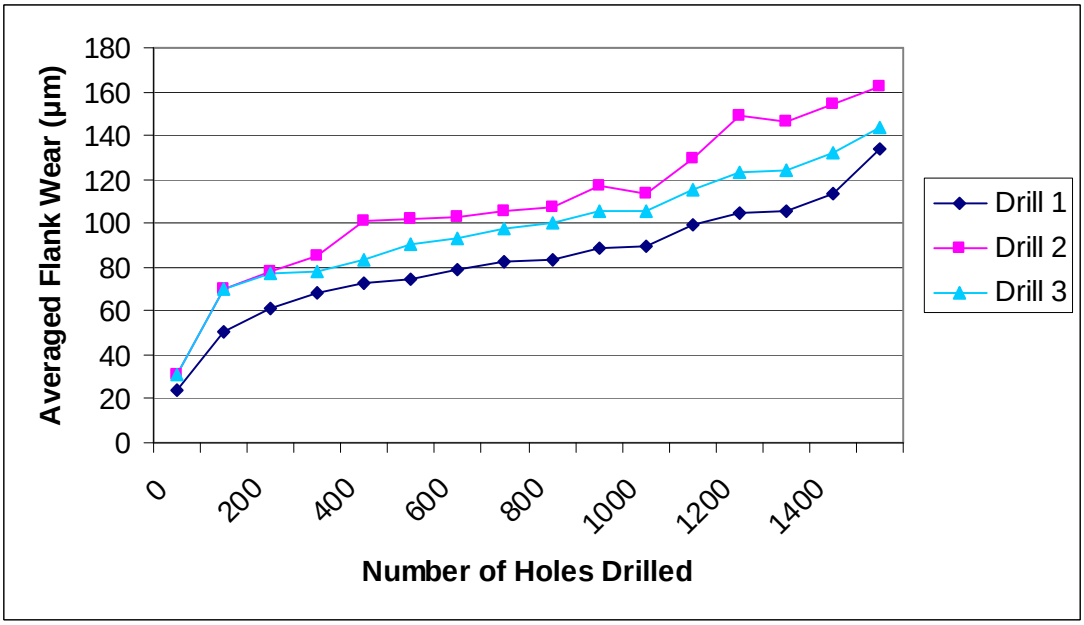

Figure 3.15: Averaged flank wear for each drill as a function of hole number

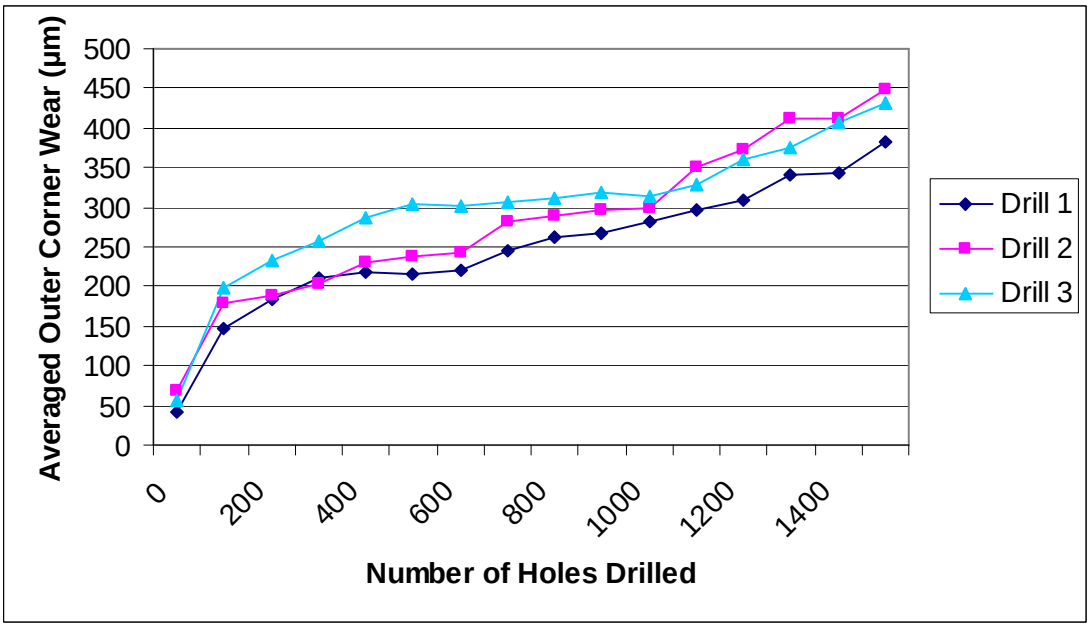

Figure 3.16: Averaged outer corner wear for each drill as a function of hole number

3.5.4 Drilling Thrust and Torque

The graphs of breakthrough thrust force and torque (measured at the instant the drill breaks through the skin) as a function of hole number are seen in Figures 3.17 and 3.18, respectively. Drill 1 generated a higher thrust force than the other drills but a slightly smaller average torque. The higher thrust force may be partially due to the fact that the black oxide coating was ground off of the tip of Drill 1 when the step was created.

It is interesting to note that, like the measurements of burr sizes, the measurements of thrust force did not show a significant increase over the wearing of the drills. This can be verified through past studies all showing a correlation between drilling thrust force and burr size [22, 27, 2].

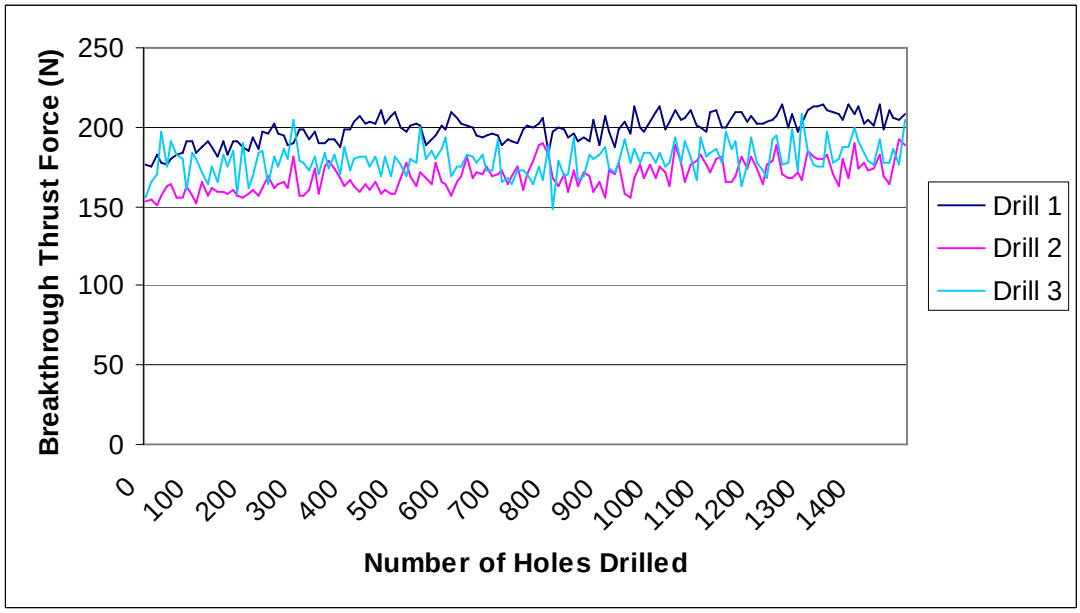

Figure 3.17: Breakthrough thrust force for each drill as a function of hole number

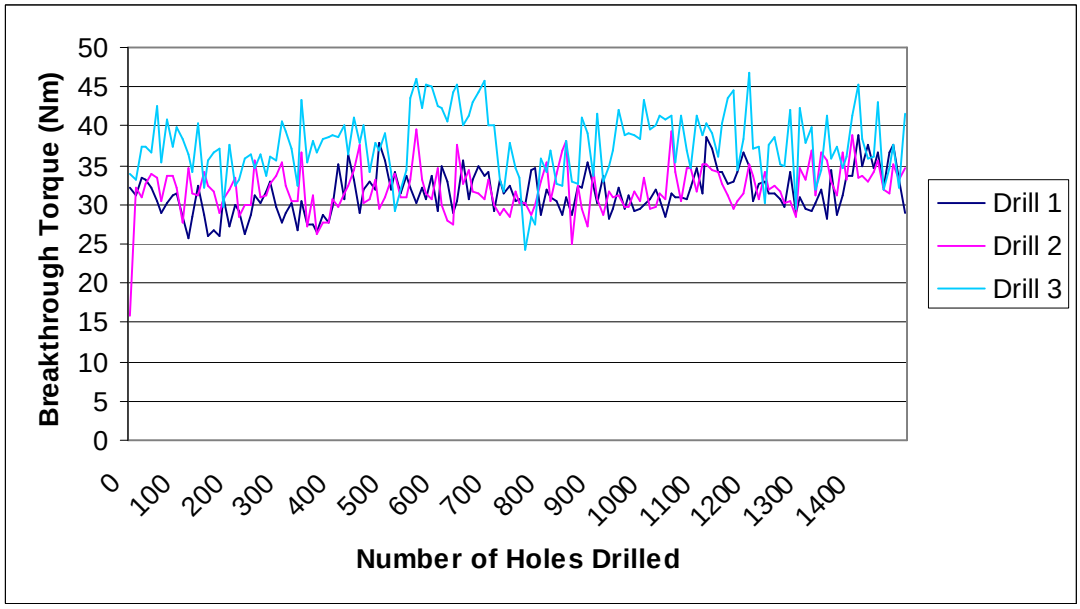

Figure 3.18: Breakthrough torque for each drill as a function of hole number

3.5.5 Summary

Table 3.3 lists the average values of the measurements made over all holes for each drill. For each measurement, the drill with the optimal value (smallest burrs, least wear, and lowest forces) is highlighted in bold type. It can be seen that Drill 1 outperforms the other two drills in every measurement taken except for thrust force.

Table 3.3: Averaged measurements for each drill over all holes

	Drill 1	**Drill 2**	**Drill 3**
Burr Exit Heights, µm ($in \times 10^{-3}$)	**64.8 (2.55)**	120.9 (4.76)	128.8 (5.07)
Burr Entry Heights, µm ($in \times 10^{-3}$)	**67.3 (2.65)**	93.2 (3.67)	71.4 (2.81)
Burr Exit Widths, µm ($in \times 10^{-3}$)	**61.0 (2.40)**	101.3 (3.99)	88.9 (3.5)
Change in Separation, µm ($in \times 10^{-3}$)	**15.5 (0.61)**	50.0 (1.97)	50.0 (1.97)
Flank Wear, µm ($in \times 10^{-3}$)	**83.2 (3.28)**	109.8 (4.32)	98.2 (3.87)
Outer Corner Wear, µm ($in \times 10^{-3}$)	**247.5 (9.74)**	281.5 (11.08)	299.2 (11.78)
Thrust Force, N (lb)	199.1 (44.75)	**168.3 (37.83)**	178.2 (40.06)
Torque, Nm (lb-in)	**31.7 (280.6)**	32.0 (283.2)	36.6 (324.0)

3.6 Discussion

The reason for the superiority of the step drill can be explained in relation to the mechanics of burr formation. Figure 3.19 shows schematically the formation of a burr using a regular drill (no step). After initial breakthrough of the drill tip (Figure 3.19(a)) most of the remaining material lying beneath the drill is cut and carried away by the drill cutting lips. Some of the material, however, either gets sheared off downward or plastically deformed into the exit burr, which is shaded black in Figure 3.19(b).

By comparison, Figure 3.20 shows the formation of an exit burr using a step drill. Figure 3.20(a) shows the chisel edge of the drill beginning to break through the material. Figure 3.20(b) shows the first diameter of the step drill breaking through, with a resulting burr slightly smaller than in Figure 3.19(b) due to the fact that the diameter is slightly smaller. In Figure 3.20(c), which shows the second diameter breaking through, much of the burr seen in Figure 3.20(b) is sheared off, resulting in a final burr height smaller than that obtained with a regular drill.

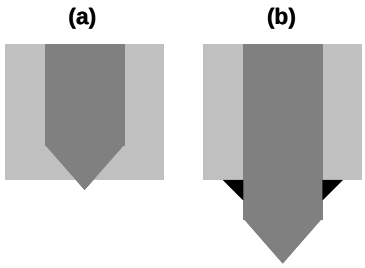

Figure 3.19: Formation of burr with regular drill

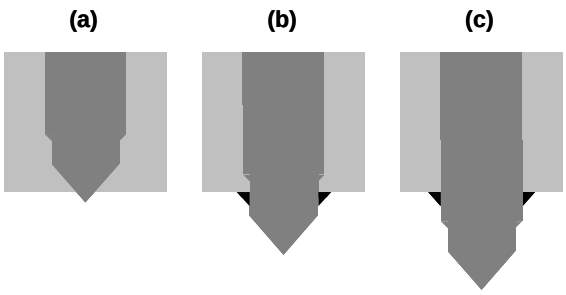

Figure 3.20: Formation of burr with step drill

Another important finding was that the effect of drill wear on burr heights and widths and on the drilling thrust and torque was not significant. Instead, unexpectedly, each of the graphs of burr sizes and drilling forces versus the number of holes drilled showed almost no increase along with the amount of drill wear. This could possibly be a result of the softness of the aluminum material, making it easily cut regardless of the amount of drill wear.

3.7 Summary

Three different drill geometries were experimentally studied to find which would produce the smallest interlayer burrs between stacked sheets of aluminum 2024-T3 layers when taking into account the effect of drill wear. The most significant finding was that a step drill with a 118° point angle (Drill 1) produced the smallest interlayer burrs, including skin exit burr heights, frame entry burr heights, skin exit burr widths, and change in separation over the tested life of the drill. The experiments also showed that for Drill 1 the burr heights and widths over the 1500 drilled holes remained nearly constant rather than increasing with drill wear and showed less variability. Furthermore,

measurements of drill wear showed that Drill 1 took the same or an even greater amount of time to reach a given amount of wear as the other two drills. Therefore, the results indicate that Drill 1 (step drill) yields the best results as far as interlayer burr formation is concerned and is the preferred drill for minimizing the same. One possible topic for future study, which was not addresses in this thesis, is the optimization of the various parameters of the step drill geometry.

CHAPTER IV

CLAMPING METHODS INVESTIGATION

4.1 Goal and Approach

Whereas the previous chapter was concerned with identifying the most suitable drill geometry for minimum burr formation during the life of the drill, this chapter describes the steps taken to optimize the other predominant factor in interlayer burr formation, namely clamping conditions. The way in which sheet metal layers are clamped together is extremely important for interlayer burr minimization in stacked layers, since the tighter that the layers are held together around the drilled hole, the less room there is for burrs to form.

The first step taken was to create a list of the ideal clamping attributes for industrial drilling applications. Next, multiple clamping concepts were brainstormed, and a single idea was selected based on its matching of the ideal attributes. From this clamping idea, two different prototypes were created and tested for their effectiveness in reducing burr sizes.

4.2 Ideal Clamping Attributes

The qualities of an ideal clamping system can be divided into attributes of functionality and implementation. Any method must be capable of reducing the space between sheet

metal layers needed for interlayer burr formation to occur as well as be practicably feasible for industrial environments.

4.2.1 Clamping Functionality

As mentioned previously, the purpose of clamping should be to hold the sheet metal layers as tightly together as possible in the area of the hole being drilled, not allowing any room for burrs to form. This goal can be further broken down into more specific clamping properties.

The most obvious attribute is that a clamp must be able to have a large force potential. This is needed to counteract the effect of the drill pushing and pulling on the workpiece. For example, as the drill is in a steady state of drilling through a layer, a large downward thrust force is exerted onto the workpiece. However, when the drill tip is breaking through a layer, the motion of the drill's helix slightly pulls the layer upward. Therefore, in the drilling of two layers of sheet metal, as the drill is exiting the first and entering the second, the first is being pulled upwards, and the second is being pushed downwards, requiring a large force to keep them together. An illustration of these forces in the drilling of two unclamped sheet metal layers is shown in Figure 4.1.

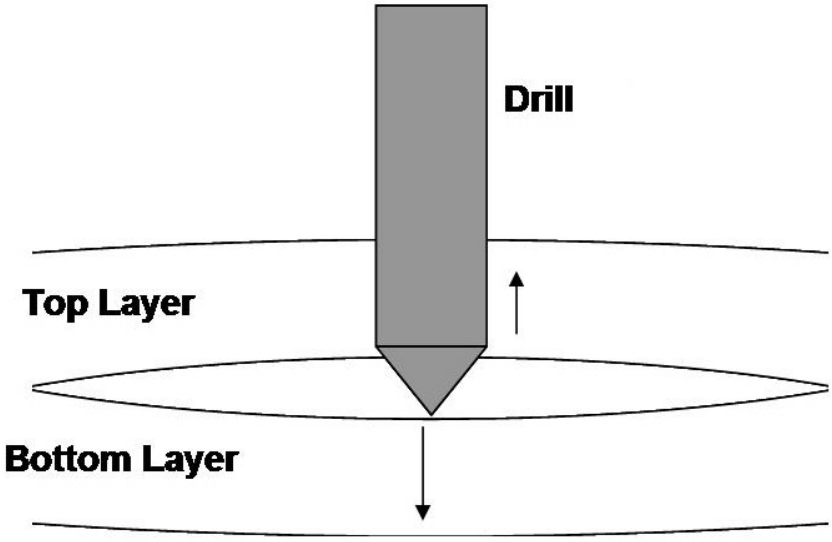

Figure 4.1: Gap formation in unclamped sheets

In order to maximize its effectiveness, a clamp should also be capable of providing a force in close proximity to the hole. Additionally, the force should be applied all around the hole rather than at just a single point on one side of the hole. This is because of the ability of thin sheet metal layers to bend and form gaps when clamping distances are large, whereas a large concentric clamping force immediately around the vicinity of the hole is the most effective method of gap prevention.

4.2.2 Clamping Practicality

In addition to being able to decrease interlayer burr sizes by minimizing the separation between sheet metal layers at hole locations, any clamping system must be capable of being implemented in industrial situations in order to have any value. Consequently, any system must be capable of being manufactured, simple for operators to use, and safe.

Additionally, a system's practicality would be improved by having a low cost and a high level of reliability in use.

To summarize, the capabilities that an ideal sheet metal clamping method should have for the minimization of interlayer burr formation are as follows:

- Provide a large clamping force
- Clamp in close proximity of the hole
- Apply force all around hole rather than at a single point
- Be easy to implement in industry and be manufacturable
- Be safe and simple for operators to use

4.2.3 Current Clamp Comparisons

Two of the most commonly used sheet metal clamping methods used in the aerospace industry are the hand clamp, seen in Figure 2.11, and the cleco clamp, seen in Figure 2.12. Figure 4.2 shows a hand clamp and a cleco clamp both being used to hold two sheet metal layers together in a setup similar to that used in Chapter III. For comparison to the ideal clamping functionality attributes listed above, the hand clamp is capable of applying a large force, but only clamps at one point relative to the hole and cannot clamp in the middle of a large workpiece. The cleco clamp, which can provide a moderate force, is a spring-loaded hole clamp that works by being pushed through a nearby existing hole and expanding to lock the two layers together. Cleco clamps are capable of being used in the middle of a workpiece but cannot be used if a nearby hole has not been drilled and also only clamps at one point.

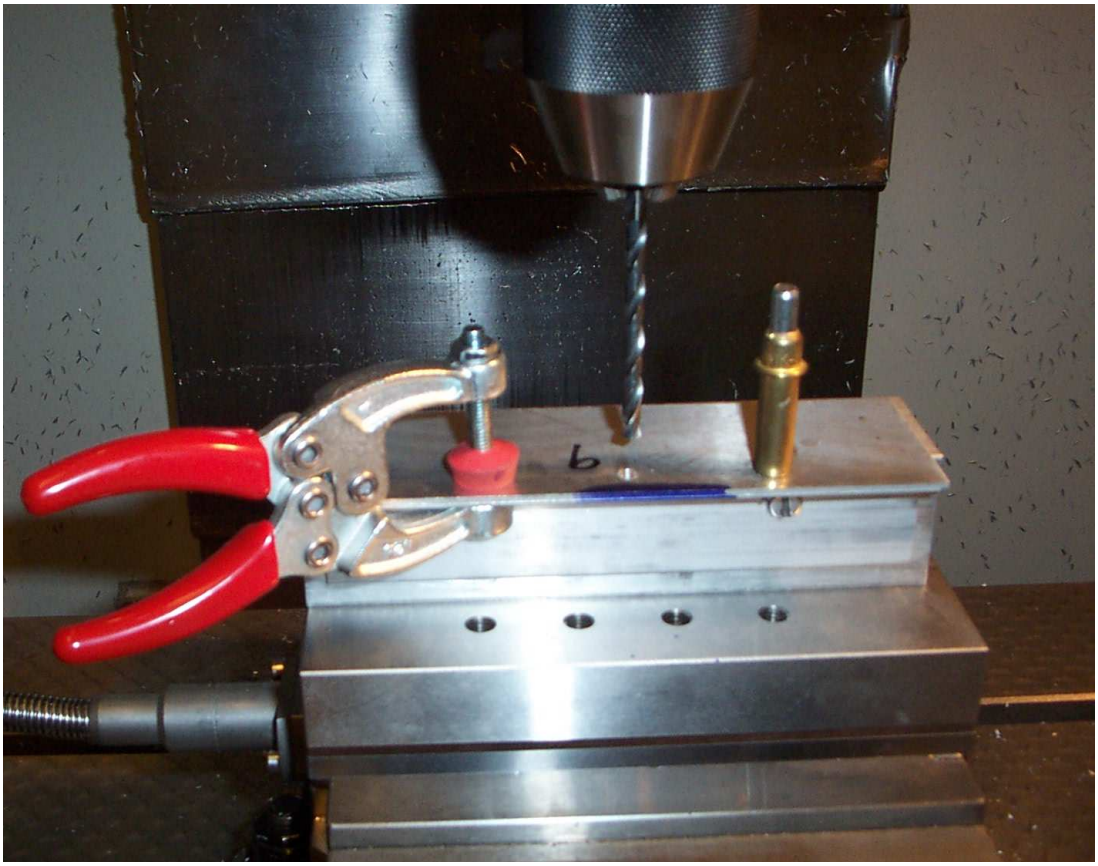

Figure 4.2: Hand clamp and cleco clamp in use [2]

4.3 New Clamping Ideas

Based on the ideal clamping attributes listed in the previous section, multiple new clamping concepts were brainstormed in an effort to create an improved system capable of reducing interlayer burr heights. The four clamping ideas examined are discussed below.

4.3.1 Long I-Beam Concept

The first concept was to have two stiff beams, such as I-beams, running along both sides of the workpiece in close proximity to the row of holes needed to be drilled. The beams would need to be long considering that many stacked sheet metal drilling operations are performed on very large workpieces. The beams could then be clamped together on either side, providing a clamping force along the entire length of the workpiece given that the beams are stiff enough. This concept is illustrated in Figure 4.3.

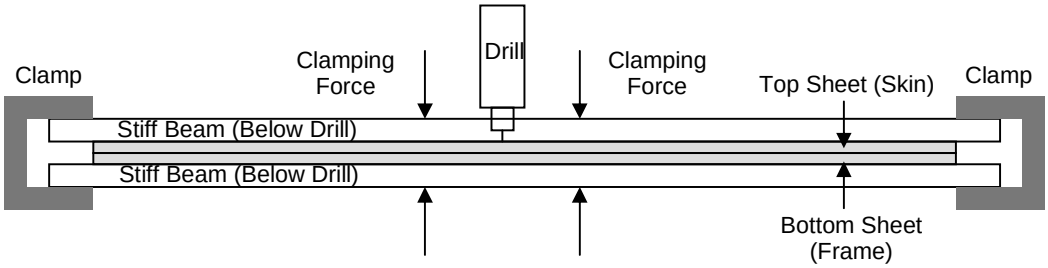

Figure 4.3: Long I-beam concept

4.3.2 Long Hand Clamp Concept

This idea was to simply use a normal clamp (such as the hand clamp discussed above) that is very large, such that it can clamp in positions closer to the center of the workpiece. The concept is shown in Figure 4.4.

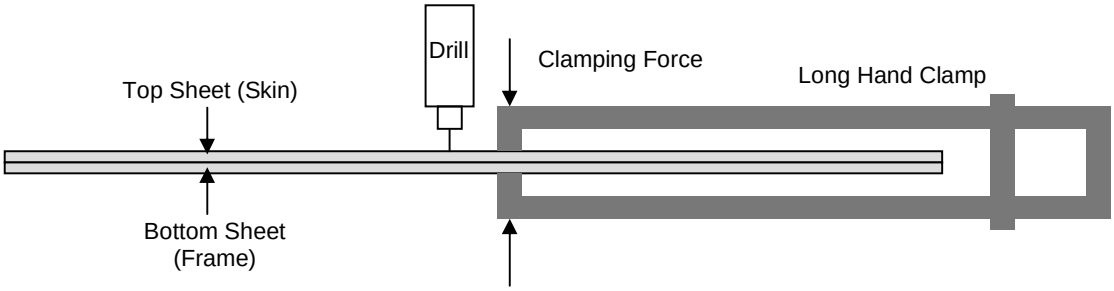

Figure 4.4: Long hand clamp concept

4.3.3 Magnetic Clamp Concept

This concept was to have an electromagnet on one side of the workpiece and some sort of ferrous metal fixture on the other side, clamping the layers together with a magnetic force. Figure 4.5 illustrates this concept. Note that the ferrous metal piece would only be needed if the sheet metal layers are non-ferrous material such as aluminum.

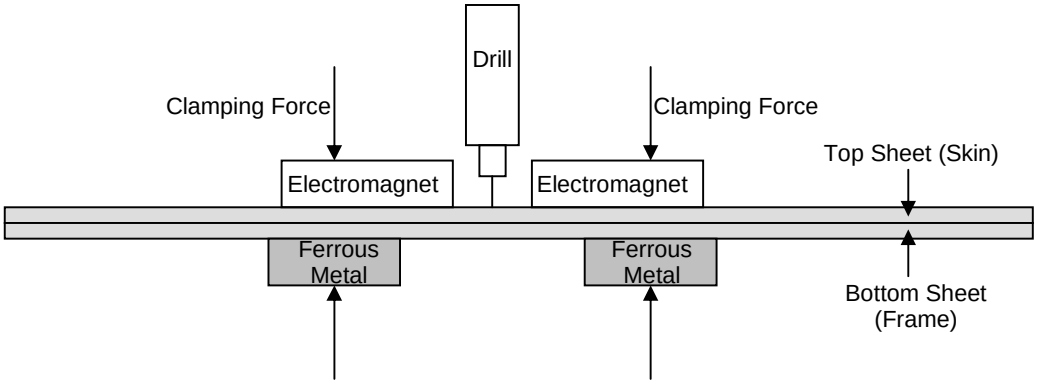

Figure 4.5: Magnetic clamp concept

4.3.4 Single-sided Clamping Concept

The final concept was to have some sort of a circular fixture that presses all around the hole being drilled on just one side of the workpiece as opposed to both sides as with

typical clamping systems. The drill would then travel through the center of the fixture to create the hole. For this to be done, having the circular fixture attached to the drill in some way would be convenient and provide simplicity, considering that many stacked sheet metal drilling operations are performed manually. The circular fixture could therefore be attached to the drill through some sort of elastic medium such as a spring or a piece of compressible material which would allow the drill to move into the workpiece relative to the fixture. The force of the circular fixture pressing against the workpiece would then hold the sheet metal layers together while the drill traveled through them. Consequently, part of the operator's total thrust force would go into pushing the layers together, and part would go into providing the drill thrust force. This concept is illustrated in Figure 4.6.

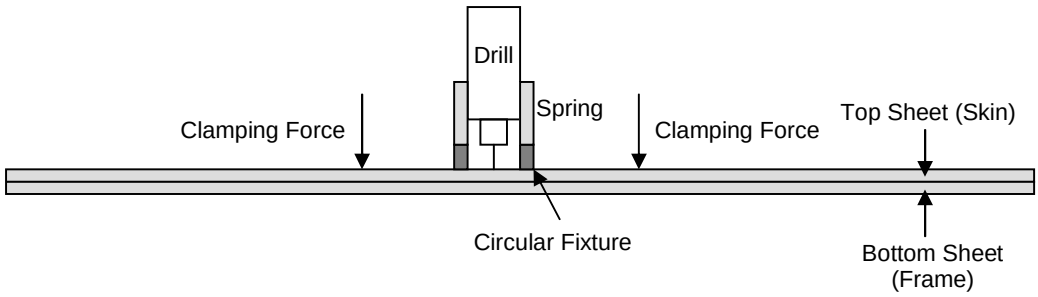

Figure 4.6: Single-sided clamping concept

4.3.5 Evaluation of Concepts

Each of the four concepts was then analyzed qualitatively and/or quantitatively based on its potential levels of functionality and practicality as described in the previous section.

For the long I-beam idea, it was decided that it would be difficult to provide a large clamping force in the center of the workpiece due to the fact that even a slight

bending of the beams would allow enough separation between the layers for interlayer burr formation to occur. Regarding its practicality, it might also be difficult or time consuming for an operator to unclamp, move, and reclamp heavy beams.

A long hand clamp would be able to provide a large clamping force closer to the center of a large workpiece, but would still only provide a force at one point relative to the hole. Manipulation of a large hand clamp in industrial use might also be difficult.

The magnetic clamp idea was unique in that it would allow a clamping force to be applied on both sides of the workpiece without having to travel around the workpiece. However, there are too many issues that would make the idea impractical for use with non-ferrous materials. Due to the fact that aluminum is nonferrous, only a small percentage of electromagnetic force can travel through depending on the layer thickness, requiring an extremely powerful electromagnet to achieve any significant clamping effect. Implementation of the idea would also be difficult due to the need to move around the large electromagnet and to manufacture the ferrous backing material based on the hole locations.

It was determined that the single-sided clamping concept was the best in terms of meeting the ideal clamping attributes discussed earlier. Because of the circular fixture, the clamping force applied could be evenly distributed immediately around the area of the hole being drilled, and the force of clamping would be limited only by the potential pushing force of the operator or machine. The idea would also be the simplest to use in that no clamping mechanism would need to be applied to the back of the workpiece, and the operator or machine would only need to push the drill into the workpiece as is done

normally in manual drilling operations. An additional advantage would be that the circular fixture would help ensure that the drill enters the workpiece perpendicular to it.

4.4 Analysis of Single-sided Clamping Idea

The clamping concept of simply pushing on one side of the workpiece around the hole was then analyzed further to ensure that it would not cause any structural problems with the workpiece and that it would in fact be able to significantly reduce the separation between the sheet metal layers.

One concern with the idea was that pushing on just one side of the thin sheet metal without any backup material on the opposite side would result in an unacceptable plastic deformation of the sheet metal. In order to test this, a finite element analysis was performed with ANSYS. Simulations were run both with a flat and a curved 6' by 6' (1.829 m by 1.829 m) panel. This shape was chosen to be large enough that the edges would be almost unaffected by the drilling force. A thickness of 1/8" (3.175 mm) was used, since industrial applications frequently stack two layers of 1/16" thick sheet metal layers. Boundary conditions were set that all four edges would have zero displacement, and SOLID45 elements were used. It was estimated that a typical drilling operator would press on a drill with 40 to 50 lbs. of force. Therefore, taking into account a safety factor of 2, a single point force of 100 lbs. (444.8 N) was applied. In both tests, this force was applied perpendicular to the workpiece at its very center. The modulus of elasticity used was 72.4 GPa, and the Poisson's ratio entered was 0.33. A mesh convergence was also performed to ensure that the mesh size employed was adequate.

A plot of the resulting deformation for the curved panel is shown in Figure 4.7. Figure 4.8 shows the resulting von Mises stress. For Aluminum 2024-T3, which was the material used in the experiments of the previous chapter, the yield stress is approximately 324 MPa (47,000 psi). However, for the flat panel test and the curved panel test, the highest resulting von Mises stresses were only 102 MPa (14,800 psi) and 77 MPa (11,100 psi), respectively. Therefore, it was determined that the resulting stresses on the sheet metal layers as a result of an operator pressing on them from one side with a typical drilling force would not be nearly enough to cause any plastic deformation.

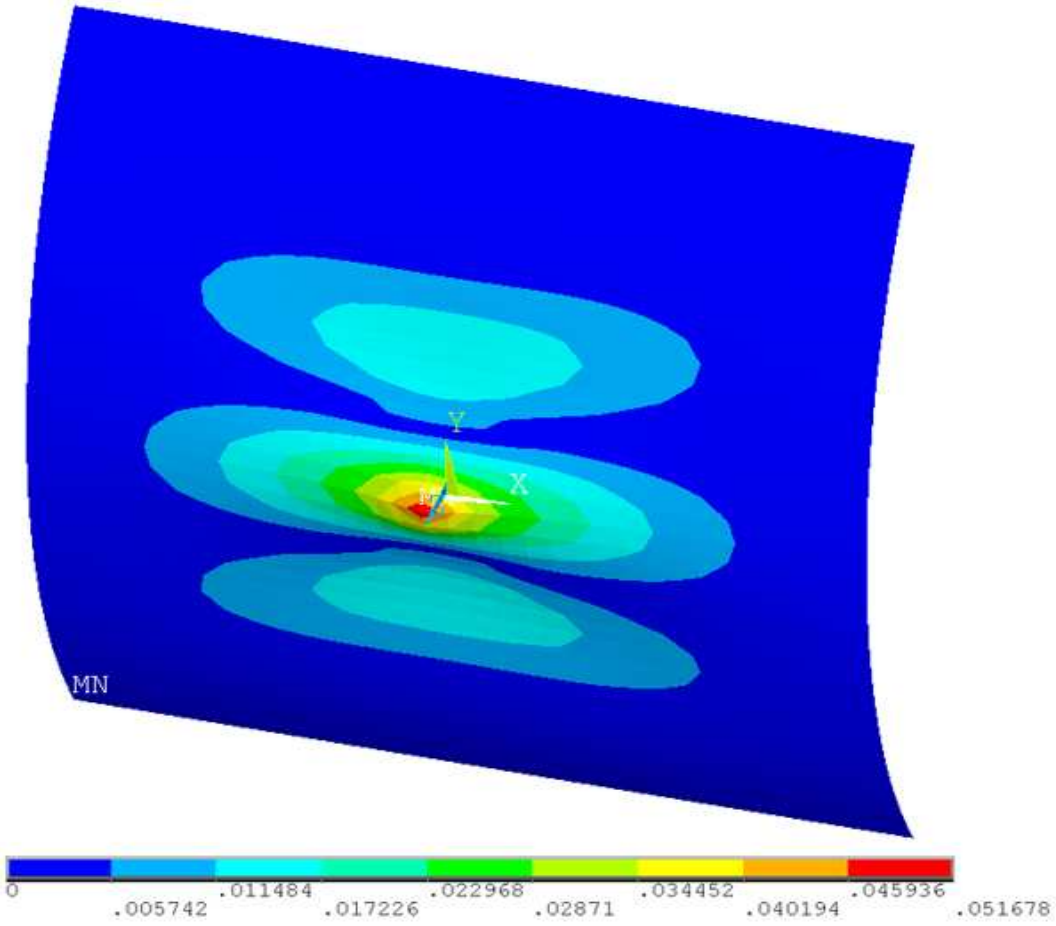

Figure 4.7: Resulting deformation from single-sided clamping (in)

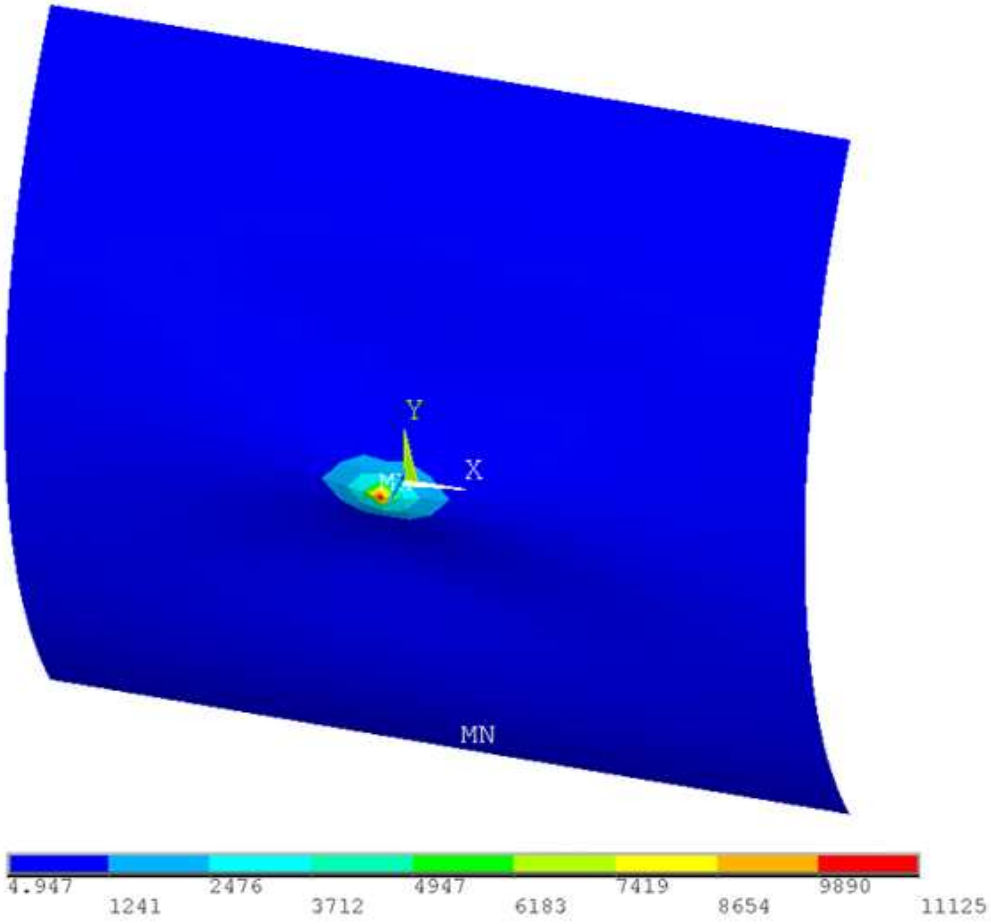

Figure 4.8: Resulting von Mises stress from single-sided clamping (psi)

The single-sided idea also needed to be analyzed to see if it would be capable of significantly reducing the separation between the sheet metal layers and what the spring stiffness of the material connecting the drill and the circular fixture would need to be. As discussed previously, the worst case scenario for when clamping is needed to keep the layers together is when the drill is breaking through the first layer, allowing it to rise up, but is pressing down against the second layer. Therefore, it was determined that the minimum force of the circular fixture against the first layer would need to be equal to or greater than the drilling thrust force acting against the second layer. In other words, as

the drill thrust force is elastically deforming the second layer downwards, the force of the circular fixture needs to match this force in order to keep the first layer elastically deformed downwards by the same amount so that the two layers remain in contact.

Based on this requirement, calculations were then made of the minimum stiffness of the spring (or other compressible material), *k*, connecting the drill to the circular fixture. Note that the following description refers to a manual drilling operation performed by an operator with the fixture attached to a hand drill such that the spring must be compressed in order for any displacement of the drill relative to the fixture to occur. Referring to the dimensions shown in Figure 4.9(a), the total spring displacement at the time the drill is pressing against the second layer at its worst case scenario (Figure 4.9(b)) is *pl*, the height of the drill point; plus d_o, the initial distance between the tip of the chisel edge and the end of the circular fixture (and the surface of the first layer); plus *t*, the thickness of one of the sheet metal layers. As mentioned previously, the clamping force of the circular fixture (force of the spring compression) when the drill displacement reaches this point needs to be greater than half of the total force of the operator pressing the drill:

$$k(pl + d_0 + t) \geq \frac{\text{Operator Force}}{2} \tag{4.1}$$

$$k \geq \frac{\text{Operator Force}}{2(pl + d_0 + t)} \tag{4.2}$$

Alternatively, the minimum clamping requirement can be specified in terms of d_o, which might be easier to change in industrial situations if the drill can be somewhat moved in and out of the collet:

$$d_0 \geq \left(\frac{\text{Operator Force}}{2k} \right) - pl - t \tag{4.3}$$

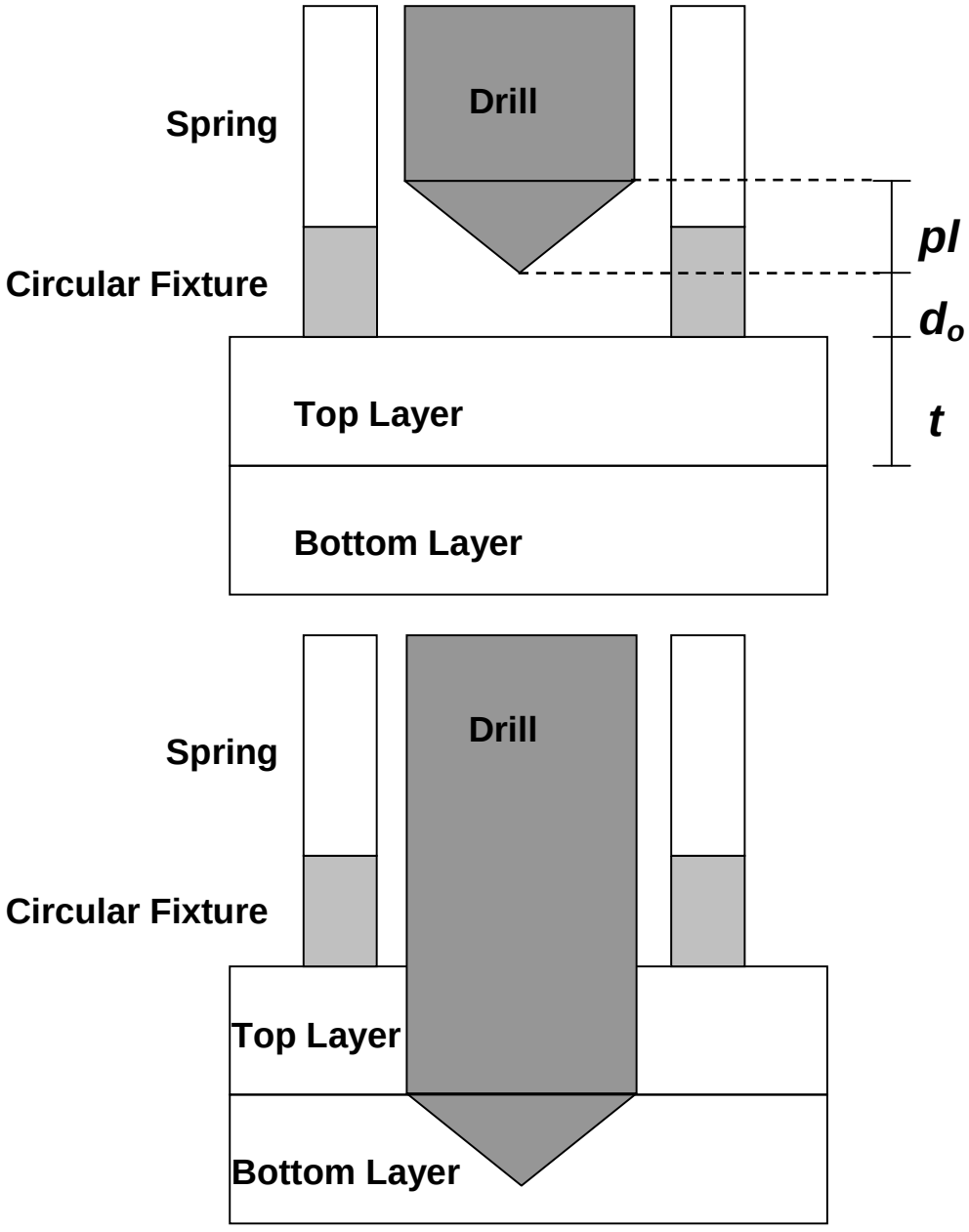

Figure 4.9: (a) Drill starting position; (b) Worst case drill position

4.5 Prototypes

Based on the single-sided clamping idea, two prototypes were assembled by adding attachments onto a small regular hand drill. The first prototype was made using a spring and is seen in Figure 4.10. The inner diameter of the spring of 55 mm was selected such that it would fit around one of the tapered diameters of the hand drill shaft, and the length of 157 mm was selected to leave a small distance between the end of the drill and the end of the spring. The spring stiffness resulted in 111 N (25 lbs.) of force at a compression of 25.4 mm (1") or 4.37 N/mm (25 lb/in). A small rubber bushing was attached to the end of the spring to soften the contact between the spring and the workpiece. The second prototype, shown in Figure 4.11 was made using a bored out 75 mm long cylinder of compressible polyurethane duct taped to a PVC cylinder. Like the spring prototype, the bored out inner diameter of the polyurethane of 55 mm was selected such that it would fit around one of the tapered diameters of the hand drill shaft. The polyurethane had a durometer rating of 40A, a tensile strength of 850 psi. (5860 kPa), and a density of 74 lb./ft^3 (1185 kg/m^3).

In order to design the spring prototype such as to be capable of holding the layers together during drilling and to provide an example of the use of the equations found in the previous section, Equation (4.3) was used to select the initial distance between the tip of the drill and the end of the circular fixture, d_0. In order to get an idea of the typical thrust force with which an operator performs a drilling operation, a drilling operator working in the aircraft manufacturing industry was asked to press a hand drill against a weighing scale with a typical manual drilling force. The force measured was approximately 178 N (40 lbs.), and was used in the calculations. As mentioned

previously, the stiffness value of the spring, *k*, was approximately 4.37 N/mm. The thickness of the sheet metal layers, *t*, with which the prototype was tested was 1.58 mm (1/16”), and the height of the drill point tested, *pl*, was 1.47 mm (.058”). Putting these values into Equation (4.3):

$$d_0 \geq \frac{178\ \text{N}}{2\left(4.37\ \text{N/mm}\right)} - 1.47\ \text{mm} - 1.58\ \text{mm}$$
$$d_0 \geq 17.3\ \text{mm} \tag{4.4}$$

Thus, the initial distance between the drill tip and the end of the circular fixture for the spring prototype was chosen to be approximately 18 mm in order to ensure that the sheet metal layers would remain clamped together during testing. For the polyurethane prototype, the stiffness of the attachment was so great that the initial distance d_0 was selected through trial and error to be approximately 1 mm.

Figure 4.10: Spring prototype

Figure 4.11: Compressible rubber prototype

4.6 Prototype Testing

After completing the prototypes, both were tested for their functionality in reducing interlayer burr formation. Tests were performed on the same setup as shown in Figure 3.4 with the skin and frame material clamped together using hand clamps and attached to the drilling force dynamometer. Rather than being clamped into the CNC machine, the dynamometer was set out at a location easier for use with the hand drill. For each prototype, a total of ten tests were performed, as well as ten tests performed with the hand drill without either of the attachments. For all three tests, a #10 drill was used with a 118° point angle, a split point, no step, and a black oxide coating (the same as Drill 2 from the experiments detailed in Chapter 3). Drill 2 was selected rather than Drill 1 since Drill 2 produced larger burrs on average, making it easier to observe any trends in burr

sizes related to the use of the clamp prototypes. The hand clamps were applied at the very ends of the two materials, a distance of approximately 135 mm (5.3”) apart from their centers. After all ten tests had been performed for each of the three cases, the top layer skin materials were taken to have their exit burr heights measured on the optical comparator.

The results of the tests are shown in Figure 4.12. As can be seen, the spring and the rubber prototypes both helped to significantly reduce average skin exit burr heights compared to the case of not using any additional attachment on the hand drill. Consequently, it can be concluded that the clamping force provided by the pushing concept is beneficial in reducing the sizes of interlayer burrs. Even if traditional clamping methods such as hand clamps and clecos continued to be used, the additional force provided by the attachment would still provide a further burr reducing contribution.

One possible disadvantage to the single-sided clamping idea is that a larger operator force would be required to feed the drill through the workpiece at the same rate, since additional operator force would be needed for clamping. Alternatively, an operator pressing with the same force as without the attachment would result in the drill feeding through the workpiece at a slower rate, requiring slightly more time per hole. However, it is important to remember that the ultimate goal of having an improved clamping system is to save significant time by eliminating the need for destacking the layers and deburring the holes.

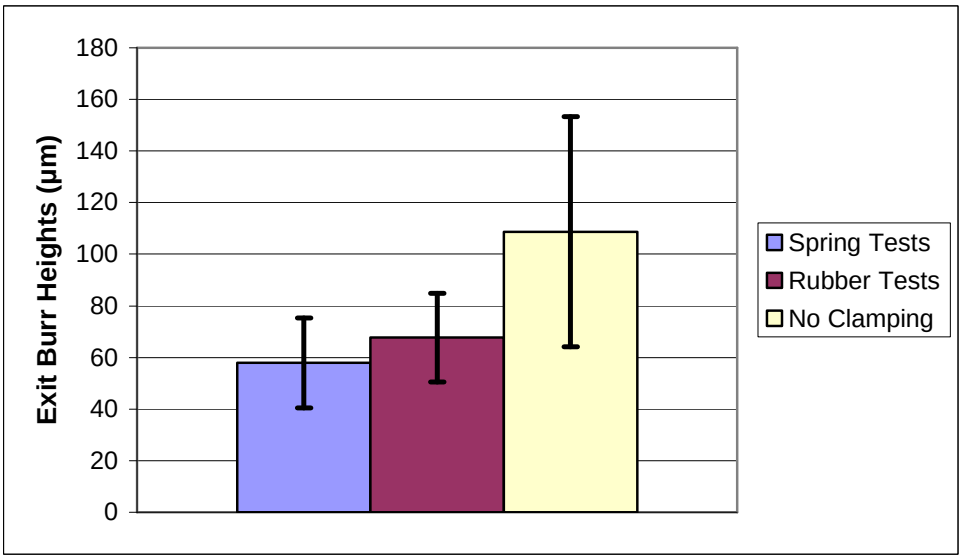

Figure 4.12: Clamping concept skin exit burr height results

4.7 Summary

It was desired to create a new method of clamping capable of reducing the sizes of interlayer burrs between sheet metal layers in industrial situations. First, ideal clamping attributes were identified such as the ability to provide a large clamping force around the entire vicinity of the hole being drilled as well as a high level of practicality and ease of use. Multiple ideas for new clamping systems were then brainstormed and evaluated based on the ideal attributes previously identified. One idea, utilizing a compressible fixture to press on the workpiece from one side, was then selected and prototyped with two different methods, one using a spring and one using a compressible piece of rubber. The two prototypes were then tested and shown to both reduce the resulting interlayer burr heights.

CHAPTER V

ANALYTICAL MODEL FOR INTERLAYER BURR FORMATION

5.1 Goal and Approach

The previous two chapters detailed efforts to reduce the sizes of interlayer burrs both through experimentation on the effects of drill geometries and through design of improved sheet metal clamping methods. This chapter describes the work done to further reduce interlayer burr sizes through an analytical model of interlayer burr formation. The goal was to create a mathematical model capable of predicting interlayer exit burr heights as a function of the various drilling parameters and conditions. From this model, the effects of the different conditions could be better understood, and ideal conditions for minimizing interlayer burr heights could be identified.

The first step in creating the model was to identify previous models for predicting exit burr heights in a single layer. The assumptions for these models were then identified, and one was selected as the most applicable for the aluminum material used in this study based on high speed videos taken of the burr formation process. This model was then modified to take into account the effect of having a second layer beneath it. The completed model was then compared to experimental results.

5.2 Analysis of Previous Models

Two analytical models of drilling exit burr heights have been reported and were discussed in section 2.4.6. Both models take various drilling parameters as inputs and output the resulting exit burr height. One of the models was created by Kim [36] and uses an energy balance equation to predict the burr initiation height (t_0 in Figure 2.9(a)) based on the various drill geometry and drilling parameters. After the burr initiation point is determined, the burr is formed via the process illustrated in the figure. The remaining material beneath the drill tip (chisel edge) is plastically deformed into a crown burr, and the sides of the crown burr stretch out until they break, forming the final exit burr height.

The second analytical drilling model, developed by Sofronas [34], is similar in that it uses an energy balance equation to determine the burr initiation height (y_1 in Figure 5.1). More specifically, the point is found at which the downward thrust force of the drill is equal to the force required to plastically deform the remaining material into a burr. However, as opposed to the Kim model, burr initiation is assumed to occur after the chisel edge of the drill has broken through the material rather than before. This model by Sofronas also builds off of an analytical drilling force model by Williams [35], which predicts the cutting forces in drilling as a function of drill geometry.

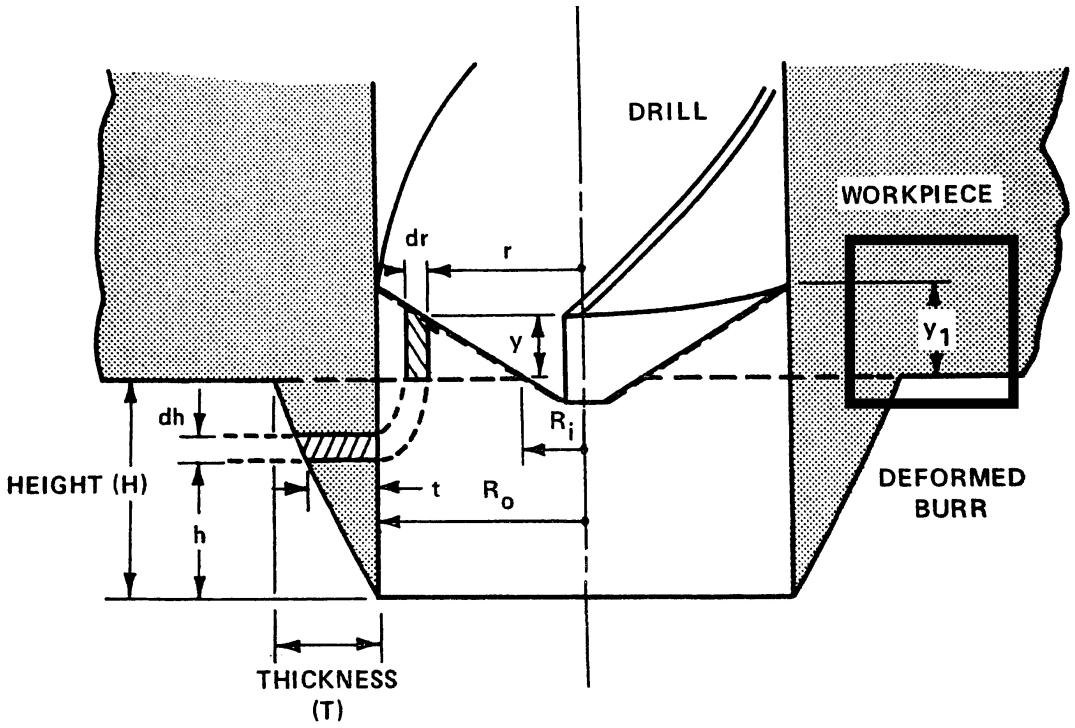

Figure 5.1: Sofronas model variables [34]

5.3 Finding Appropriate Model

Based on the assumptions made by the two models, one model needed to be selected as the most applicable for the aluminum sheet metal used in this study. The Kim model assumed that burr initiation begins before the drill tip has exited the workpiece, whereas the Sofronas model assumed that the tip exits first. Consequently, the Kim model assumed a more ductile material than the Sofronas model.

In order to better understand the mechanics of burr formation in the Aluminum 2024-T3 sheet metal used, it was decided to take high speed videos of the burr formation process. The tests were performed with Drill 2 from Chapter 2 but without the split point (118° point angle, 20° helix angle, black oxide coating, no step). The parameters were

kept the same as well, with a speed of 4500 rpm and a feed rate of 18 in/min (457 mm/min) or 0.004 in/rev (0.1016 mm/rev). The videos were taken at a rate of 7000 frames per second. Some videos were taken from the side of two workpieces clamped together at both close and far clamping distances (25 mm from hole and 70 mm from hole each, respectively) in order to gain a better understanding of the interlayer burr formation process. Some videos were also taken from underneath a single layer to better see the regular exit burr formation process and then used for comparison with the exit burr formation processes described by the two models.

Images from the high speed videos of skin exit burr formation in a single layer are shown in Figure 5.2. In the figure, the camera is pointed at an upward angle from underneath the single sheet metal layer, such that the chisel edge of the drill can be seen breaking through the bottom. After observation of the videos, it was apparent that rather than the final burr shape forming as a result of a crown burr, as in the Kim model, the final burr shape begins to form as a result of material being bent after the tip of the drill begins to break through, similar to that assumed in the Sofronas model. One observed difference from the Sofronas model was that a jagged burr formed as opposed to a uniform burr around the hole. However, this only further verified the applicability of the Sofronas model due to the fact that jagged burrs are formed as a result of low ductility materials, which the model assumes.

Although this might seem to invalidate the burr height results of the model for this case, it was assumed that the Sofronas model results, rather than predicting the uniform height, could be used to predict the maximum burr heights of the jagged burrs.

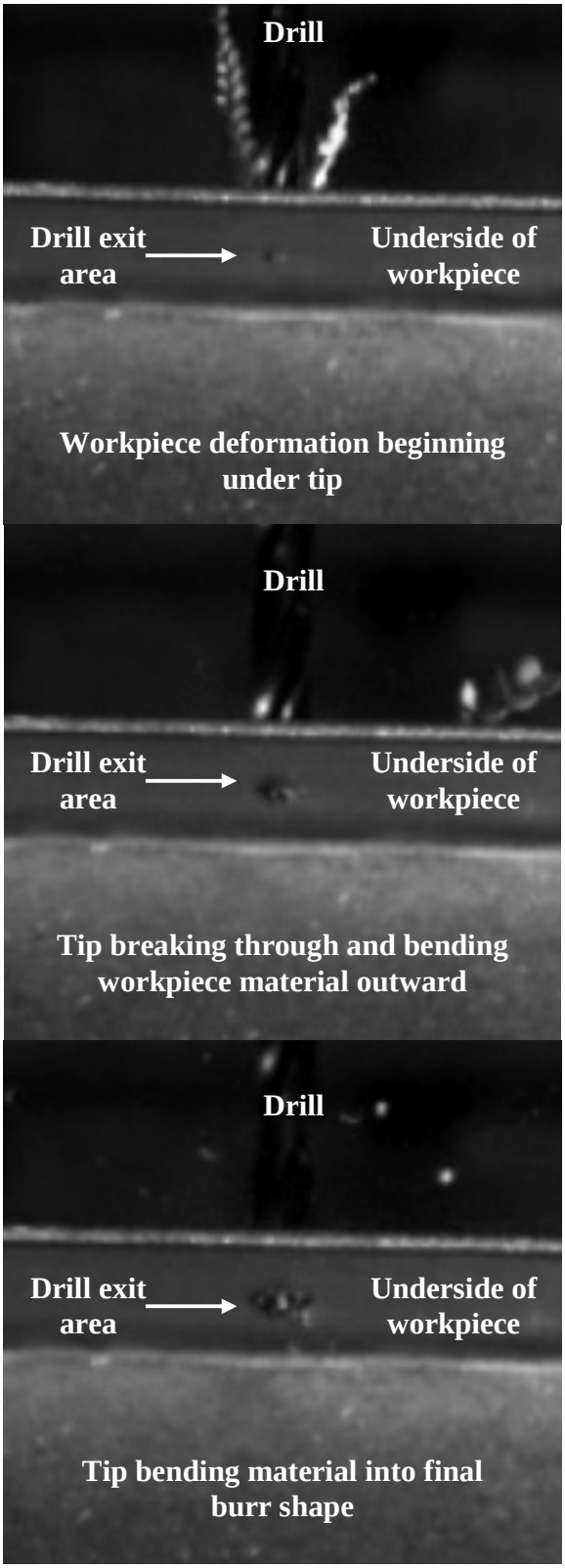

Figure 5.2: High speed video captures of exit burr formation in single aluminum layer

In addition to stating that the drill tip breaks through the workpiece before burr initiation, the Sofronas model makes other assumptions such as stating that chips form in the same manner as in oblique cutting and that no material is cut after burr initiation. The material is also assumed to be homogeneous, isotropic, rigid, perfectly plastic, and incompressible. The assumptions that are made by the William's model for drilling forces [35], which is used by Sofronas, include the cutting velocity being normal to the cutting edge, the main cutting edge being straight, and the feed velocity being negligible.

5.4 Sofronas Model Derivation

For the sake of completeness, Sofronas' exit burr height model [34], which forms the basis for the interlayer burr height model in this thesis, is summarized here. The Sofronas model for predicting exit burr heights is divided into two parts. In the first part, the initiation height y_1 at which the burr begins to form is determined. This parameter is illustrated above in Figure 5.1. Next, the geometry of the remaining workpiece material underneath the drill at burr initiation is used to determine the final burr height and thickness as a result of plastic deformation, as shown in Figure 2.8.

5.4.1 Finding Burr Initiation Height

The burr initiation height y_1 is found through an energy balance equation. It is assumed that burr initiation begins when the power input due to the drilling force vector and its velocity is equivalent to the power required to shear the supporting slab of material. An

illustration of this slab along with the various parameters used is shown in Figure 5.3. Thus, the governing equation for finding the initiation height is:

$$\vec{F} \cdot \overrightarrow{V_{drill}} = \tau_{\omega} \left|\vec{A}\right| \left|\Delta \overrightarrow{v_{slab}}\right|$$

where $\vec{F}$ is the total drilling force vector, τ_{ω} is the material shear strength, and $\left|\vec{A}\right|$ is the magnitude of area needed to be sheared. However, the drill velocity vector $\overrightarrow{V_{drill}}$ and the relative velocity of the sheared slab material $\left|\Delta \overrightarrow{v_{slab}}\right|$ are the same, such that:

$$F = \tau_{\omega} \left|\vec{A}\right| \tag{5.1}$$

where F is the scalar magnitude of force in the direction of the slab's motion. The magnitude of area will be derived first, followed by the force magnitude.

The total sheared area can be created with the vectors $\vec{V}_1$, $\vec{V}_2$, $\vec{V}_1$*, and $\vec{V}_2$*, where x_1* and z_1 are other parameters that will be determined by the analysis in addition to y_1, and β is the drill's point angle

$$\vec{V}_1 = (y_1 \tan\beta)\hat{i} + (-y_1)\hat{j}$$
$$\vec{V}_2 = (x_1^*)\hat{i} + (-y_1)\hat{j} + (-z_1)\hat{k}$$

The area of the plane formed by $\vec{V}_1$ and $\vec{V}_2$ is:

$$\overrightarrow{A_{12}} = \frac{1}{2}\vec{V}_1 \times \vec{V}_2$$

which results in a magnitude of:

$$\left|\overrightarrow{A_{12}}\right| = \frac{y_1}{2}\sqrt{\left[x_1^{*2} + z_1^2\left(1+\tan^2\beta\right)\right] - 2x_1^* y_1 \tan\beta + y_1^2 \tan^2\beta}$$

The vectors $\vec{V}_1$* and $\vec{V}_2$* can be related to $\vec{V}_1$ and $\vec{V}_2$ through geometry, and the area of the plane formed by $\vec{V}_1$* and $\vec{V}_2$* can be found:

$$\vec{V}_1^* = \left(\frac{y_1 - d}{y_1}\right)\vec{V}_1$$

$$\vec{V}_2^* = \left(\frac{y_1 - d}{y_1}\right)\vec{V}_2$$

$$\left|\vec{A}_{12}^*\right| = \left(\frac{y_1 - d}{y_1}\right)^2 \left|\vec{A}_{12}\right|$$

The third area is bounded by $\vec{V}_2$ and $\vec{V}_2^*$ and can be found using the additional vectors:

$$\vec{V}_y = (-y_1)\,\hat{j}$$

$$\vec{V}_y^* = \left[-(y_1 - d)\right]\hat{j}$$

The area and its magnitude are then calculated as:

$$\overrightarrow{A_{22}} = \frac{1}{2}\left(\vec{V}_y \times \vec{V}_2 - \vec{V}_y^* \times \vec{V}_2^*\right)$$

$$\left|\vec{A}_{22}\right| = \frac{y_1}{2}\left[1 - \left(\frac{y_1 - d}{y_1}\right)^2\right]\sqrt{z_1^{\,2} + x_1^{*2}}$$

The following dimensionless parameters are then substituted into the equations:

$$\delta = \frac{x_1^*}{y_1}$$

$$\gamma = \frac{z_1}{y_1}$$

$$\varepsilon = \frac{f}{2y_1} \qquad \text{where } f = \text{feed per revolution}$$

The final area summation term is then written as:

$$\left|\vec{A}\right| = \frac{{y_1}^2}{2}\left[\delta^2 + \gamma^2\left(1+\tan^2\beta\right) - 2\delta\tan\beta + \tan^2\beta\right]^{\frac{1}{2}}\left[1+\left(1-\varepsilon\right)^2\right] + \frac{{y_1}^2}{2}\left[1-\left(1-\varepsilon\right)^2\right]\left(\gamma^2+\delta^2\right)^{\frac{1}{2}} \tag{5.2}$$

Next, the scalar magnitude of force in the direction of the slab's motion is derived. According to the parameters in Figure 5.3, the drilling force vector can be expressed as:

$$\vec{F} = \left(-F_{xy}\cos\beta\right)\hat{i} + \left(-F_{xy}\sin\beta\right)\hat{j} + \left(-F_z\right)\hat{k}$$

Taking the dot product of this force with a unit vector in the direction of $\vec{V}_2$ (the direction of the slab's motion) results in the scalar force value *F*:

$$F = \frac{-F_{xy}\left(x_1 * \cos\beta - y_1\sin\beta\right) + F_z z_1}{\left(x_1 *^2 + {y_1}^2 + {z_1}^2\right)^{\frac{1}{2}}} \tag{5.3}$$

Equation (5.3) can also be simplified with the use of the following relationship between F_{xy} and F_z derived by Williams [35]:

$$F_{xy} = F_z\tan\left(\lambda - \upsilon\right) \tag{5.4}$$

where λ is the drill's friction angle, and υ is the normal rake angle. λ and υ were found for use in the model using these other expressions given by Williams [35], where *H* is the helix angle and *q* is the ratio of the drill's web thickness to diameter, which can be easily measured with a microscope:

$$\tan\upsilon = \frac{\left(1-q^2\sin^2\beta\right)\tan(H)}{\left(1-q^2\right)^{\frac{1}{2}}\sin\beta} - \frac{q\cos\beta}{\left(1-q^2\right)^{\frac{1}{2}}}$$

$$\lambda \simeq \frac{\pi}{6} + \frac{\upsilon}{2}$$

Equations (5.2) and (5.3) are next plugged into Equation (5.1) and simplified with the use of Equation (5.4) and the dimensionless parameters to obtain the following equation:

$$\frac{F_z}{\tau_\omega {y_1}^2} = \frac{\left(\delta^2+\gamma^2+1\right)^{\frac{1}{2}}\left[\delta^2+\gamma^2\left(1+\tan^2\beta\right)-2\delta\tan\beta+\tan^2\beta\right]^{\frac{1}{2}}\left[1+\left(1-\varepsilon\right)^2\right]}{2\gamma-2\left[\tan\left(\lambda-\upsilon\right)\right]\left(\delta\cos\beta-\sin\beta\right)} + \frac{\left[1-\left(1-\varepsilon\right)^2\right]\left(\gamma^2+\delta^2\right)^{\frac{1}{2}}}{2\gamma-2\left[\tan\left(\lambda-\upsilon\right)\right]\left(\delta\cos\beta-\sin\beta\right)} \tag{5.5}$$

The following expression which relates the cutting force to the drill geometry was also found by Williams:

$$\frac{F_z}{\tau_\omega {y_1}^2} = \left(\varepsilon\tan\beta\right)\left[\frac{\cos\left(\lambda-\upsilon\right)}{\sin\phi\cos\left(\phi+\lambda-\upsilon\right)}\right] \tag{5.6}$$

$$\text{with } \phi = \frac{\pi}{4}+\frac{\upsilon-\lambda}{2}$$

Putting together Equations (5.5) and (5.6) results in two equations with four unknowns, ε, γ, δ, and $\xi = \frac{F_z}{\tau_\omega {y_1}^2}$. Two additional equations are attained by stating that δ and γ should be adjusted to result in a minimum value for ξ:

$$\frac{\partial\xi}{\partial\delta} = 0 \tag{5.7}$$

$$\frac{\partial\xi}{\partial\lambda} = 0 \tag{5.8}$$

Equations (5.5), (5.6), (5.7), and (5.8) are then solved with a computer solution which uses the following steps:

1. Ranges of values are assigned to γ, ε, and δ until a minimum value is found for the right side of Equation (5.5). The corresponding value of δ (and consequently x_1*) is then finalized.
2. With the values of δ and ε used to find the minimum in the previous step, γ is then varied until a minimum is attained, and this value of γ (and consequently z_1) is recorded.
3. δ and γ are then plugged into Equation (5.5), and the value of ε is varied until the right sides of Equations (5.5) and (5.6) are equalized, resulting in the final value of ε.
4. The initiation height y_1 is then found as $\boxed{y_1 = \frac{f}{2\varepsilon}}$.

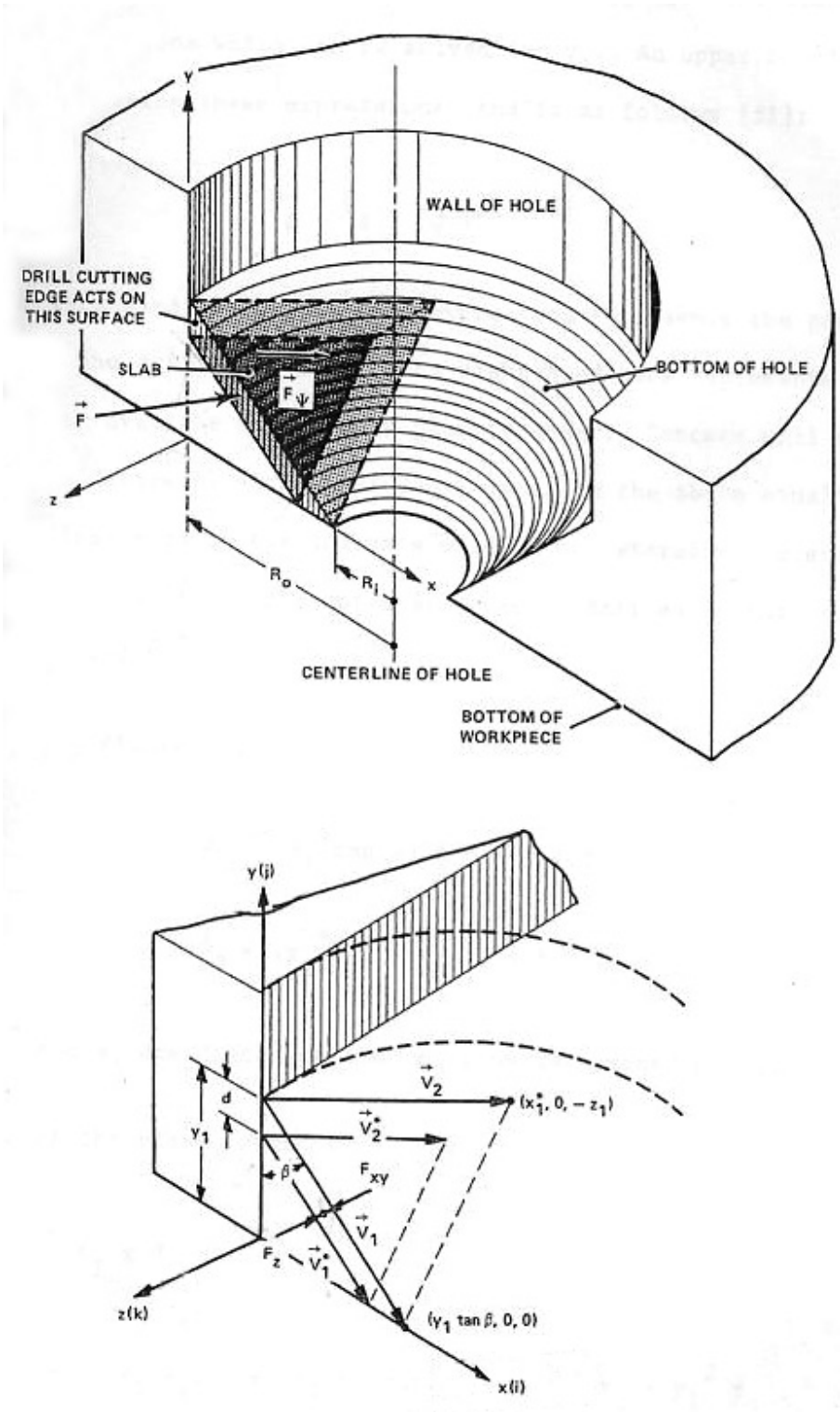

Figure 5.3: Sofronas initiation height parameters [34]

5.4.2 Finding Final Burr Geometry

After the burr initiation height is found, it is assumed that no additional material is cut, and that all of the remaining material is bent downwards into the final exit burr shape. Referring to the parameters in Figure 5.1, the assumption of no volume change results in:

$$2\pi r y \mathrm{d}r = 2\pi R_0 t \mathrm{d}h \tag{5.9}$$

Rearranging and putting in logarithmic form results in:

$$\ln\frac{R_0}{r} + \ln\frac{dh}{dr} + \ln\frac{t}{y} = 0 \tag{5.10}$$

which is equivalent to:

$$\varepsilon_\theta + \varepsilon_r + \varepsilon_t = 0 \tag{5.11}$$

where ε_θ is the circumferential strain, ε_r is the radial strain, and ε_t is the thickness strain. The variable y can be rewritten and substituted into the equation:

$$y = \frac{r - R_i}{\tan\beta}$$

$$\ln\frac{R_0}{r} + \ln\frac{dh}{dr} + \ln\frac{t}{\left(\frac{r - R_i}{\tan\beta}\right)} = 0 \tag{5.12}$$

It is then assumed that only radial stress is present, such that $\varepsilon_\theta = \varepsilon_t$, which implies:

$$\varepsilon_r = -2\varepsilon_\theta$$

$$\ln\frac{dh}{dr} = -2\ln\frac{R_0}{r}$$

$$\frac{dh}{dr} = \left(\frac{r}{R_0}\right)^2$$

$$\int_0^h R_0^{\,2} dh = \int_{R_i}^r r^2 dr$$

$$h = \frac{r^3 - R_i^{\,3}}{3R_0^{\,2}}$$

which at its highest point $r = R_0$, gives the final burr height H:

$$\boxed{\mathrm{H} = \frac{R_0^{\,3} - R_i^{\,3}}{3R_0^{\,2}}} \tag{5.13}$$

where $R_i = R_0 - y_1 \tan\beta$ through geometry

The final burr thickness is then found by recalling that:

$$\varepsilon_\theta = \varepsilon_t$$

$$\ln\frac{R_0}{r} = \ln\frac{t}{\left(\frac{r - R_i}{\tan\beta}\right)}$$

$$\frac{R_0}{r} = \frac{t}{\left(\frac{r - R_i}{\tan\beta}\right)}$$

$$r = \frac{R_0 R_i}{R_0 - t\tan\beta} \tag{5.14}$$

Plugging this value of r into the equation $h = \frac{r^3 - R_i^{\,3}}{3R_0^{\,2}}$ and solving for t results in:

$$t = \frac{R_0}{\tan\beta}\left[1 - \left(\frac{R_i^{\,3}}{3R_0^{\,2}h + R_i^{\,3}}\right)^{\frac{1}{3}}\right] \tag{5.15}$$

Substituting in h = H and t = T results in:

$$\boxed{\mathrm{T} = \frac{R_0 - R_i}{\tan\beta} = y_1} \tag{5.16}$$

5.5 New Model Assumptions

After deciding that the interlayer burr formation model should be built upon the Sofronas model for regular burr formation, it was necessary to make assumptions about the effect of the second layer's presence on the formation of the first layer's exit burr. Figure 5.4 shows screen captures from the high speed videos of two-layered drilling taken from the side. The first image shows the drill performing steady state cutting through the first layer with the two layers both slightly bent downwards and pressed together due to the drilling thrust force. The second image is from the instant after the chisel edge of the drill has already broken through the first layer and is cutting through the second layer. Separation between the two layers can be seen due to the fact that the first layer sprung back up as the drill exited it, while the second layer remains slightly bent downwards due to the thrust force.

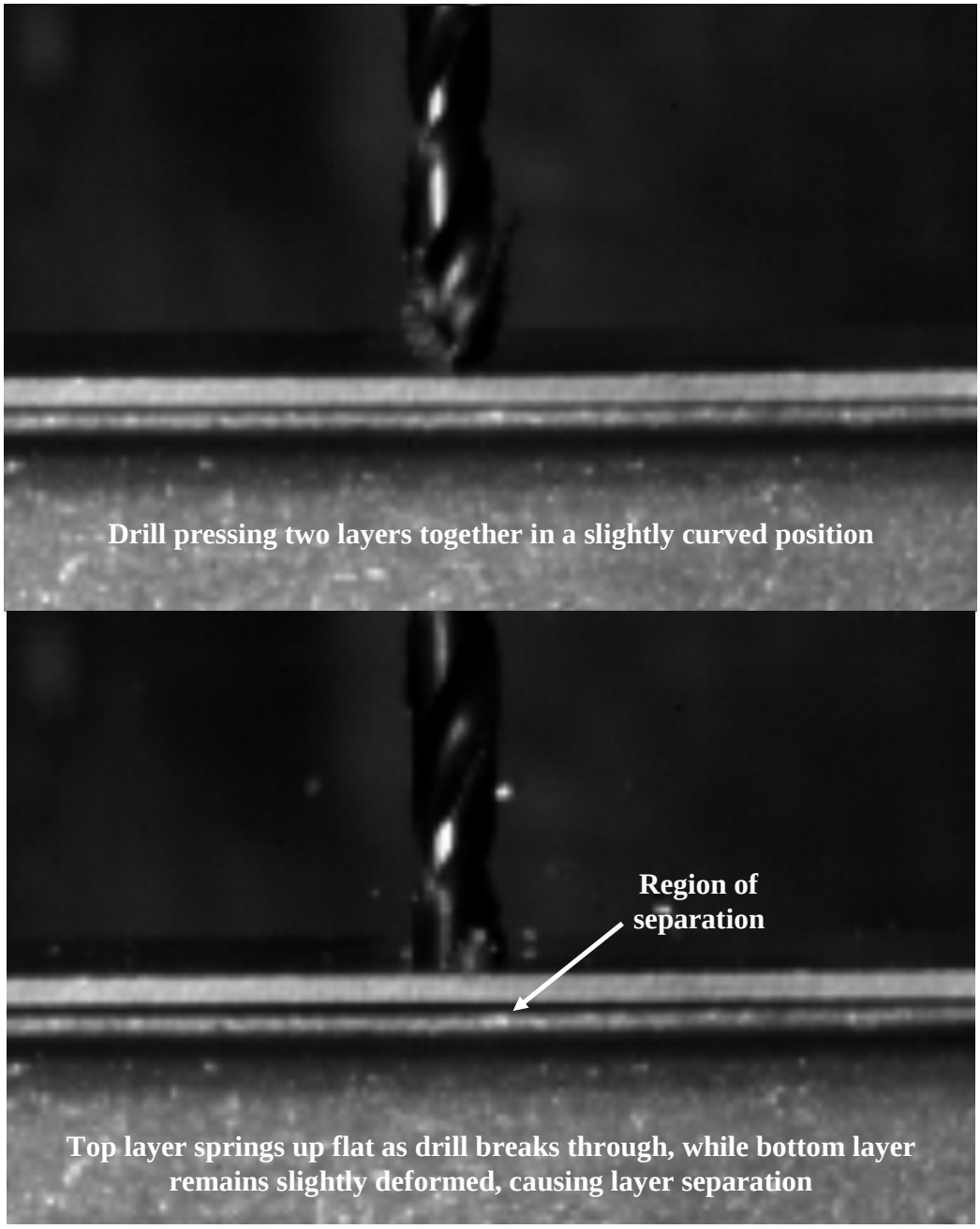

Figure 5.4: High speed captures of interlayer formation

Based on these observations, the following assumptions were proposed for construction of the interlayer burr formation model. At the point of burr initiation (the point at which the material underneath the drill chisel edge becomes plastically deformed

into the exit burr), the two layers are still pressed together and remain in contact as in the first image of Figure 5.4. Consequently, at this burr initiation point, the elastic force required to bend the second layer downwards acts upwards on the bottom side of the burr about to be formed, reducing the burr initiation height. In other words, the presence of the second layer pressing against the bottom of the first layer increases the amount of first-layer material that gets cut by the drill and reduces the amount of material that gets bent down into a burr. This concept is illustrated in Figure 5.5. The first drawing shows the single-layer initiation point y_1 of the Sofronas model, while the second drawing shows the reduced initiation point y_2 of the new interlayer model. The second drawing also shows the force required to deform the second layer which acts against the forming burr and reduces its initiation height.

Immediately after this initiation point, it is assumed that the burr is allowed to form freely without any interference from the second layer due to the first layer springing upwards. This makes sense considering that, for geometrical reasons, the plastic deformation of the burr material must take place either during or before the top layer springs upwards. Consequently, the second half of the Sofronas model, which uses geometry to predict how the material underneath the drill tip at burr initiation will form into its final shape is still valid. Therefore, the only change from the Sofronas model to this model is the reduced burr initiation height due to the presence of the second layer.

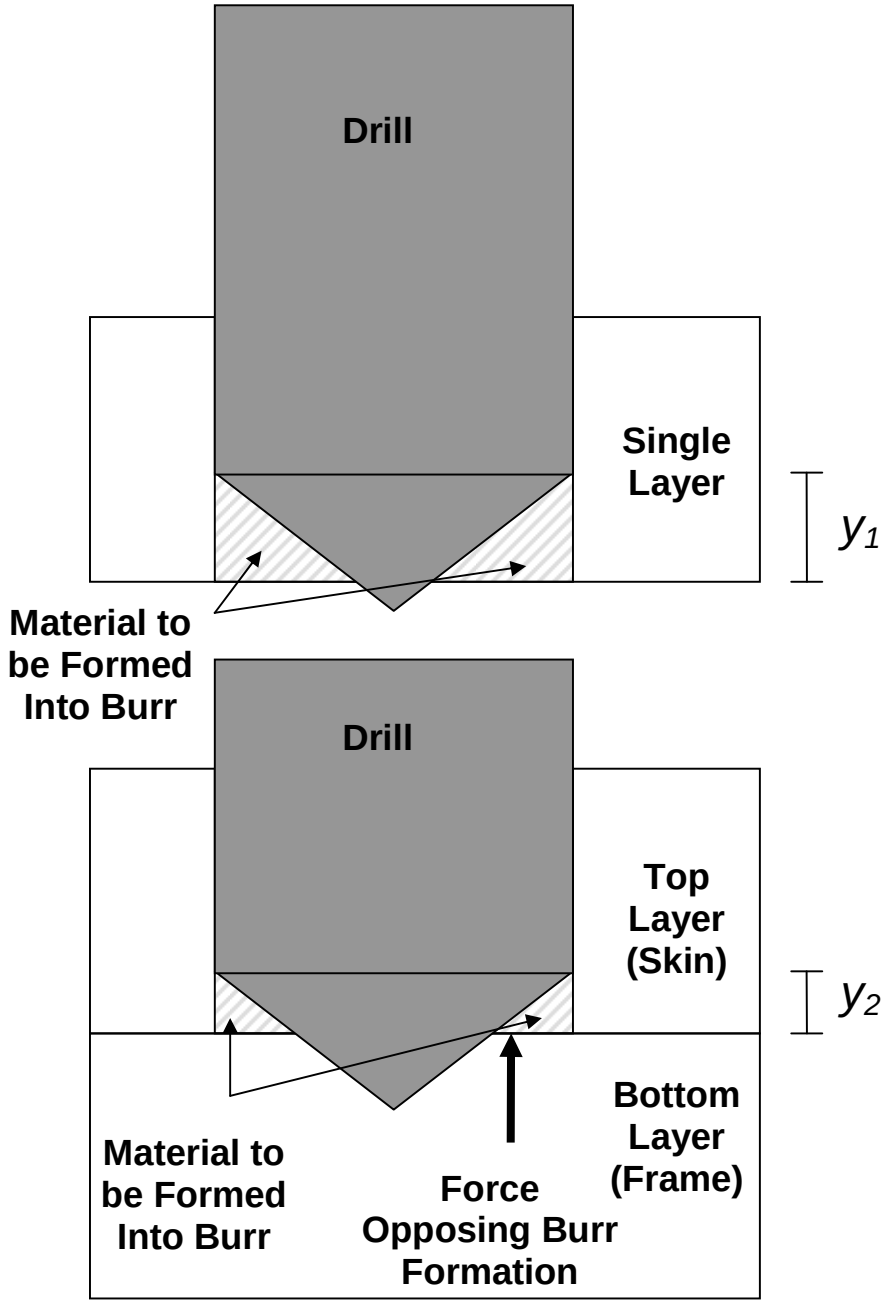

Figure 5.5: Sofronas model initiation point and new model initiation point

5.6 New Model Calculations

From the Sofronas model, the initiation height y_1 was found from the following equation [35]:

$$\frac{F_z}{\tau_\omega y_1^2} = \varepsilon \tan\beta \left[\frac{\cos(\lambda - \upsilon)}{\sin\phi \cos(\phi + \lambda - \upsilon)} \right] = A \tag{5.17}$$

where F_z is the cutting force of the drill, τ_ω is the shear flow stress of the workpiece material, β is half the point angle of the drill, φ is the chip shear plane angle, λ is the friction angle, υ is the normal rake angle, and ε is the ratio of the drill feed to the initiation height. For simplicity in future calculations, the entire right hand side of this equation was defined as *A*.

From equation (5.11) above,

$$y_1 = \sqrt{\frac{F_z}{A\tau_\omega}} \tag{5.18}$$

From the drill geometry, Sofronas derived the following expression relating the cutting force F_z to the thrust force F_{thrust}:

$$F_z = \frac{F_{thrust}}{\sin\beta \tan(\lambda - \upsilon)} = BF_{thrust} \tag{5.19}$$

$$\text{with } B = \frac{1}{\sin\beta \tan(\lambda - \upsilon)}$$

Combining equations (2) and (3):

$$y_1 = \sqrt{\frac{BF_{thrust}}{A\tau_\omega}} \tag{5.20}$$

Next, the initiation height equation in (4) was modified to include the fact that a certain percentage of the force of deforming the second layer opposes the thrust force in

determining the burr initiation height. Recall that the initiation point is determined as the point at which the drilling thrust force is equal to the force required to plastically shear the remaining material under the drill. In other words, the term F_{thrust} in equation (4) can be thought of as the net force required to shear the burr material underneath it. Therefore, for the new interlayer model, the term cF_d was subtracted from F_{thrust}, where F_d is the force required to deform the second layer downward and c is the percentage of the elastic deformation force of the second layer that acts against the forming burr to reduce the initiation height. Consequently, the equation for the new interlayer initiation height was calculated as follows:

$$y_2 = \sqrt{\frac{B(F_{thrust} - cF_d)}{A\tau_\omega}} = \sqrt{\frac{BF_{thrust}}{A\tau_\omega} - \frac{BcF_d}{A\tau_\omega}} = \sqrt{y_1^2 - \frac{BcF_d}{A\tau_\omega}} \tag{5.21}$$

where c is the percentage of the elastic deformation force of the second layer that acts against the forming burr to reduce the initiation height.

From this new initiation height, the final geometry of the burr is calculated in the same way as in the second half of the Sofronas model, which assumes no volume change and negligible circumferential stress. The equation for the final interlayer exit burr height is therefore the same as Equation (5.9) but with the new initiation height, and is given as:

$$H = \frac{R^3 - (R - y_2 \tan\beta)^3}{3R^2} \tag{5.22}$$

where R is the radius of the drilled hole.

5.7 Possible Model Completion Methods

From Equation (5.16), all that is needed to find the interlayer burr height is the new burr initiation height, y_2. From Equation (5.15), the only term needed to find y_2 is cF_d, where F_d is the force required to deflect the second layer downwards during drilling, and c is the percentage of this force that acts against the forming burr to reduce its initiation height.

One possible method for determining cF_d is to calculate each term individually. F_d could be calculated experimentally by deflecting a single sheet metal layer to different displacement values while simultaneously using a dynamometer to measure the amount of force required to do so and using a deflection gauge to measure the amount of workpiece deflection. A relationship could then be established between workpiece deflection and deflection force for any given material. Then, for any set of drilling conditions, the amount of workpiece deflection during drilling could be measured and used to find F_d. The value of c could then be found either through the use of an analytical model or a finite element model.

Alternatively, the entire term cF_d could be calibrated through the use of experimental data. For any set of experimental conditions, all of the terms in Equation (5.15) could be calculated except for cF_d and y_2. However, any interlayer burr height resulting from the experiments could be used to calculate its burr initiation height, y_2, before formation. This could be done by rearranging Equation (5.16):

$$y_2 = \frac{R - \sqrt[3]{R^3 - 3R^2H}}{\tan\beta} \tag{5.23}$$

where H is the experimental interlayer burr exit height. Rearranging Equation (5.15), the term cF_d can then be found as:

$$cF_d = \left(y_1^{\,2} - y_2^{\,2}\right)\left(\frac{A\tau_\omega}{B}\right) \tag{5.24}$$

5.8 Calibration with Experimental Results

In order to test if the model captures the experimental trends correctly, a program was written in MATLAB to receive as inputs the various drilling parameters and to output the final interlayer burr height. This code is included in Appendix G.

In order to find a value of cF_d to complete the model, it was decided to perform calibration experiments rather than calculate the values of the terms individually. This is due to the fact that finding a precise value of c through an analytical model or a finite element simulation would require further refinement of the model that was deemed to be outside the timeline for this thesis. In addition, model calibration would allow a quick check of the ability of the model to capture the experimental trends correctly.

To calibrate the value of cF_d for the new model, it was decided to perform experimental tests at different feed values. All of the tests were performed with a drill the same as Drill 3 from Chapter 2 (135° point angle, 20° helix angle, black oxide coating, split point, no step). Drill 3 (with no step) was chosen as opposed to Drill 1 since the model is currently only applicable for drills without a step. Stacks of two layers of 1/16" (1.59 mm) thick Aluminum 2024-T3 were used as in Chapter III. A total of ten tests were performed for each of three feeds of 0.004, 0.0045, and 0.005 in/rev (0.102, 0.114, and 0.127 mm/rev) at a spindle speed of 4500 rpm. The resulting interlayer burr heights were then measured and averaged using an optical comparator. During each test

the thrust forces were recorded with a dynamometer, and the average breakthrough thrust force was calculated for each feed rate.

For each of the three cases, the respective feed rate along with the other drill geometry parameters were plugged into the MATLAB height prediction program. The average breakthrough thrust force was entered into the program as F_d, as it was assumed that the breakthrough thrust force measured by the dynamometer would be proportional to the force going into deforming the second layer downwards. The appropriate value of c was then found by trial and error such that the program would return a height value the same as that found experimentally. From the three values of c found, an average of the three was taken.

This average c value was then plugged into the MATLAB program for each of the three feed cases to get the final model predicted results. The predicted values along with the experimentally measured values and their standard deviations are shown in Figure 5.6. As can be seen, the program outputs somewhat accurate predictions for the 0.0045 and 0.005 in/rev feed rates but significantly underestimates the burr height for the 0.004 in/rev case. However, it is important to note that the model correctly predicts that burr heights will increase with higher feed values. As mentioned earlier, a more accurate model could be created by finding the term cF_d through a more detailed analytical or finite element contact model as opposed to a simple calibration model. This will be the subject of future work.

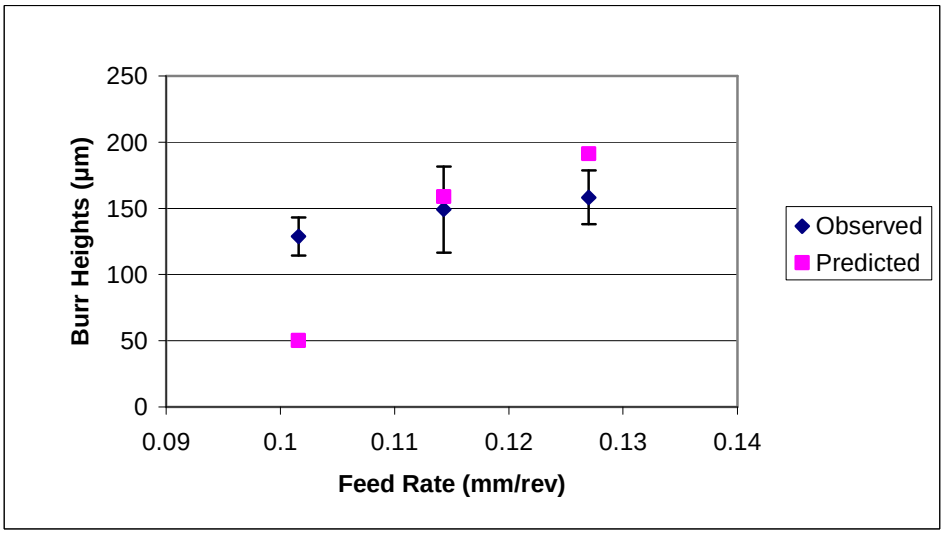

Figure 5.6: Predicted and observed values of burr heights vs. feed rates with c = 0.02594 (averaged from observed values of all three)

5.9 Summary

It was desired to create an analytical model of interlayer burr formation such that interlayer burr heights could be predicted based on the various drilling parameters and drill geometries. First, previous models of exit burr formation in single layers were analyzed, and high speed videos were taken in order to select which model was most applicable. Based on this model by Sofronas, additional assumptions regarding the geometry of interlayer burr formation were made and used to create the final burr height model. This model was then calibrated and compared to experimental results using different feed values.

Although the model did not accurately predict the interlayer burr heights in all cases, it correctly showed the direct correlation between burr heights and feed values. In order to improve the model to make accurate predictions in all cases, more work needs to

be performed to more accurately predict the term cF_d. This could perhaps be completed through the use of an analytical or a finite element model.

CHAPTER VI

CONCLUSIONS

6.1 Overview

This thesis described work done to understand burr formation in hole drilling at the interface of stacked layers of metal sheets. This is important in order to increase the structural integrity of the layers and to possibly eliminate the need for costly deburring operations. Research was performed in three different areas: experimental parameter optimization, clamping design, and analytical model derivation. The experiments were performed using three different drill geometries in order to find the geometry that minimizes interlayer burr formation and to ascertain the relationship between burr sizes and drill wear. A new clamping system for holding sheet metal layers together during drilling was designed, prototyped, and tested for its effectiveness. Finally, an analytical model was constructed for determining interlayer burr sizes as a function of the various drilling parameters.

6.2 Experimental Findings

6.2.1 Interlayer Drilling Burr Experiments

Experiments were performed using three different drill geometries, selected in order to study the effects of having different point angles and of having a step ground into the end of the drill. Each test run was performed over 1500 holes in order to observe the effects

of drill wear on the interlayer burr sizes. Measurements were periodically taken of burr heights, burr widths, drill wear, and the drilling forces. The major findings of the study were as follows:

- Burr sizes were significantly reduced with the use of a step drill (Drill 1) due to the fact that the second diameter drills away some of the burr formed from the first diameter
- Drill 1 burr sizes remained nearly constant rather than increasing with drill wear
- Burr heights were not significantly effected by drill wear in general
- Drill 1 burr sizes showed less variability than the other two geometries studied
- Drill 1 reached any given amount of wear slower than the other two drills

6.2.2 Clamping Methods Investigation

A new clamping system was designed in order to further reduce burr heights. Clamping is important in reducing interlayer burr sizes due to the fact that less separation between the layers allows less room for burrs to form. Ideal clamping attributes were identified and used to select one clamping idea out of multiple ideas brainstormed. This idea involved a circular fixture pressing the workpiece layers together from one side immediately around the area of the hole being drilled. For simplicity in use, this fixture could be attached to the drill and allowed to move relative to the drill via a spring or other compressible material. This idea was then prototyped in two different ways, which were both tested and shown to reduce burr heights relative to using only hand clamps.

6.2.3 Interlayer Burr Formation Analytical Model

It was desired to create an analytical model such that the various drilling geometries and parameters could be input and used to find the resulting burr sizes. Such a model could be used to find the optimal conditions for interlayer burr minimization and to better understand burr formation in stacked sheet metal in general. First, a previously derived model for regular exit burr formation was chosen based on high speed videos of burr formation in the Aluminum 2024-T3 used in this study. This model was then adapted to take into account the presence of a second layer based on assumptions also found using high speed videos. Comparison of the final model with experimental results showed correct correlations, but not completely accurate results, indicating a need for more work to be performed.

6.3 Future Work

More work could be performed related to all three of the interlayer burr minimization strategies detailed above: optimizing drill point geometries and clamping systems and obtaining a greater understanding of the mechanics behind the interlayer burr formation process.

In this study, it was found that a step drill minimizes interlayer burrs as well as a lower point angle. However, it was not found exactly which point angle is the best, nor were parameters such as the drill's helix angle, lip angle, relief angle, or any of the other step drill geometry parameters studied. Finding optimized drill point geometries is something that is also dependent on the workpiece material used. So the best geometry

for the Aluminum 2024-T3 used in this study would be different from that for another material, requiring more experimental studies for each material.

Clamping systems are another very important aspect in interlayer burr formation. The tighter and closer that workpiece layers can be held together in the vicinity of the hole being drilled, the less room there is for burrs to form. Technically, if layers could be held together extremely tightly at the exact hole location, they could act as a single layer, and no interlayer burr would form. Therefore, until this goal is reached, there will always be room for clamping improvements though the use of new innovative systems.

As just mentioned, in order to completely optimize drill point geometries experimentally, an extensive number of studies would need to be performed due to the large amount of variable geometry parameters and the fact that each workpiece material has different properties that affect these parameters. Consequently, it is important that an analytical model be developed that is capable of accurately predicting interlayer burr sizes without a large amount of experimentation needed. In order to accomplish this, more needs to be known about the interlayer burr formation process, and exactly what the effects are of the clamping force and the presence of the second layer on the burr formation process.

APPENDIX A

MATLAB CODE FOR DETERMINING BREAKTHROUGH THRUST AND TORQUE

```
clear all
close all
clc

directory = 'F:\Documents\Georgia Tech\Research\Measurements\Force
Measurements\Drill 1 Run 1\';

for hole = 1:9
    thrustforces = 0;  %clear variable from previous loop run
    torques = 0;
    filename = sprintf('d1r1h00%d', hole);
    loadfile = strcat(directory, filename, '.lvm');
    data = importdata(loadfile);
    time = data(:,1);  %get time from first column of .lvm file
    thrustforces = data(:,3);  %get forces from fourth column of .lvm
file
    torques = data(:,4);
    m = length(thrustforces);
    stop = 0;
    for i = 2:m-1
        if ((thrustforces(i) > 0.2) && (stop == 0)) %if drill is
beggining to make contact
            x = thrustforces((i+192):(i+218));  %then breakthrough
occurs around these points
            y = torques((i+192):(i+218));
            maxforce(hole) = mean(x);
            maxtorque(hole) = mean(y);
            stop = 1;
        end
    end
end

for hole = 10:99
    thrustforces = 0;  %clear variable from previous loop run
    torques = 0;
    filename = sprintf('d1r1h0%d', hole);
    loadfile = strcat(directory, filename, '.lvm');
    data = importdata(loadfile);
    time = data(:,1);  %get time from first column of .lvm file
    thrustforces = data(:,3);  %get forces from fourth column of .lvm
file
    torques = data(:,4);
    m = length(thrustforces);
    stop = 0;
```

```
    for i = 2:m-1
        if ((thrustforces(i) > 0.2) && (stop == 0))
            x = thrustforces((i+192):(i+218));
            y = torques((i+192):(i+218));
            maxforce(hole) = mean(x);
            maxtorque(hole) = mean(y);
            stop = 1;
        end
    end
end

for hole = 100:1500
    thrustforces = 0;  %clear variable from previous loop run
    torques = 0;
    filename = sprintf('d1r1h%d', hole);
    loadfile = strcat(directory, filename, '.lvm');
    data = importdata(loadfile);
    time = data(:,1);  %get time from first column of .lvm file
    thrustforces = data(:,3);  %get forces from fourth column of .lvm
file
    torques = data(:,4);
    m = length(thrustforces);
    stop = 0;
    for i = 2:m-1
        if ((thrustforces(i) > 0.2) && (stop == 0))
            x = thrustforces((i+192):(i+218));
            y = torques((i+192):(i+218));
            maxforce(hole) = mean(x);
            maxtorque(hole) = mean(y);
            stop = 1;
        end
    end
end

%multiply by amplfication factor to get metric units:
maxtorque = maxtorque * 50;
maxforce = maxforce * 50;

%create thrust and torque plots, find best fit lines, and display r^2
value
holes = 1:1500;
coeff1 = polyfit(holes, maxforce, 1);
bestfit1 = coeff1(1)*holes + coeff1(2);
coeff2 = polyfit(holes, maxtorque, 1);
bestfit2 = coeff2(1)*holes + coeff2(2);
plot(holes, maxforce, holes, maxtorque, holes, bestfit1, holes,
bestfit2)
[a,b,c,d] = r_squared(holes, maxforce);
a1 = num2str(a);
a2 = strcat('r^2 = ', a1);
text(500, 100, a2);
title('Breakthrough Thrust Force and Torque Vs. Hole Number');
xlabel('Hole Number');
ylabel('Breakthrough Thrust Force (N), Torque (N-cm)');
```

APPENDIX B

EXIT BURR HEIGHT RESULTS

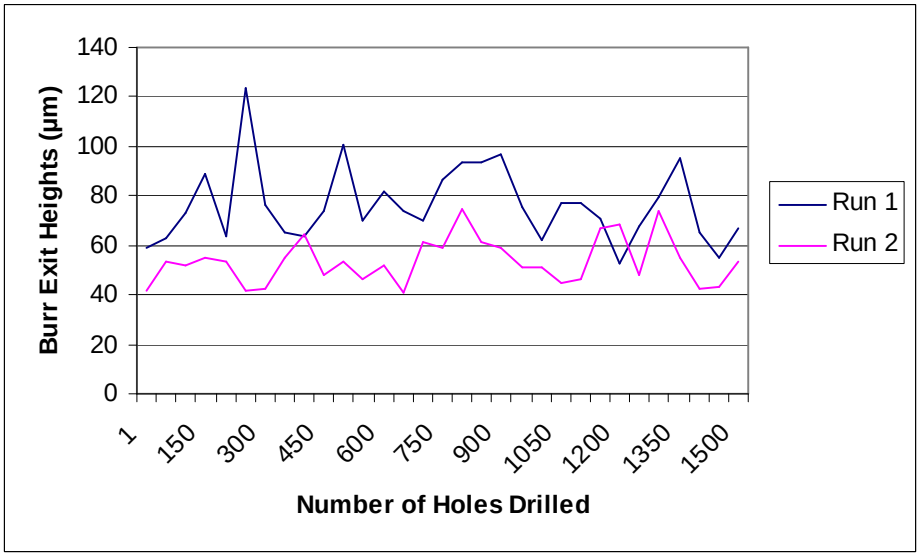

Figure B.1: Individual burr exit heights for drill 1

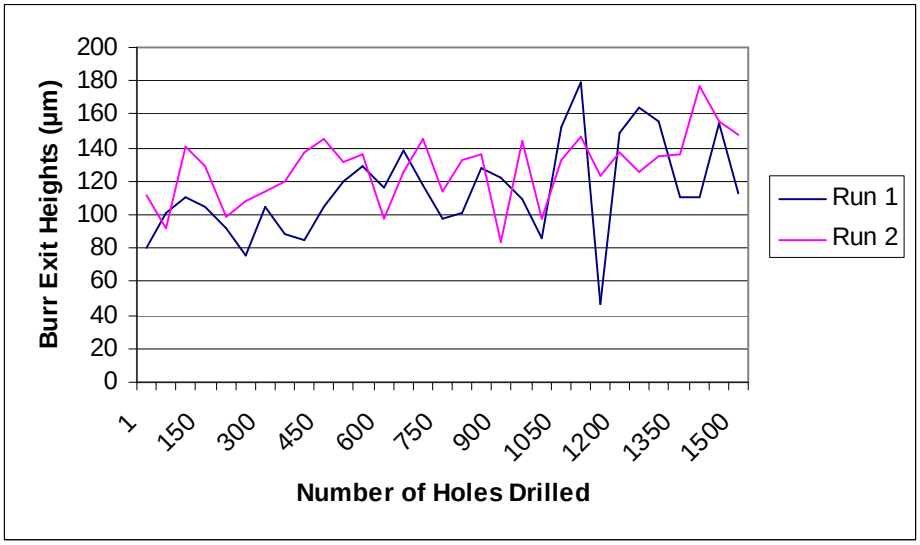

Figure B.2: Individual burr exit heights for drill 2

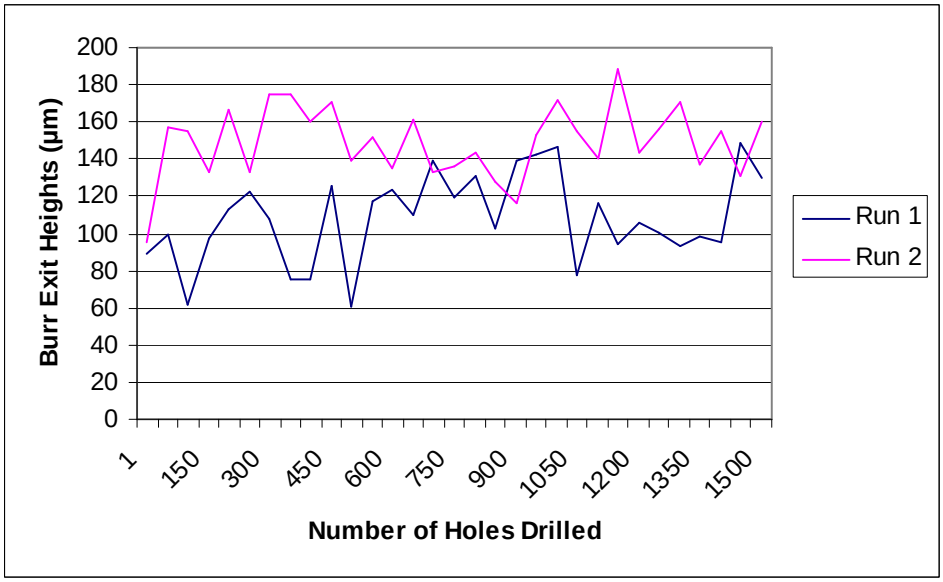

Figure B.3: Individual burr exit heights for drill 3

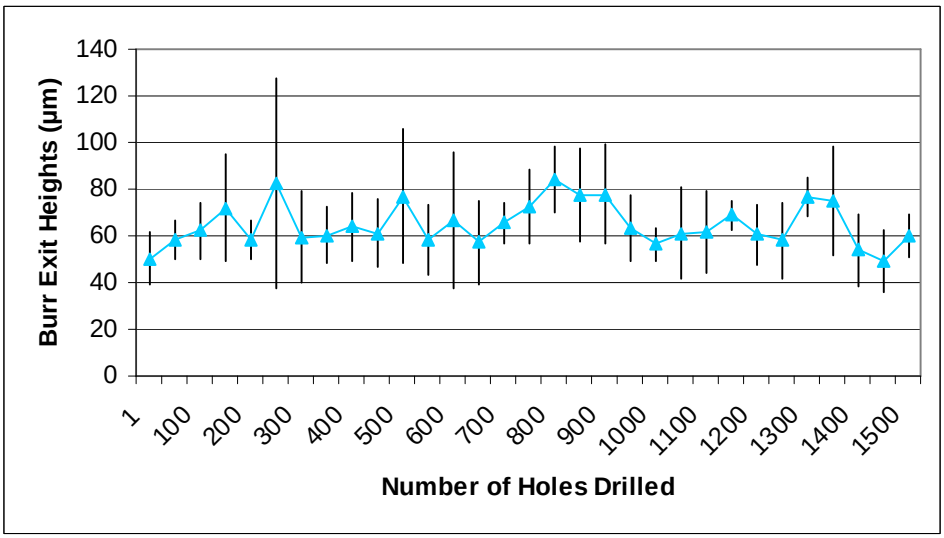

Figure B.4: Averaged burr exit heights for drill 1 (with std bars)

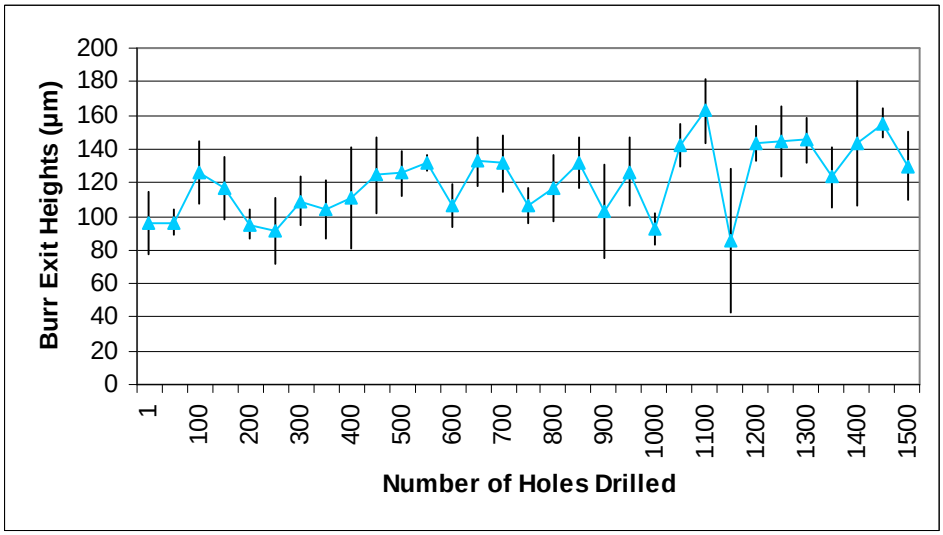

Figure B.5: Averaged burr exit heights for drill 2 (with std bars)

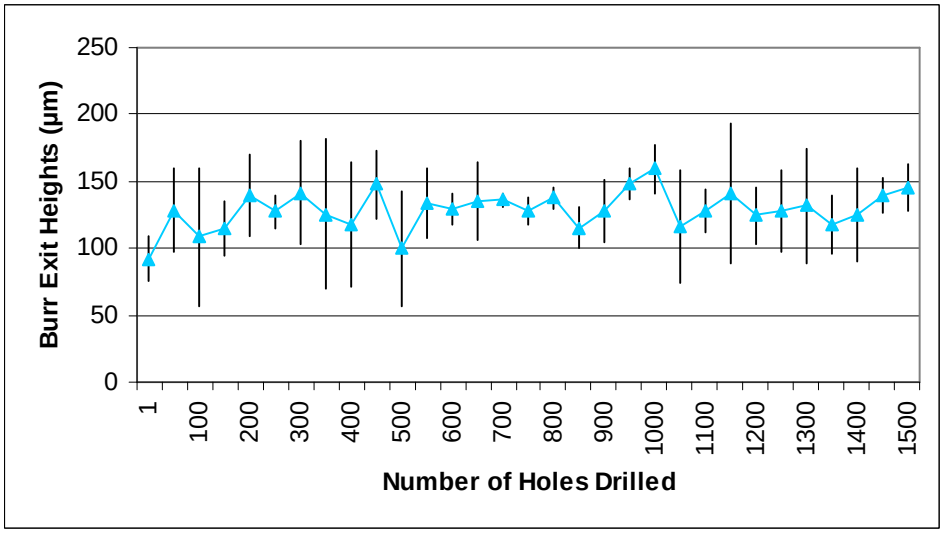

Figure B.6: Averaged burr exit heights for drill 3 (with std bars)

APPENDIX C

ENTRY BURR HEIGHT RESULTS

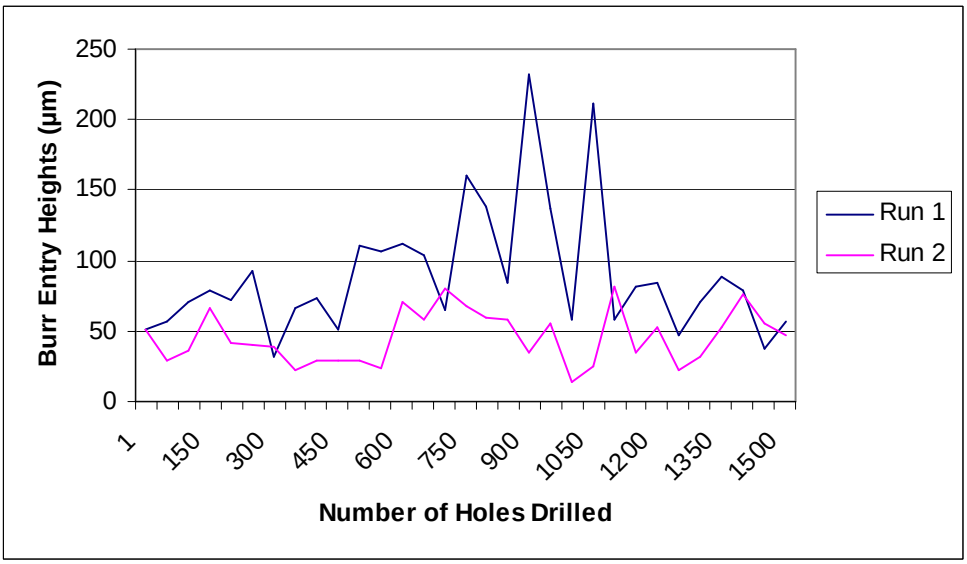

Figure C.1: Individual burr entry heights for drill 1

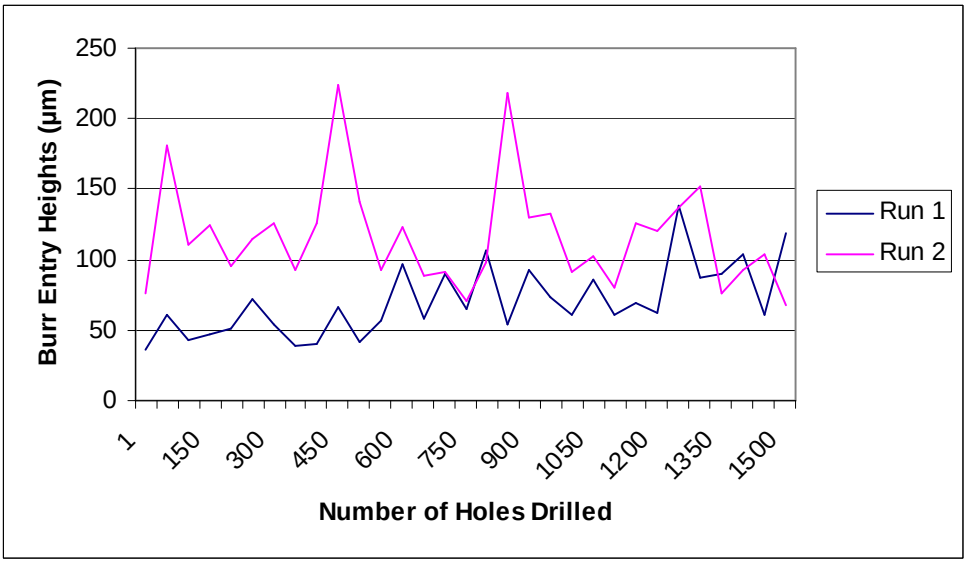

Figure C.2: Individual burr entry heights for drill 2

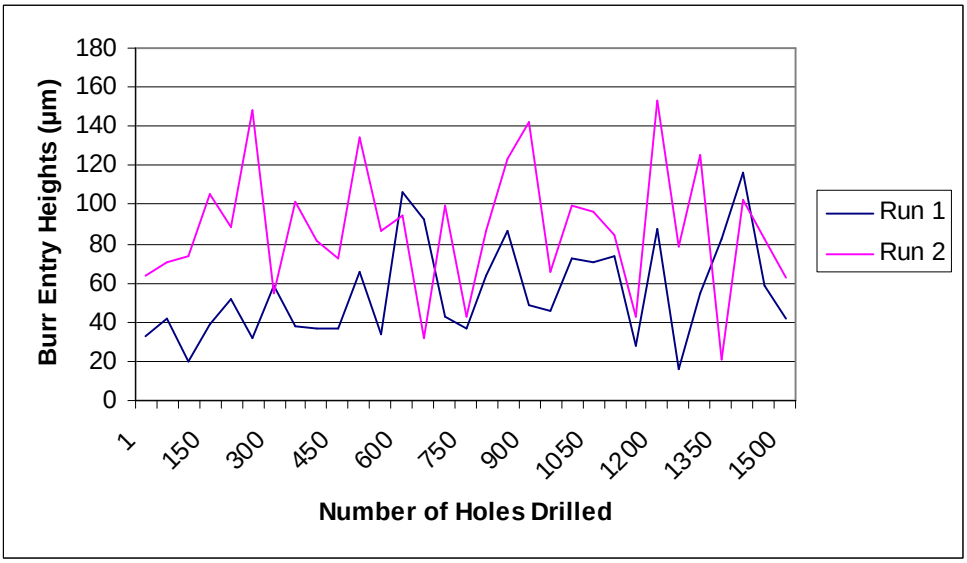

Figure C.3: Individual burr entry heights for drill 3

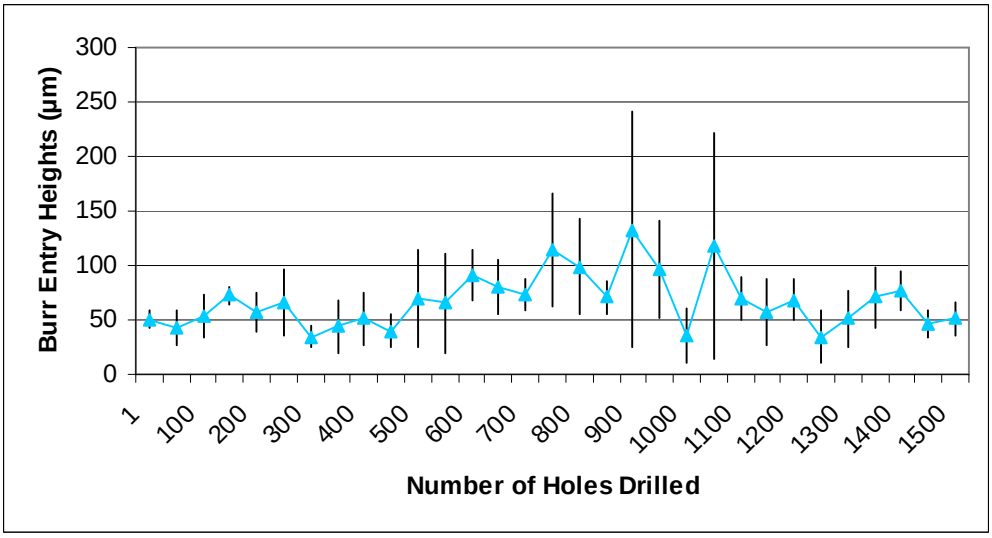

Figure C.4: Averaged burr entry heights for drill 1 (with std bars)

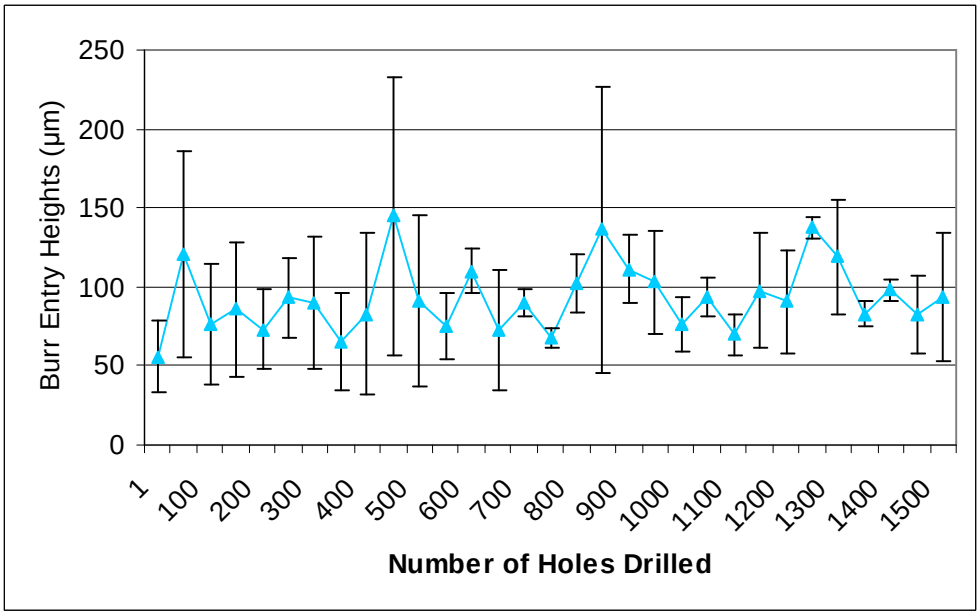

Figure C.5: Averaged burr entry heights for drill 2 (with std bars)

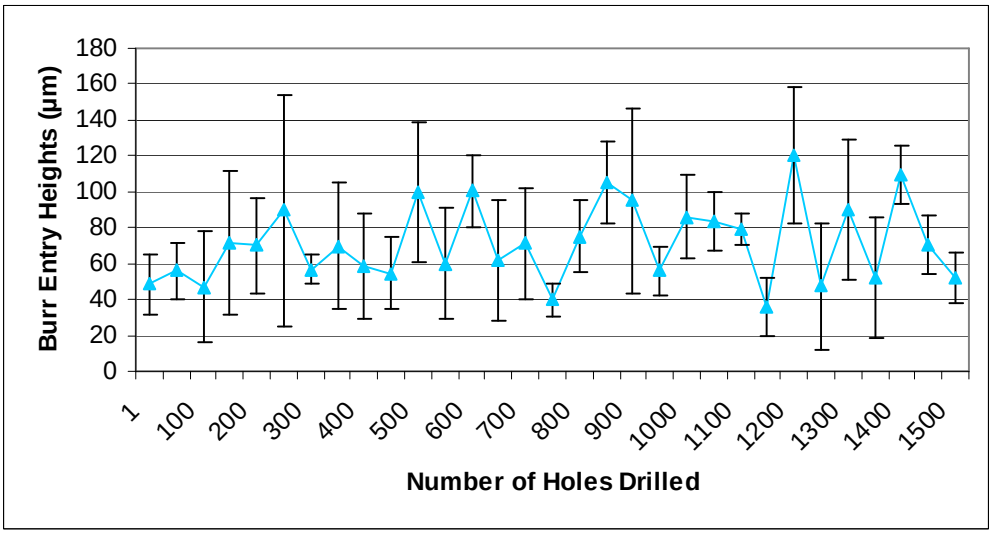

Figure C.6: Averaged burr entry heights for drill 3 (with std bars)

APPENDIX D

BURR WIDTH RESULTS

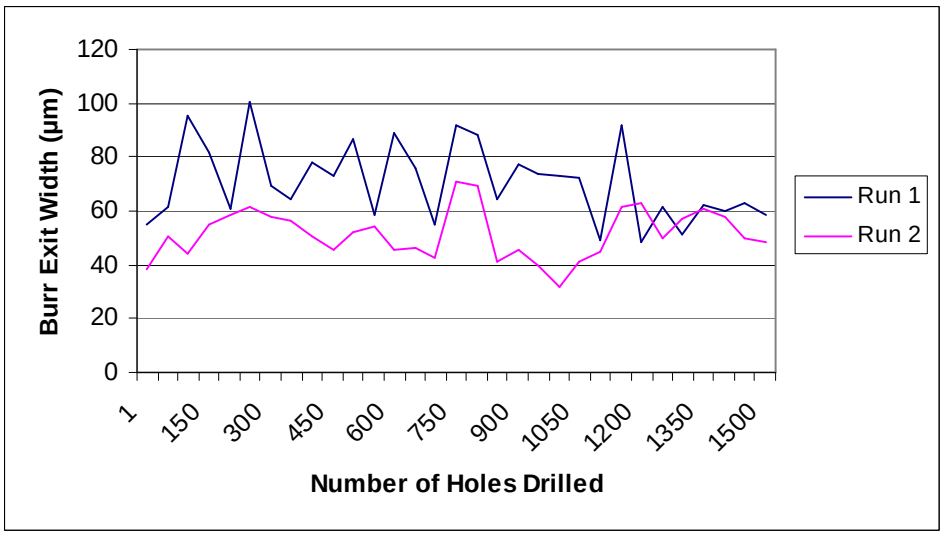

Figure D.1: Burr exit widths for drill 1

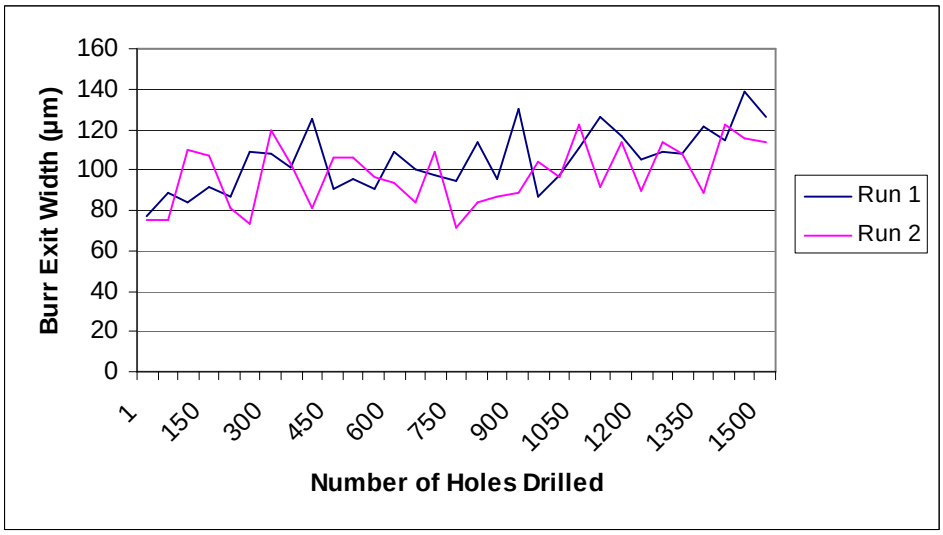

Figure D.2: Burr exit widths for drill 2

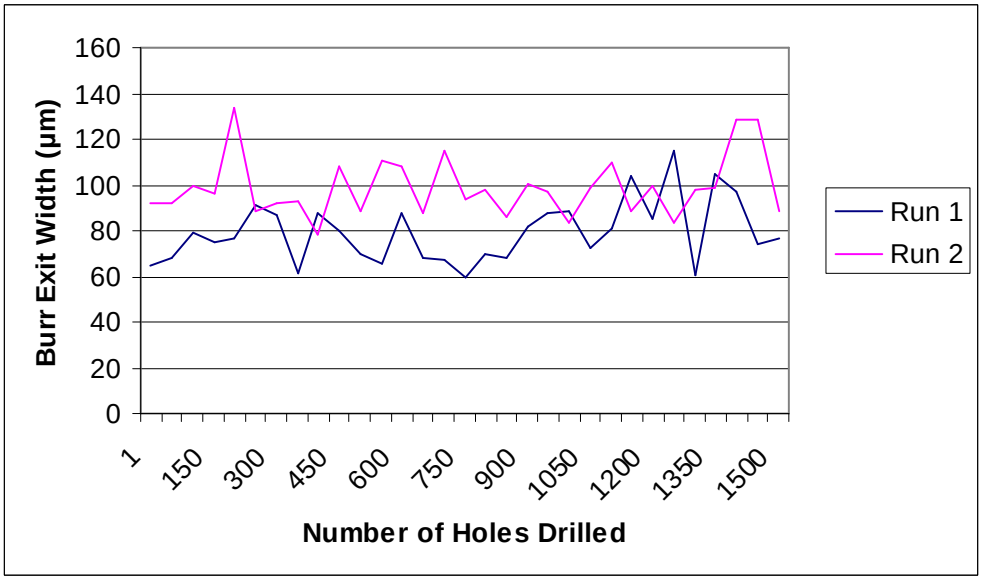

Figure D.3: Burr exit widths for drill 3

APPENDIX E

AVERAGED DRILL FLANK WEAR RESULTS

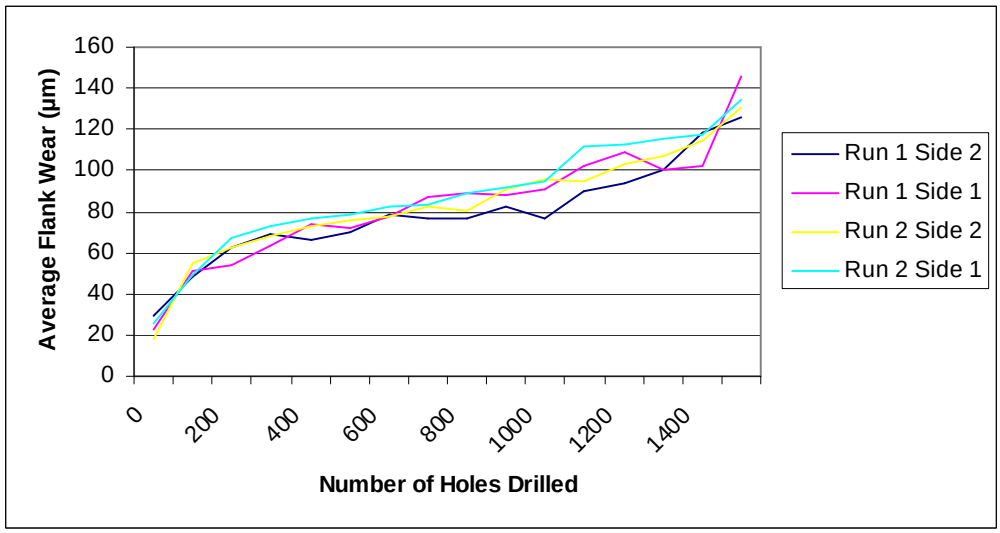

Figure E.1: Average flank wear for drill 1 (for each side)

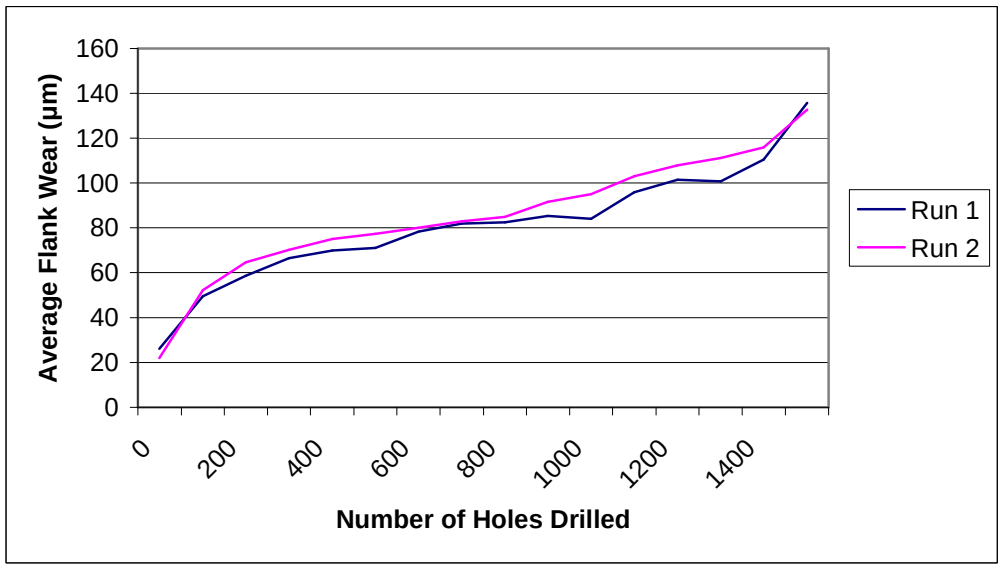

Figure E.2: Average flank wear for drill 1 (for each run averaged)

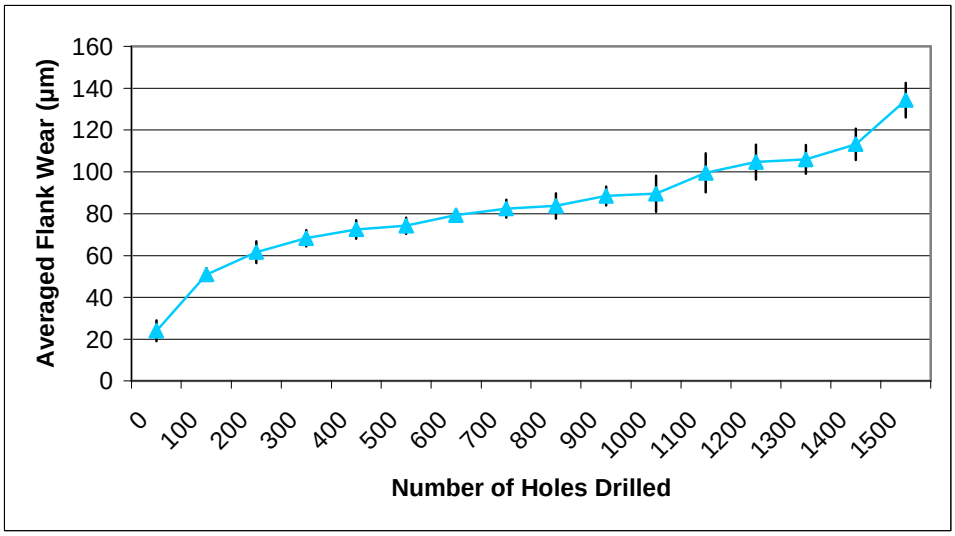

Figure E.3: Average flank wear for drill 1 (with std bars)

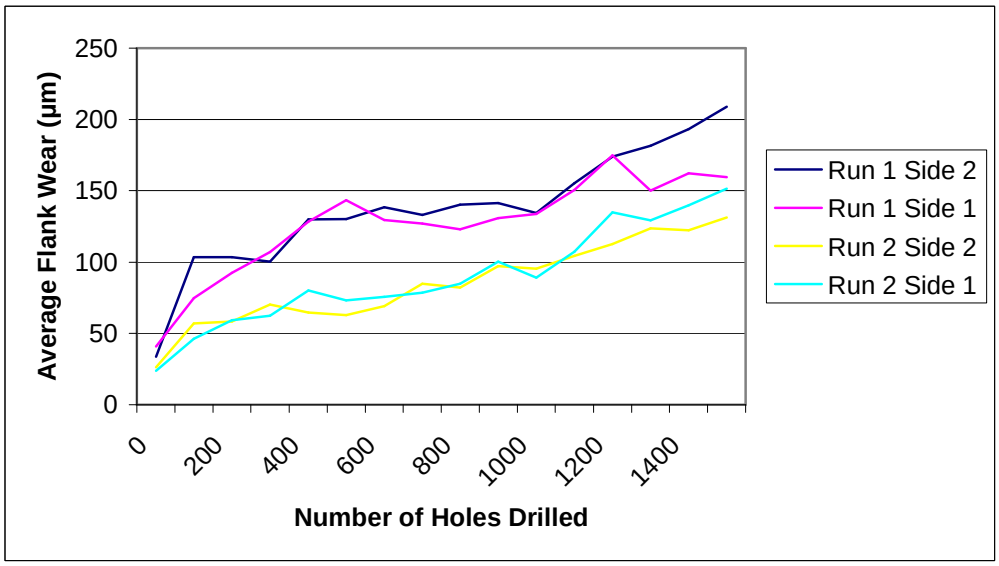

Figure E.4: Average flank wear for drill 2 (for each side)

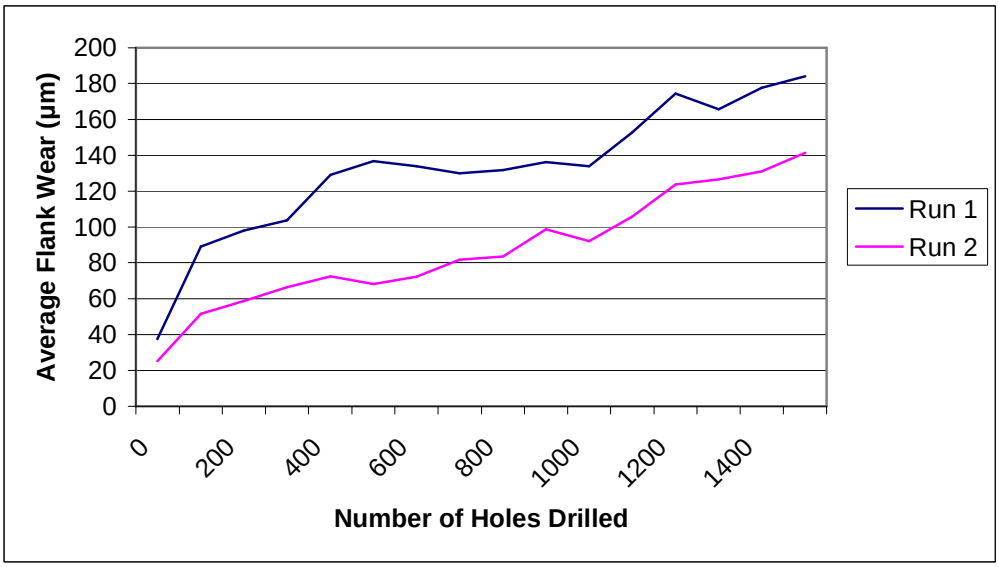

Figure E.5: Average flank wear for drill 2 (for each run averaged)

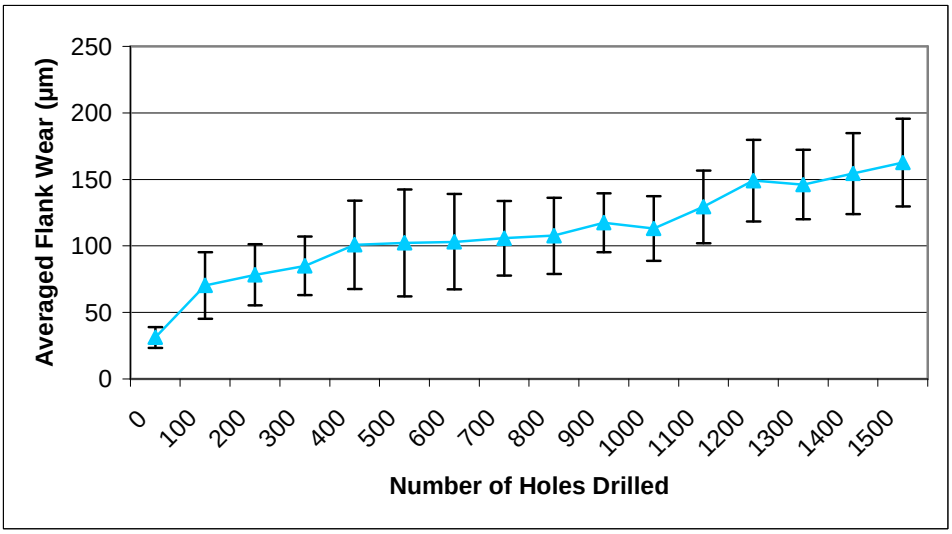

Figure E.6: Average flank wear for drill 2 (with std bars)

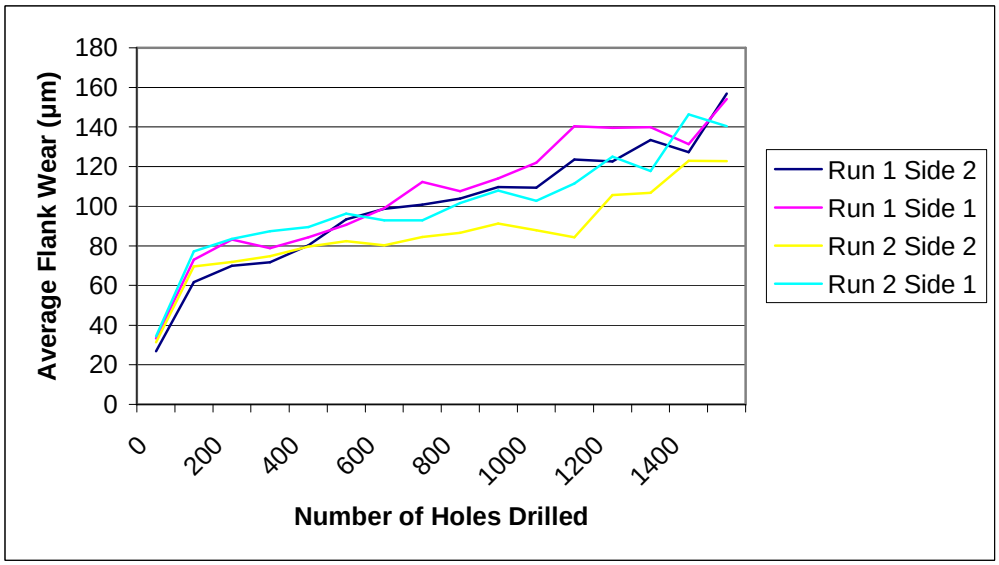

Figure E.7: Average flank wear for drill 3 (for each side)

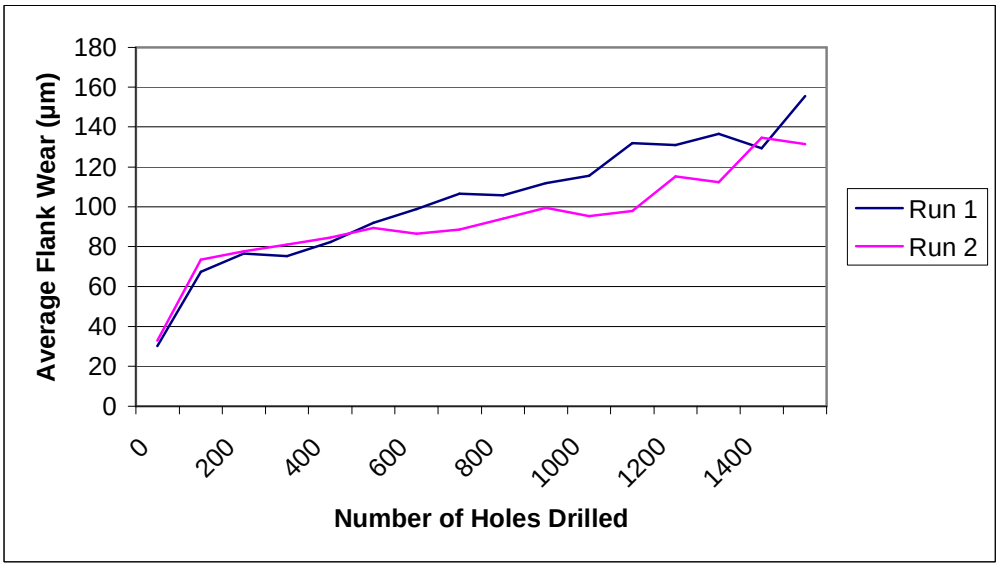

Figure E.8: Average flank wear for drill 3 (for each run averaged)

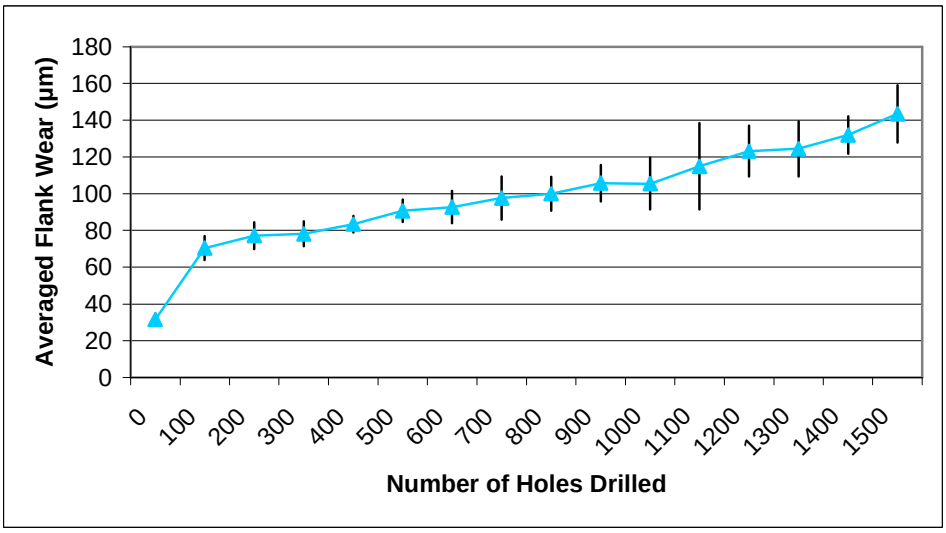

Figure E.9: Average flank wear for drill 3 (with std bars)

APPENDIX F

DRILL OUTER CORNER WEAR RESULTS

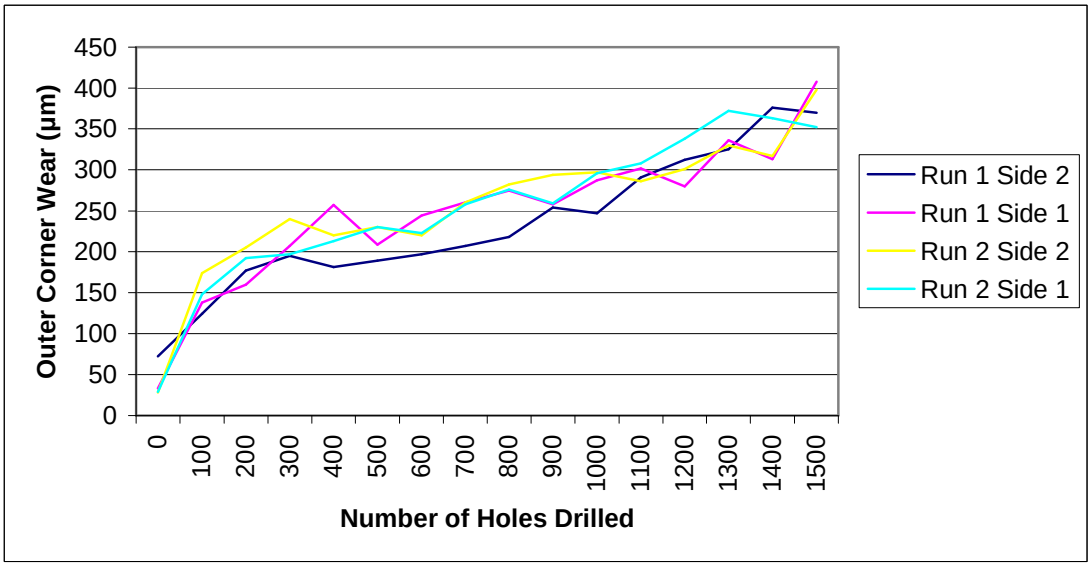

Figure F.1: Outer corner wear for drill 1 (for each side)

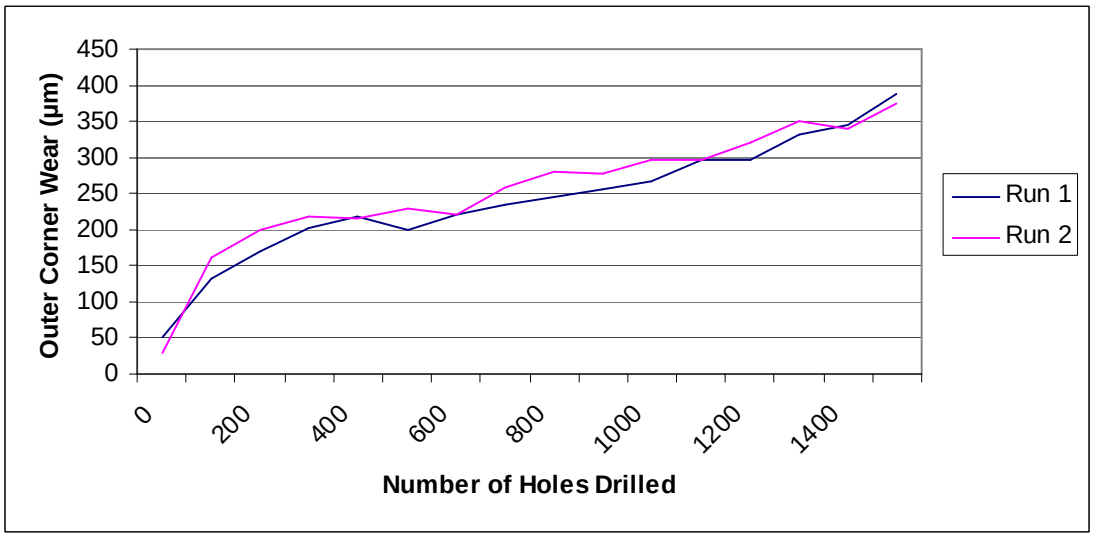

Figure F.2: Outer corner wear for drill 1 (for each run averaged)

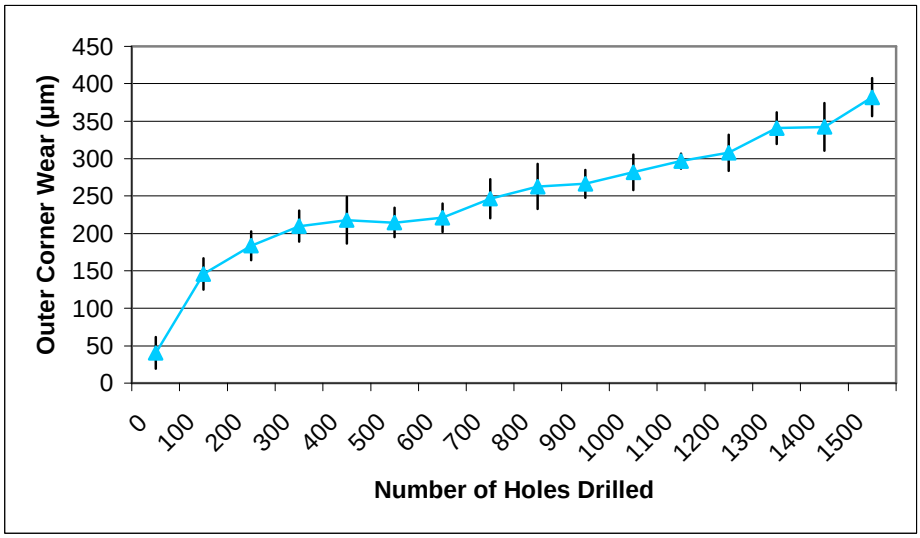

Figure F.3: Outer corner wear for drill 1 (with std bars)

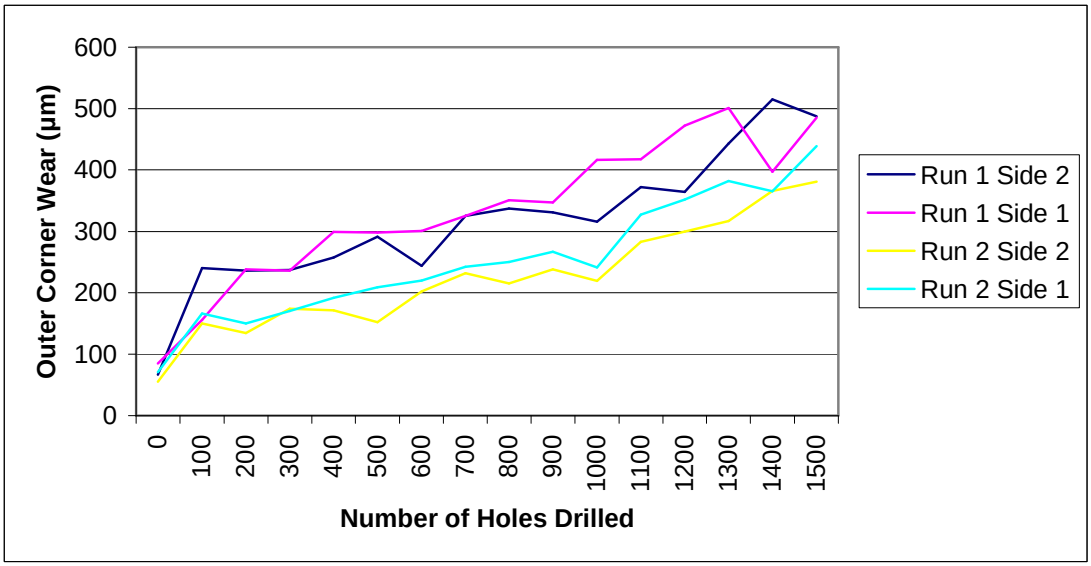

Figure F.4: Outer corner wear for drill 2 (for each side)

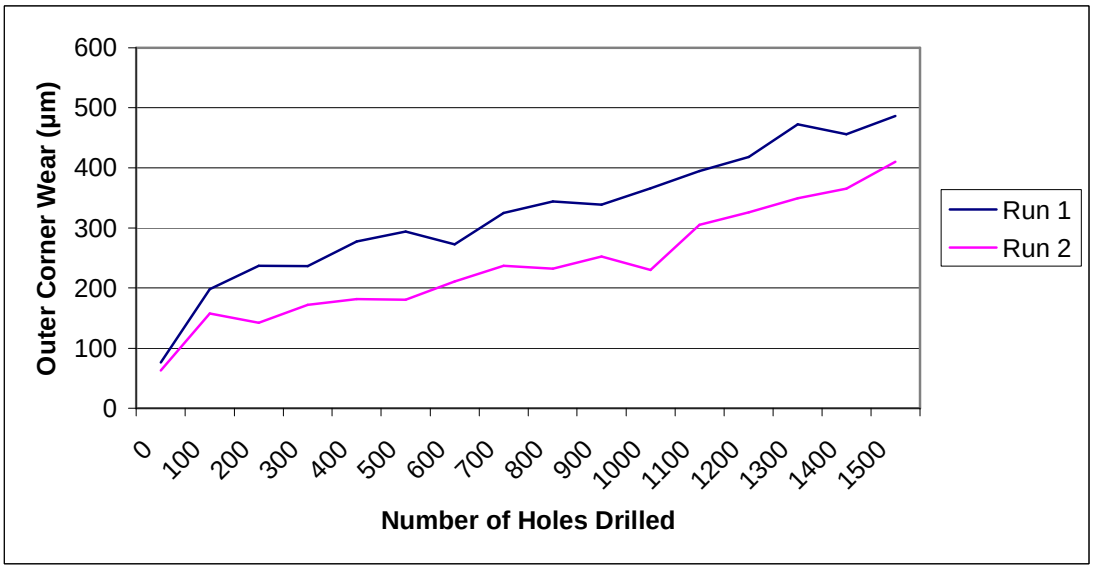

Figure F.5: Outer corner wear for drill 2 (for each run averaged)

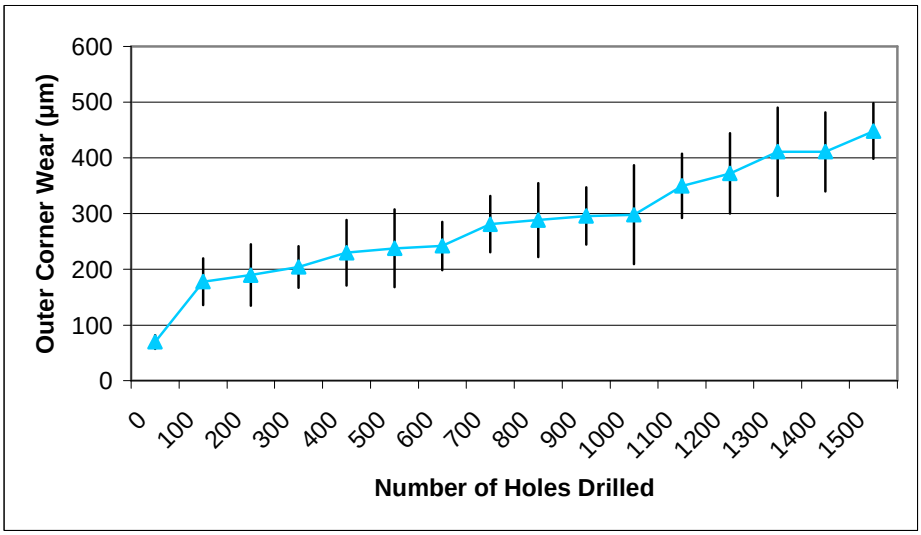

Figure F.6: Outer corner wear for drill 2 (with std bars)

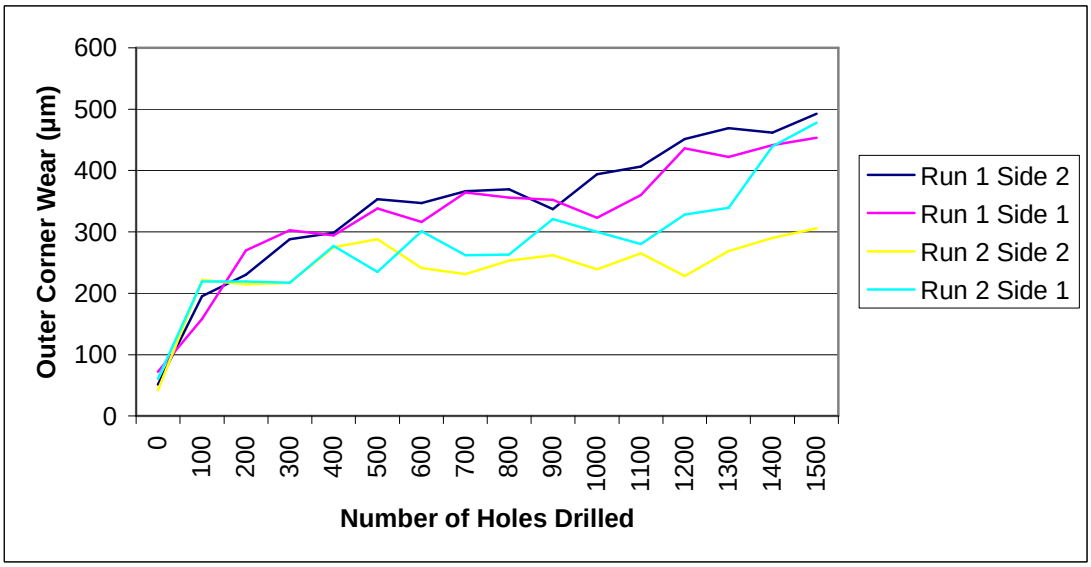

Figure F.7: Outer corner wear for drill 3 (for each side)

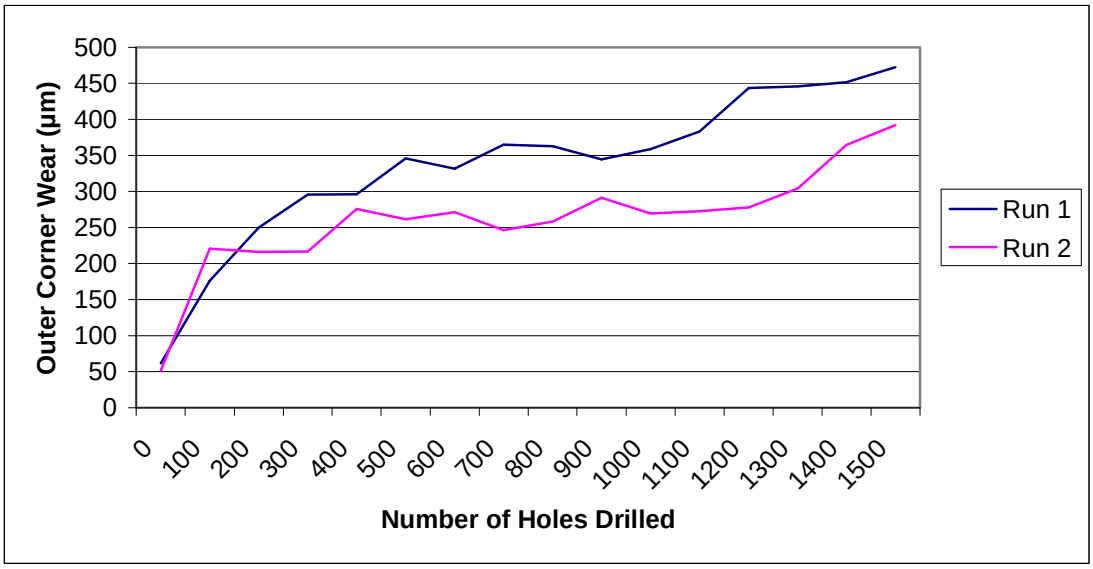

Figure F.8: Outer corner wear for drill 3 (for each run averaged)

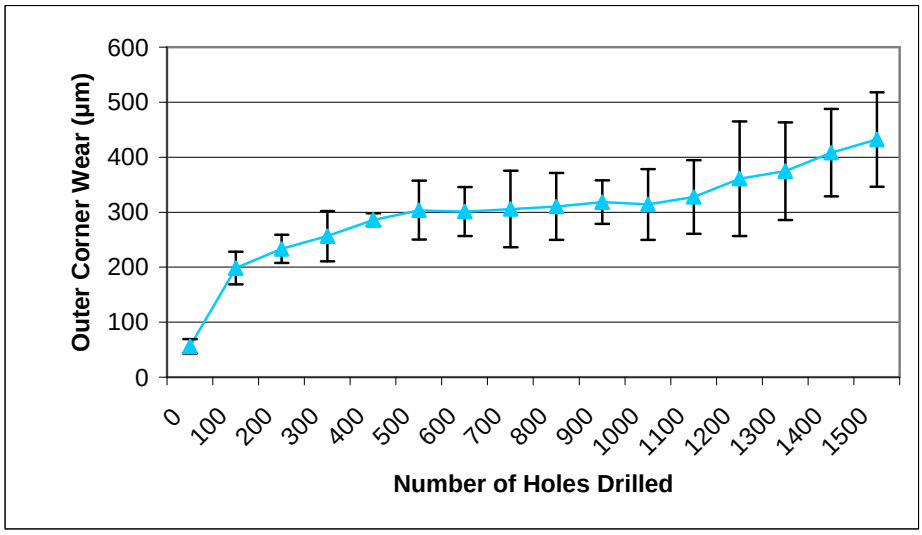

Figure F.9: Outer corner wear for drill 3 (with std bars)

APPENDIX G

MATLAB CODE FOR DETERMINING RESULTS OF INTERLAYER MODEL

```
%Changable Parameters:
Thrustfactor = .03815; %c (percentage of deformation force acting
against burr)
averagethrustforce = 178.2; %average thrust force measured from
dynamometer
feed = .005; %feed per revolution
pointangle = 135; %drill point angle
helix = 20;  %drill helix angle
webthickness = .0274; %drill web thickness
shearstress = 283000000;  %material shear stress
drillradius = .1935 / 2; %drill radius

%Extra Parameters:
beta = ((pointangle/2) * (pi/180)); %converting point angle to radians
helixangle = helix * (pi/180); %converting helix angle to radians
q = webthickness / (2*drillradius); %dimensionless parameter used in
future calculations
tanrakeangle = (((1 - (q^2 * (sin(beta)^2)))*tan(helixangle))/(((1 -
q^2)^.5)*sin(beta))) - ((q * cos(beta))/((1 - q^2)^.5));
rakeangle = atan(tanrakeangle); %calculating rake angle (from William's
model)
frictionangle = (pi/6 + rakeangle/2); %calculating friction angle (from
William's model)
phi = (pi/4) + ((rakeangle - frictionangle)/2); %calculating chip shear
plane angle (from William's model)

%Initialized Variables for Calculations:
deltafinal = 0;
epsilontest = 0;
epsilonfinal = 0;
gammafinal = 0;
summin1 = 10; %for determining delta
summin2 = 10; %for determining gamma
summin3 = 10; %for determining epsilon
sumfinal = 0;

%Determining Parameter Delta
for gamma = .02:.02:1
    for epsilon = .2:.2:1.6
        for delta = .01:.01:.8
            a = (delta^2 + gamma^2 + 1)^.5;
            b = (delta^2 + (gamma^2 * (1 + (tan(beta))^2)) - (2 * delta
* tan(beta)) + (tan(beta))^2)^.5;
```

```
            c = 1 + (1 - epsilon)^2;
            d = (delta * cos(beta)) - (sin(beta));
            e = 2 * (gamma - (tan(frictionangle - rakeangle) * d));
            f = 1 - (1-epsilon)^2;
            g = (gamma^2 + delta^2)^.5;
            sum1 = (a*b*c + f*g)/e;
            if sum1 < summin1
                epsilontest = epsilon;
                deltafinal = delta; %delta
                summin1 = sum1;
            end
        end
    end
end

%Determining Parameter Gamma
for gamma = .02:.02:1
    a = (deltafinal^2 + gamma^2 + 1)^.5;
    b = (deltafinal^2 + (gamma^2 * (1 + (tan(beta))^2)) - (2 *
deltafinal * tan(beta)) + (tan(beta))^2)^.5;
    c = 1 + (1 - epsilontest)^2;
    d = (deltafinal * cos(beta)) - (sin(beta));
    e = 2 * (gamma - (tan(frictionangle - rakeangle) * d));
    f = 1 - (1-epsilontest)^2;
    g = (gamma^2 + deltafinal^2)^.5;
    sum2 = (a*b*c + f*g)/e;
    if sum2 < summin2
        gammafinal = gamma; %gamma
        summin2 = sum2;
    end
end

%Determining Parameters Epsilon and A
for epsilon = .001:.001:.5
    a = (deltafinal^2 + gammafinal^2 + 1)^.5;
    b = (deltafinal^2 + (gammafinal^2 * (1 + (tan(beta))^2)) - (2 *
deltafinal * tan(beta)) + (tan(beta))^2)^.5;
    c = 1 + (1 - epsilon)^2;
    d = (deltafinal * cos(beta)) - (sin(beta));
    e = 2 * (gammafinal - (tan(frictionangle - rakeangle) * d));
    f = 1 - (1-epsilon)^2;
    g = (gammafinal^2 + deltafinal^2)^.5;
    sum3 = (a*b*c + f*g)/e;
    sum4 = stressratio * epsilon * tan(beta) * ((cos(frictionangle -
rakeangle))/(sin(phi)*cos(phi + frictionangle - rakeangle)));
    if abs(sum4-sum3) < summin3
        epsilonfinal = epsilon; %epsilon
        summin3 = abs(sum4-sum3);
        sumfinal = sum4; %A
    end
end

y1 = feed / (2*epsilonfinal); %calculating Sofronas initiation height
sum5 = 1 / (sin(beta)*tan(frictionangle - rakeangle)); %calculating B
y3 = y1 * (25.4/1000); %converting y1 to metric
```

```
y2 = (y3^2 -
((sum5*Thrustfactor*averagethrustforce)/(sumfinal*shearstress)))^(1/2);
%calculating new interlayer initiation height in metric
y4 = y2 * (1000/25.4); %converting y2 to inches
Rj = drillradius - (y4 * tan(beta)); %calculating value of inner burr
material radius
Predictedheight = (drillradius^3 - Rj^3) / (3 * drillradius^2);
%calculating final interlayer burr height
```

REFERENCES

[1] J.C. Aurich. Characterization of burr formation in grinding and prospects for modelling. *Annals of the CIRP*, 54(1):313-316, 2005.

[2] T.R. Newton, J. Morehouse, S.N. Melkote, S. Turner. An experimental study of interfacial burr formation in drilling of stacked aluminum sheets. *Transactions of NAMRI/SME*, 36:437-444, 2007.

[3] D.F. Galloway. Some experiments on the influence of various factors on drill performance. *Transactions of the ASME*, 79:191-231, 1957.

[4] Y. Altintas. *Manufacturing Automation*. Cambridge University Press, Cambridge, 2000.

[5] S.L. Ko, J.E. Chang, G.E. Yang. Burr minimization scheme in drilling. *Journal of Materials Processing Technology*, 140:237-242, 2003.

[6] S.L. Ko, J.E. Chang. Development of drill geometry for burr minimization in drilling. *Annals of the CIRP – Manufacturing Technology*, 52:45-48, 2003.

[7] R.S. Xia, S.M. Mahdavian. Experimental studies of step drills and establishment of empirical equations for the drilling process. *International Journal of Machine Tools and Manufacturing*, 45:235-240, 2004.

[8] R.A. Williams. A study of the basic mechanics of the chisel edge of a twist drill. *International Journal of Production Research*, 8(4):325-343, 1970.

[9] M. Kanai, K. Iwata, S. Fujii, Y. Kanda. Statistical characteristics of drill wear and drill life for the standardized performance tests. *Annals of the CIRP*, 27:61-66, 1978.

[10] L.K. Gillespie, P.T. Blotter. The formation and properties of machining burrs. *Transactions of the ASME*, 66-74, 1976.

[11] D. Dornfeld, S. Min, J. Kim, J. Hewson, C.H. Chu, P. Tyler. Burr prevention and minimization for the aerospace industry. *SAE Technical Paper Series*, 1999-01-2292, 1999.

[12] S.L. Ko. A study on burr formation mechanism. *Transactions of the ASME*, 113:75-87, 1991.

[13] M. Hashimura, D. Dornfeld. Analysis of burr formation mechanism in machining process. *SME Technical Paper*, MR95-178, 1995.

[14] L.K. Gillespie. The measurement of burrs. *SME Technical Paper*, MR74-993, 1974.

[15] J.J. Claus, S.J. Kotula. The characterization and removal of burrs with three-dimensional abrasives. *SME Technical Paper*, MR77-426, 1977.

[16] L.K. Gillespie. Effects of measurement technique and experimental design in the analysis of burrs. *SME Technical Paper*, MR75-985, 1975.

[17] U. Heisel, M. Schaal. Burr formation in intersecting holes. *Production Engineering Research and Development*, 2:55-62, 2008.

[18] J. Kim, S. Min, D. Dornfeld. Optimization and control of drilling burr formation of AISI 304L and AISI 4118 based on drilling burr control charts. *International Journal of Machine Tools and Manufacture*, 41:923-936, 2001.

[19] A. Vijayaraghavan, D. Dornfeld. Challenges in modeling machining of multilayer materials. *Consortium on Deburring and Edge Finishing*, 2005.

[20] J. Choi, S. Min, D. Dornfeld. Finite element modeling of burr formation in drilling of a multi-layered material. *Consortium on Deburring and Edge Finishing*, 2004.

[21] A. Sofronas, K. Taraman. Model development for exit burr thickness as a function of drill geometry and feed. *SME Technical Paper*, MR76-253, 1976.

[22] Y. Hasegawa, S. Zaima, A. Yuki. Burr in drilling aluminum and a prevention of it. *SME Technical Paper*, MR75-480, 1975.

[23] S. Basavarajappa, G. Chandramohan, M. Ashwin, M. Prabu, K. Mukund. Analysis of burr formation during drilling of hybrid metal matrix composites using design of experiments. *International Journal of Machining and Machinability of Materials*, 1(4):500-510, 2006.

[24] A. Sofronas. The effect of system stiffness, workpiece hardness and spindle speed on drilling burr thicknesses. SME Technical Paper, MR76-132, 1976.

[25] J. Stein, D. Dornfeld. Burr formation in drilling miniature holes. *Annals of the CIRP*, 46(1):63-66, 1997.

[26] L.K. Gillespie. *Burrs Produced by Drilling (Topical Report)*. Bendix Kansas City: BDX-613-1248, 1976.

[27] S.S. Pande, H.P. Relekar. Investigations on reducing burr formation in drilling. *International Journal of Machine Tool Design and Research*, 26(3):339-348, 1985.

[28] U. Heisel, M. Luik, R. Eisseler, M. Schaal. Prediction of parameters for the burr dimensions in short hole drilling. *Annals of the CIRP*, 54(1):79-82, 2005.

[29] L.K.L. Saunders. A finite element model of exit burrs for drilling of metals. *Finite Elements in Analysis and Design*, 40:139-158, 2003.

[30] Y. Guo, D. Dornfeld. Finite element analysis of drilling burr minimization with a backup material. *Transactions of the NAMRI/SME*, 26:207-212, 1998.

[31] S. Min, D. Dornfeld, J. Kim, B. Shyu. Finite element modeling of burr formation in metal cutting. *Machining Science and Technology*, 5(3):307-322, 2001.

[32] I.W. Park, D.A. Dornfeld. A study of burr formation processes using the finite element method: part II—the influences of exit angle, rake angle, and backup material on burr formation processes. *Journal of Engineering Materials and Technology*, 122:229-237, 2000.

[33] A.A. Toropov, S.L. Ko. A new burr formation model for orthogonal cutting of ductile materials. *Annals of the CIRP*, 55(1), 2006.

[34] A. Sofronas. The formation and control of drilling burrs. Doctoral dissertation, University of Detroit, 1975.

[35] R.A. Williams. A study of the drilling process. *Journal of Engineering for Industry*, 96:1207-1215, 1974.

[36] J. Kim, D. Dornfeld. Development of an analytical model for drilling burr formation in ductile materials. *Transactions of the ASME*, 124:192-198, 2002.

[37] S. Min. Investigation of the interlayer burrs by drilling of multi-layered materials. *Laboratory for Manufacturing Automation Research Reports*, University of California, Berkeley, 1999.

[38] M.C. Avila, J.D. Gardner, C. Reich-Weiser, A. Vijayaraghavan, D. Dornfeld. Strategies for burr minimization and cleanability in aerospace and automotive manufacturing. *SAE Transactions*, 114(1):1073-1082, 2005.

[39] J. Choi, S. Min, D. Dornfeld, M. Alam, T. Tzong. Modeling of inter-layer gap formation in drilling of a multi-layered material. *Proceedings of the 6th CIRP Workshop on Modeling of Machining*, McMaster University, Hamilton, Ontario, May 19-20, 2003.

[40] H.P. Hoang, S.L. Ko. Burr measurement system for drilled hole at inclined exit surface. *Proceedings of the CIRP International Conference on Burrs*, Kaiserslautern, Germany, April 2-3, 2009.

[41] V. Franke, L. Leitz, J.C. Aurich. Burr measurement: a round robin test comparing different methods. *Proceedings of the CIRP International Conference on Burrs*, Kaiserslautern, Germany, April 2-3, 2009.

[42] V. Krishnaraj, S. Vijayarangan, P. Davim. An experimental and statistical study on the effect of drill geometries on force and hole quality in drilling of glass fibre reinforced plastic. *International Journal of Materials and Product Technology*, 32(2-3):264-275, 2008